2015

Characterization Of Real-World Particle Number Emissions During Re-Ignition Events From A 2010 Light-Duty Hybrid-Electric Vehicle

Matthew Beach Conger
University of Vermont

CHARACTERIZATION OF REAL-WORLD PARTICLE NUMBER EMISSIONS DURING RE-IGNITION EVENTS FROM A 2010 LIGHT-DUTY HYBRID-ELECTRIC VEHICLE

A Thesis Presented

by

Matthew B. Conger

to

The Faculty of the Graduate College

of

The University of Vermont

In Partial Fulfillment of the Requirements
For the Degree of Master of Science
Civil and Environmental Engineering

May, 2015

Defense Date: November 17, 2014
Thesis Examination Committee:

Britt A. Holmén, Ph.D., Advisor
Ruth M. Mickey, Ph.D., Chairperson
Donna M. Rizzo, Ph.D.
Cynthia J. Forehand, PhD., Dean of the Graduate College

Abstract

Despite the increasing popularity of hybrid-electric vehicles (HEVs), few studies have quantified their real-world particle emissions from internal combustion engine (ICE) re-ignition events (RIEVs). RIEVs have been known to occur under unstable combustion conditions which frequently result in particle number emission rates (PNERs) that exceed stabilized engine operation. Tailpipe total PN (5 to 560 nm diameter) emission rates (#/s) from a conventional vehicle (CV) and hybrid electric vehicle (HEV) 2010 Toyota Camry were quantified on a 50 km (32 mi) route over a variety of roadways in Chittenden County, Vermont using the Total On-board Tailpipe Emissions Measurement System (TOTEMS). While HEVs are known to have significant fuel conserving benefits compared to conventional vehicles, less is known about the relative emissions performance of HEVs. This study is the first to characterize RIEVs under a range of real-world driving conditions and to directly compare HEV and CV PNER during driving on different road sections.

A total of 28 CV and 33 HEV sampling runs were conducted over an 18-month period under ambient temperatures ranging between -4 and 35 °C. A road classification based upon speed and intersection density divided the route into four different road sections: Freeway, Rural, Urban I and Urban II. Due to the distinct on-off cycling of the HEV ICE, a new operational mode framework (ICE OpMode) was developed to characterize shutdown, off, re-ignition and stabilized HEV ICE operation. Road section was found to affect overall ICE OpMode distribution, with HEV engine-off operation averaging 57%, 36% and 5% of total operation for combined Urban, Rural and Freeway road sections, respectively. Re-ignition frequency was found to range between 11 and 133 events per hour, with spatial density ranging between 0.1 and 5.6 events per kilometer of roadway. A total of 3212 re-ignition events were observed and recorded, and mean HEV PNER during RIEVs, on average, ranged between 2.4 and 4.4 times greater than that of HEV Stabilized operation. Approximately 65% of all re-ignition events resulted in a peak PNER exceeding the 95% percentile for all ICE-on activity in both vehicles (9.3×10^{11} #/s), known as a High Emission Event Record (HEER).

Comparisons between vehicles found an average of 37% and 7% fuel conserving benefits of the HEV during Urban I and Freeway driving, respectively. However, a different effect was found for PN emissions. During Urban I driving, where RIEVs were most frequent, on average HEV PNER was 2.3 times greater than overall mean CV PNER. For Freeway driving, where the HEV operated similar to a conventional vehicle, mean CV PNER was 2.4 times greater than mean HEV PNER. PNER from partial re-ignition events following an incomplete ICE shutdown (no period of prior engine off operation) were on average 1.65 times greater than those occurring when the ICE shutdown for at least one second.

The typical fuel consumption benefits of HEVs in urban driving are associated with a tradeoff in PN emissions. The HEV ICE operating behavior has implications for the spatial distribution of PN hot-spots as well as the associated micro-scale modeling of alternative vehicle technology emissions. It is likely that building a model of HEV behavior based upon CV activity will be appropriate, with consideration of a hybridization factor and, as a result of these analyses, a re-ignition factor.

Acknowledgements

While the pathway to completion of this master's thesis has been delayed beyond reasonable expectation, it has been possible only with the constant support and guidance of the gracious Dr. Britt Holmén, who has endured the most in countless hours of google-chat conferencing and discussion of my excessively numerous analyses. Dr. Holmén, with her tireless work ethic, attention to detail and scientific rigor, has served as an ideal role model throughout this five-year journey. Throughout my time with the Transportation and Air Quality lab team, she has given me the space to pursue that which both has served the needs of the Signature Project #2 goals but also my own areas of interest within the field of vehicle efficiency and emissions. If given the space and time, I would have unhesitatingly pursued further academic enterprise in the field of transportation and air quality under her tutelage. It is to Dr. Holmén I dedicate this body of work.

I am thankful to my committee members, Dr. Donna and Dr. Ruth Mickey for their patience and willingness to work with a non-traditionalist such as myself.

A critical pillar in my studies, Matlab coding, research methods and child care needs has been the selfless and brilliant Karen Sentoff, who has not only guided SP2 TOTEMS to its completion but has provided the support I needed, without hesitation or expectation, for which I am eternally grateful. Other members of the TAQ lab team who have provided emotional and academic support include Tyler Feralio, John Kasumba, and Jim Dunshee. Additional support and academic liasons came from my fellow TRC scholar Dale Azaria as well as my co-researcher Jonathan Dowds and my supervisor Jim Sullivan at the Transportation Research Center.

I last but not least I would like to thank my partner and wife for her persistent encouragement and support, from all parts of the world –Vermont, Turkey, and now Kenya – without whom I would never have embarked upon this endeavor, and whose own pursuit of her dream as a foreign service officer has been an inspiration for my own life path.

Table of Contents

List of Tables

List of Figures

Acronyms

General Nomenclature

A/F	Air-to-Fuel Ratio
AT-PZEV	Advanced Technology Partial Zero Emission Vehicle
BES	Battery Electric System
CAA	Clean Air Act
CAFE	Corporate Average Fuel Economy
CO	Carbon Monoxide
CV	Conventional Vehicle
DI	Direct Injection
DOE	Department of Energy
ECU	Electronic Control Unit
EEPS	Engine Exhaust Particle Sizer
EF	Emission Factor
EPA	Environmental Protection Agency
EV	Electric Vehicle
FC	Fuel Consumption
FTP	Federal Test Procedure
GPS	Global Positioning System
HC	Hydrocarbons
HEER	High Emission Event Record
HEV	Hybrid-Electric Vehicles
HWFET	Highway Fuel Economy Test
HSD	Hybrid Synergy Drive (Toyota)
ICE	Internal Combustion Engine
MOVES	MOtor Vehicle Emissions Simulator
MY	Model Year
NAAQS	National Ambient Air Quality Standards
NEDC	New European Driving Cycle
NYCC	New York City Cycle
PEMS	Portable Emissions Measurement System
PFI	Port Fuel Injection
PNEF	Particle Number Emission Factor
PNER	Particle Number Emission Rate
PZEV	Partial Zero Emission Vehicle
RIEV	Re-Ignition EVent
Qexhaust	Exhaust Flow Rate
SI	Spark Ignited
SOC	Battery State of Charge
SULEV	Super Ultra Low Emissions Vehicle
TOTEMS	Total On-Board Tailpipe Emissions Measurement System
TWC	Three-way Catalyst
UCDS	Unified Cycle Driving Schedule (LA92)
UCPC	Ultrafine Condensation Particle Counter
UDDS	Urban Dynamometer Driving Schedule (LA4 or FTP72)
ULEV	Ultra Low Emission Vehicle
VMT	Vehicle Miles Traveled
VSP	Vehicle Specific Power

Dimensional Units Nomenclature

atm	Atmospheres
°C	degree Celsius
Hz	Hertz
°K	Kelvin
kg	Kilograms
km	Kilometers
kph	Kilometers per Hour
kW/ton	Kilowatts per Metric Ton
L	Liters
L/100 km	Liters per 100 kilometers
lpm	Liters per minute
m	Meters
mg	Milligrams
mg/s	Milligrams per second
mL	Milliliter
mL/s	Milliliter per second
mph	Miles per hour
RPM	Revolutions per minute
#/sec	Particle count per second
#/km	Particle count per kilometer
#/cc	Particle count per cubic centimeter

1 Motivation

Coming from a background in residential construction, my original intent in applying to the University of Vermont Civil and Environmental Engineering Department was to seek a degree which would help me pursue my passion for improving structural integrity and reducing building energy demands. In my first semester, however, after taking Dr. Holmén's Transportation and Air Quality class, I became motivated by the tremendous gains being made in fuel efficiency within the transportation sector. Additionally, Dr. Holmén's ongoing Signature Project #2 (SP#2) Total On-board Tailpipe Emissions Measurement System (TOTEMS) study provided a wealth of real world driving data from which I could develop several avenues of investigation.

My initial interest for a thesis investigation lay in the development of a look-ahead eco-driving model, using the fuel rate data, GPS route locations and dashboard video from the TOTEMS study to identify driver behaviors which result in minimal fuel consumption. Alas, while the data were plentiful, the design of the SP#2, with only two vehicles and one driver, did not meet necessary breadth to provide generalizations to improve the understanding of the effects of eco-driving techniques. Instead, my focus turned to the recognition of a new automotive phenomenon inherent in the operation of hybrid-electric vehicle – the re-ignition – and the relatively unexplored impact upon emissions.

While much of the work shown below is novel and the techniques are my own, a significant body of methodological development, data collection and alignment are owed to the TOTEMS team, which includes Dr. Holmén, Mitchell Robinson, and Karen Sentoff, as well as the external assistance from the team at Resource System Group, Inc., who together over a five-year period have collaborated to bring this study to fruition. Four critical works cited here provide the basis for much of the methodology and database development required for my analysis. These include two reports to the University of Vermont Transportation Research Center: the first titled "The On-Board Tailpipe Emissions Measurement System (TOTEMS): Proof-of-Concept" (Holmén et al. 2009) and the second being the final report "Light-Duty Gasoline Hybrid-Electric and Conventional Vehicle Tailpipe Emissions Under Real-World Operating Conditions" (Holmén et al. 2014). Additionally, the theses of Mr. Robinson and Ms. Sentoff, in fulfillment of their Civil

and Environmental masters' degrees: "Second-by-second on-board real-world particle number emissions for comparable conventional and hybrid-electric gasoline vehicles in a city driving environment" (Robinson 2011) and "Characterization of gas-phase emissions from comparable conventional and hybrid gasoline vehicles during real-world operation" (Sentoff 2013). None of the work I have achieved here would be possible without the countless hours of instrumentation development and data alignment performed through collaborations with these authors.

2 Introduction

Hybrid-electric vehicles (HEVs) are becoming an increasingly important component of the domestic and world-wide light-duty vehicle (LDV) passenger fleet. Light-duty HEVs were first introduced into the U.S. market in the late 1990's with the first generation Toyota Prius and Honda Insight. With increasing popularity of HEVs, the number of models has expanded considerably, and by 2013 ten different manufacturers offered 56 HEV models on the U.S. passenger vehicle market (U.S. DOE 2013). HEV passenger vehicle purchases over the past 5 years have increased on average 12%, and in 2013 represented 3.19% of all passenger vehicle sales (Electric Drive Transportation Association 2014). The HEV share of the light-duty vehicle market is estimated to reach 9% by 2020 (NREL 2009), and a projected 38% of new sales by 2040 (U.S. EIA 2014).

On-board battery electric systems (BES) vary considerably between HEV models, resulting in different categories of hybridization (micro, mild, full, plug-in). As seen in Table 1 below, the increasing levels of hybridization involve the application of more complex electrical operations to reduce the use of the internal combustion engine (ICE). Most HEVs on the road today are categorized as "full" HEVs, utilizing engine stop/start technology when the vehicle is at idle, regenerative braking capacity to capture energy typically lost to heat during deceleration, and an electric motor (EM) to assist in vehicle propulsion. In 2013, the top ten selling HEVs in the U.S. were all full hybrid models (Electric Drive Transportation Association 2014).

Electric motors maintain high efficiency under high RPM, can be operated independent of driver demand and are thus complementary to internal combustion engine (ICE) torque deficiencies (Villatico 2014). The addition of this electrical power plant allows for the downsizing of the

vehicle's ICE, with further fuel economy improvements possible with use of a more efficient Atkinson thermodynamic combustion cycle (Rajagopalan, et al. 2003; Schouten et al. 2002; Zhao and Xu 2013). The mean fuel economy of MY 2009 HEV passenger vehicles was on average 30% higher than that of comparable conventional vehicles (UNEP 2009).

Table 1. Levels of Electric Hybridization.

	Level of Hybridization			
Vehicle Capacity	**Micro**	**Mild**	**Full**	**Plug-in**
ICE shuts off and on while at idle	Yes	Yes	Yes	Yes
Employs regenerative braking	No	Yes	Yes	Yes
Uses an electric motor to assist ICE	No	Yes	Yes	Yes
Can drive using only the electric motor	No	No	Yes	Yes
Recharges battery from electric grid	No	No	No	Yes

Tailpipe emissions from motor vehicles are known to have significant impact upon the environment and public health, and are known to affect local air quality and contribute significantly to changes in global climate. Some of the mobile source gaseous pollutants are currently regulated under the National Ambient Air Quality Standards (NAAQS), including carbon monoxide (CO), oxides of nitrogen (NO_x), sulfur dioxides (SO_x) and Particle Matter (PM). Obvious benefits arise with the HEV in terms of fuel savings, yet there is not yet a wealth of investigation into the effects of vehicle hybridization upon pollutant emissions. While a liter of gasoline burned in a hybrid ICE results in similar pollutant emissions as that of a liter of gasoline burned in a comparable conventional ICE, the new modes of operation of the HEV ICE differ in

real world driving compared with the CV, with the HEV ICE shutting off and on while the CV remains on continuously.

Mobile source emissions, both on- and off-road, present local air quality concerns as well as larger issues associated with global climate change. In the United States, the on-road vehicle fleet was estimated to contribute 42% of carbon monoxide, 40% of oxides of nitrogen, 29% of total hydrocarbon atmospheric emissions in 2010 (EPA 2012). Globally, efforts to reduce transport-related pollutants are not likely to be achieved by reductions in vehicle miles traveled (VMT) as developing countries such as China see a rapid expansion of passenger car use, with one prediction of global vehicle ownership reaching 2 billion by year 2030 (Dargay et al. 2007). Yet here in the United States, adoption of regulations and developing technologies have taken a primary role in reducing criteria pollutant inventories by 60% over the past 30 years (EPA 2012). The implementation of Corporate Average Fuel Economy (CAFE) standards has steadily resulted in improved fleet fuel efficiencies over the past 40 years, with the goal of reducing dependence upon foreign oil. Today, improved fuel economy is viewed as a means to mitigate greenhouse gas emissions (GHG) and has in part incentivized the development of alternative technologies including HEVs and pure electric vehicles (EVs), which displace on-board gasoline consumption with other energy sources provided from the grid (Samaras and Meisterling 2008; Lutsey and Sperling 2009). Despite the rising penetration of electrified and semi-electrified vehicles, the ICE remains the prevalent source of propulsion for LDV domestically and globally, with less than $1/10^{th}$ of 1% of the 2010 fleet operating on electric power alone (DOE 2012). Though hybridization of the fleet will likely mitigate the emissions and fuel use, sparse information is available to date that compares HEVs with their conventional counterparts in real-world operation.

3 Background

3.1 HEV Re-ignition Events (RIEVs)

As demonstrated in Table 1 above, the one energy conserving strategy employed by all HEVs is the stop-start function, allowing the ICE to shut down during most standstill operation or 'idling' events. Following a period of ICE shutdown – typically, under low power demand driving conditions - the ICE of a hybrid vehicle will "re-ignite" to meet the requested increased power demand associated with acceleration. Traditionally, these events have been identified with conventional vehicle operation as 're-starts', yet this term is technically ambiguous and requires more precise definition. Under typical operating conditions, re-ignition events (RIEVs) occur while the engine is warm, as opposed to a conventionally defined ICE "cold start", which occurs while the engine is within 10 degrees Fahrenheit of ambient temperature (U.S. EPA 1993). Warm starts occur when the ICE temperature is elevated but the catalytic converter has cooled, while the EPA (1993) has defined a "hot start" as one during which both engine and catalytic converter are at elevated temperatures. A hot start as defined by the EPA requires a previous ICE-on period of at least four minutes from a cold start (two minutes to raise the catalyst temperature and additional two minutes for the coolant to reach 140 °F), assuming standard ICE design features. These definitions of warm and hot starts, designed to identify emissions behavior in conventional vehicles during trip chaining events, do not adequately characterize HEV RIEV conditions with frequent ICE on-off cycling.

The micro-hybrid re-ignition is enabled through the use of an efficient integrated starter generator (ISG), replacing both the traditional starter motor and alternator. The ISG is typically belt driven and relies on a higher voltage conventional starter battery to provide auxiliary power during

standstill (Friedrich and Girardin 2009). A micro-hybrid power train receives no assistance from the battery and relies solely on the ICE for propulsion. In the mild hybrid, where a higher voltage BES provides power to the wheels through the electric motor, a RIEV is achieved, similar to the mico-hybrid, solely following standstill conditions, but with the BES providing some propulsive assistance to the ICE (Bitsche and Gutmann 2004). With full and plug-in HEV models, the RIEV can occur after standstill operation or when the vehicle is in motion following a mode of electric-only propulsion (Bayindir et al. 2011).

Little if any direct investigation of HEV re-ignition events has been conducted under real-world driving conditions. RIEVs have been spatially associated with urban driving, particularly at intersections where ICE-off operation under low speed and load is followed by an increase in power demand (Robinson and Holmén 2011). There is a necessary association between periods of ICE-off and RIEVs, yet the ICE-off phenomena and their duration are dependent upon many variables. ICE-off operation varies by full HEV powertrain type (series, parallel, series-parallel), computerized power management strategies, battery state of charge (SOC), vehicle speed and instantaneous power demand (Rajagopalan et al. 2003; Liu and Peng 2008; Villatico 2014; Bayindir et al. 2011; Chau and Wong 2002). Zhai (2011) identified specific thresholds of maximum speed (40 mph) and acceleration (2.5 mph/s) for ICE-off operation for a first generation MY 2001 Toyota Prius. Testing on a MY 2004 Prius showed that ICE-off operation was 59% greater in urban driving under the New York City drive cycle (NYCC) compared with highway driving using the Highway Fuel Economy Test cycle (HWFET) (Christenson et al. 2007).

While extensive studies have examined the optimal management of the BES to maintain fuel efficient operation and battery thermal stability in full HEVs (Liu and Peng 2008; Liu and Li

2012; Chaturvedi et al. 2010; Koot et al. 2005; Zhu et al. 2004), charge depletion strategies for plug-in HEVs (Gonder and Markel 2007; Banvait et al. 2009; Tribioli et al. 2014) and route look-ahead dynamic programming strategies using telematics (Manzie et al. 2007; Tae 2008; Ganji and Kouzani 2010; Larsson et al. 2012), the characterization of RIEVs and their driving factors remain largely unexplored.

3.2 Ambient effects upon HEV operation

The effects of increased temperature upon real-world conventional vehicle operation include an overall general decrease in fuel consumption due to decreased internal resistance and air drag as well as reduced engine idling (Eccleston and Hurn 1978). Investigations of effects of temperature on HEV operation have been shown to largely affect ICE-off activity. Under a NYC dynamometer test cycle at ambient temperatures of 20˚C and -18˚C , a MY 2006 Toyota Prius and a Ford Escape both experienced a three-fold decrease in ICE-off operation, from 66% to 20% for the Prius and from 55% to 18% for the Escape (Christenson et al. 2007). Sentoff (2013) found moderate effects from temperature changes for a 2010 Hybrid Toyota Camry, with only a 7% increase in ICE-off operation between cold (<5°C) and warm (>22°C) seasonal temperatures. Battery performance in HEVs has been shown to deteriorate with colder ambient temperatures (Smith and Wang 2006), but overall effects may depend upon driving conditions and auxiliary power requirements such as cabin heating and cooling. Duarte et al. (2014) showed correlation between lower battery state of charge (SOC) and reduced frequency of electric-only propulsion, with 90% of standstill operation in a MY 2011 Prius occurring with the ICE off. Sentoff (2013) found that average SOC decreased 6% from cold (<5°C) to hot (>29°C) temperature operation in the MY 2010 Hybrid Camry. Fonteras et al. (2008) found fuel usage to fluctuate 12% as a function of season for a 2006 Toyota Prius, with highest fuel consumption rates occurring during

winter (mean temperature of 11.4 °C) and lowest occurring during spring (mean temperature of 22.8 °C).

3.3 Health Effects and Regulation of Particulate Emissions

Recent studies provide evidence of correlation between exposure to particulate matter (PM) and increased rates of lung disease, cardiopulmonary disease, diminished childhood lung development and mortality (Gauderman et al. 2004; MacNee and Donaldson 2003). Ultrafine particles (diameter <= 100 nm) are able to penetrate deeper into the respiratory system and are associated with increased chronic health issues (Pope et al. 2002). This penetration is due to the higher total surface-area-to-volume ratio of smaller particles that facilitates adsorption and leads to greater potential toxicological effects (MacNee and Donaldson 2003). Inhalation of smaller diameter particles is also shown to result in elevated total particle deposition fraction because they bypass the natural defense system within the lungs (Kittelson 1998).

3.3.1 Particulate Regulation

Particles emitted during the combustion process exhibit complex behavior in the tailpipe due to nucleation, condensation, coagulation, and adsorption, and are thus difficult to measure. Under the Clean Fuel Fleet Exhaust Emission Standards, particulate matter is currently only regulated on a mass basis (g/mi) in diesel powered vehicles (U.S. EPA 2014a). Airborne particulate matter of aerodynamic diameter 2.5 micrometers and smaller ($PM_{2.5}$) is a regulated criteria pollutant under the National Ambient Air Quality Standards (U.S. EPA 2014b). Inconsistencies arise with regulation of PM based solely on mass in regards to tailpipe emissions as there is a general lack of correlation between particle number and particle mass in vehicle exhaust (Robinson and Holmén 2011; Kittelson 1998). While particles in the nanoparticle mode (diameter less than 50 nm) constitute 90% or more of the total particle number, they only account for between 1% and

20% of total particle mass in spark-ignited engine exhaust (Kittelson 1998). Beginning in September of 2014, all SI gasoline direct injection (DI) LDVs sold in Europe must meet a stringent particle *number* (PN) emission factor requirement of 6 x 10^{12} #/km, and by 2016 this will become more restrictive by an order of magnitude to meet the Diesel LDV limit 6 x 10^{11} #/km (MECA 2013). Direct injection gasoline engines differ from port fuel injection (PFI) engines in the delivery of the fuel mixture to the cylinder, with DI engines having better control of the fuel-air mixture and flame propagation under low engine loads, contributing in part to overall reduced fuel use compared with PFI engines (Harada et al. 1997). While particle number is not currently regulated in the U.S. for SI LDV engines, it is important to recognize that the size of the particle has more potential health significance than does the overall mass, and therefore PN-based standards should be considered for regulatory adoption (MECA 2013). Eventually, it is likely that the U.S. will follow suit in adoption of PN tailpipe regulations similar to those found in Europe.

3.3.2 Particulate Matter from Mobile Sources

PM emitted from mobile sources is significant. One study in 1996 showed an estimated 43% of all UFP mass inventory in the California South Coast Air Basin came from on-road vehicles (U.S. EPA 2014c), while an estimated 36% of all European particles less than 300 nm in 2005 were emitted from road transport (Health Effects Institute 2013). Traditionally, diesel vehicles have been the primary mobile emitters of particulate air pollution and were the primary focus of particulate emissions research, yet recent technological advances have significantly decreased diesel vehicle PM emission factors (g/mi) over the past 20 years (Farnlund et al. 2001; Dallmann and Harley 2010). This in turn has fostered an interest in particulate emissions from SI light-duty passenger vehicles (LDVs). LDVs comprise over 55% of vehicle miles traveled and 65% of all gasoline fuel consumed from mobile sources (Sawyer et al. 2000; Puentes and Tomer 2009).

Real-world studies of particulate emissions from LDVs in high temporal resolution are lacking, especially for HEVs, and testing of CVs has been limited to roadside sampling (Agus et al. 2007; Gouriou et al. 2004), dynamometer testing in idealized lab conditions (Kasper et al. 2005; Harris and Maricq 2001; Lee et al 2009; Kayes et al. 2000) or using chase vehicles (Merkisz et al. 2009). Recent studies of particulate emissions using on-board portable emissions measurement systems (PEMS) have focused primarily upon heavy-duty and light-duty diesel vehicles (Durbin et al. 2008; Merkisz, Pielecha, and Gis 2009; Huang et al. 2013), while investigation of real world on-board LDV HEVs emissions have been limited. On-road studies have examined of particle number emission factors (PNEF) for roadway fleets across several cities, with overall ranges between 10^{13} and 10^{14} particles/km per vehicle, and fleet make-up including heavy-duty diesel vehicle (HDDV) trucks of 5% - 6% (Jamriska and Morawska 2001; Gramotnev et al. 2003; Kittelson, et al. 2004; Zhang et al. 2005). More recent studies of PN emission factors have been limited, and no recent studies have examined PNEF on-board newer hybrid LDVs.

3.4 Factors Affecting Tailpipe Particulate Emissions

While much of the early focus upon PM emissions was dedicated to the examination of heavy-duty diesel vehicles (HDDVs), recent advancements in diesel particulate filters and national shifts to low sulfur fuels has resulted in dramatic reductions in HDDV particulate emissions (Burtscher 2005). With these changes in diesel technology, a new focus upon spark ignition (SI) particulate emissions is emergent. Environmental factors have been shown to affect tailpipe particulate emissions from conventional SI vehicles. PM emission rates for stabilized operation were shown to negatively correlate with air temperature (Mulawa et al. 1997). Particle number concentrations between 15 and 30 nanometers were most significantly affected by temperature, attributable to increased particle nucleation at lower ambient air temperatures (Jamriska et al. 2008). Effects of

higher relative humidity were shown to positively influence particle formation in the lower diameter accumulation mode (50-150 nm), suggesting particle growth from smaller size ranges due to condensation and an overall increase in primary soot emissions (Jamriska et al. 2008). Engine load has been shown to largely influence particle number emissions from SI engines with a general increase in PN concentration with increased load across all engine sizes (Farnlund et al. 2001; Kayes et al. 2000; Kittelson et al. 2006).

3.4.1 PN Emissions from HEV Re-ignition Events

Under dynamometer testing, HEVs and conventional vehicles have shown similar emission patterns for criteria pollutants HC and NOx under heavy engine loading, with emission rates increasing during acceleration and at high speeds (Christenson et al. 2007). The effects of HEV ICE on/off cycling during low speed driving conditions, however, were shown to result in a two-fold increase in high emission events (HEEs), or PN emission rates (PNER, in particles per second or #/s) above the 90th percentile, compared with the conventional vehicle driven along the same route (Robinson 2011). Christienson (2007) found that the 2004 Toyota Prius and 2005 Ford Escape had sporadic high Total Hydrocarbon (THC) emission rates, possibly attributed to catalyst cooling as a result of ICE-off operation. Robinson (2011) found that 85% of all HEV HEEs occurred as a result of re-ignition during city driving. During engine ignition, fuel injection rates were found to be 210% – 240% greater than those of steady-state operation (Yu et al. 2008a), and these fuel-rich conditions have been associated with increases in unburned hydrocarbons (Kittelson et al. 2006).

3.4.2 Three-way Catalysts and the Air-to-Fuel Ratio

In all modern vehicles, the use of the three-way catalyst (TWC) exhaust system to remove gaseous pollutants CO, NO_x and hydrocarbons (HC) simultaneously relies upon stabilized operating temperatures and ideal combustion stoichiometry (Brandt et al. 2000). The effective

removal of CO, HC and NO_x in a TWC are highly dependent upon the air-to-fuel ratio (A/F) as seen in Figure 1 below. A/F is a measure of the mass of air injected into the engine divided by the mass of fuel injected. Stoichiometric operation occurs when A/F = 14.7, generating ideal conditions for complete combustion of gasoline fuels. A/F is also expressed using the Greek letter Lambda (λ). Lambda is the actual measured A/F ratio divided by the stoichiometric A/F ratio, thus an actual A/F ratio of 14.7 results in λ = 1.0. It is generally assumed that fuel consumption under stoichiometric conditions results in the lowest HC and CO emissions and as a result particle number emissions (Lee et al. 2009). The TWC functions to convert CO to CO_2, HC to H_2O and CO_2, and NO_x to N_2 during incomplete combustion (Brandt et al. 2000). The following general chemical equations represent these pollutant conversions:

$$2CO + 2NO \rightarrow 2CO_2 + N_2 \qquad \textit{Equation 3.1}$$

$$[HC] + NO \rightarrow N_2 + CO_2 + H_2O \qquad \textit{Equation 3.2}$$

During fuel-rich conditions (enrichment, λ < 1) and during fuel-lean conditions (enleanment, λ > 1), the modern electronic control unit (ECU) monitors the oxygen content of the exhaust upstream and downstream of the TWC several times per second, allowing for adjustments to the fuel injection rate and air flow to keep λ within a target range either side of 1.0. As can be seen in Figure 1, fuel-rich conditions (λ < 1) can significantly reduce HC and CO removal while fuel-lean conditions (λ > 1) can significantly reduce NO_x removal. Thus, optimal removal of all three pollutants is dependent upon maintenance of Lambda within a specific window. Enrichment in CVs is typically associated with greater power demand and acceleration, while enleanment occurs with reduced power demand and decelerations (Li et al. 2008).

As is seen in Figure 2, TWC conversion efficiency of all three pollutants is extremely temperature dependent. While CV exhaust systems are able to maintain elevated TWC temperatures during all operation, the HEV TWC is subject to different thermal conditions. Because of the frequent on-off ICE cycling and extended periods of cooling of the exhaust system, consistent maintenance of optimal catalyst temperature may not be possible in hybrid vehicles (Reyes et al. 2006), thus suggesting that re-ignition events may result in relatively high emission rates compared to stabilized steady-state activity.

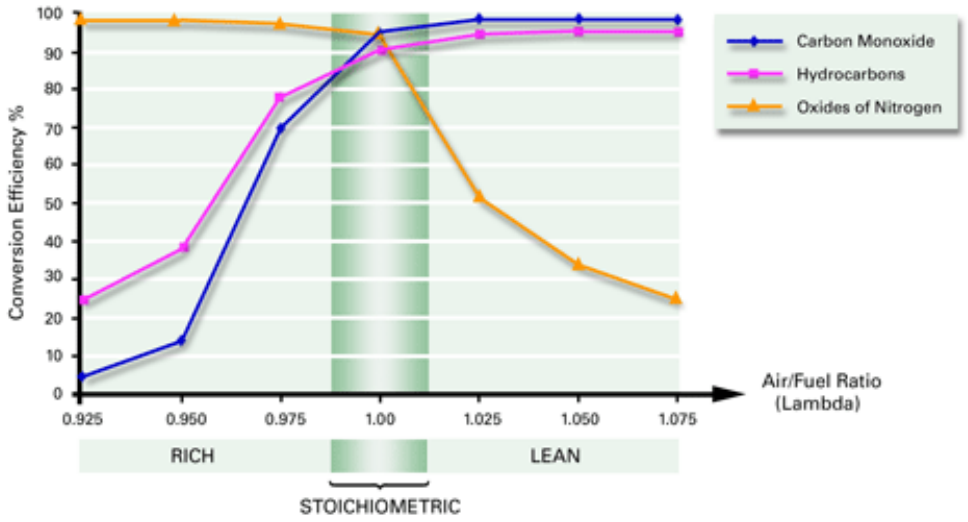

Figure 1.Typical conversion efficiency for a spark ignition Three-way Catalyst vs. Air-to-Fuel Ratio (A/F). Source: Johnson Matthey, 2014.

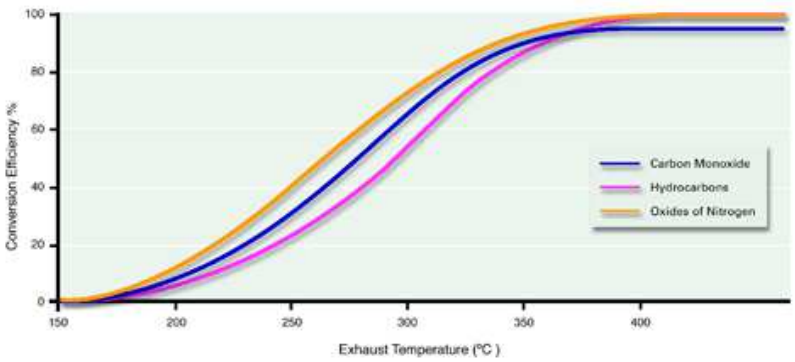

Figure 2. Effect of temperature on TWC conversion efficiency (%) for a typical spark ignition engine, Lambda = 1. Source: Blackthorn, 2014.

3.5 On-board Portable Emissions Measurement Systems

3.5.1 Historic Emissions Study Methods

Several methods have been applied to generate estimates of mobile source emissions, with each having its merits and drawbacks. Traditionally, these have included tunnel, remote sensing, dynamometer and portable emission measurement system studies (PEMS). The most popular method, chassis dynamometer studies, are conducted in controlled laboratory environments with vehicles operated over simulated driving cycles with fixed ambient conditions, with emissions typically collected from bag analysis over portions of a drive cycle (EPA 2009). This method allows for the most convenient testing of numerous vehicle makes, of varying mileage and condition, without the need for specialized accessorization for each vehicle. While this method has the benefit of repeatable and standardized data collection and has been the traditionally accepted method for quantifying tailpipe emissions, bag analysis can be limited in providing detailed emissions at finer temporal resolution under transient operation (Frey et al. 2003). Dynamometer testing furthermore is not responsive to the effects of ambient factors and varying road conditions. One study showed acceleration and deceleration rates of simulated drive cycles to be significantly lower than those found in real-world driving (Li et al. 2008), while another showed that emission rates from dynamometer tests can significantly differ from emissions testing in actual driving environments (Barth et al. 2006).

Studies using tunnel and remote sensing techniques typically have measured mobile source emissions from a composite vehicle fleet using stationary, road side equipment over a specified time period such as rush hour in highly urbanized areas. These investigations allow for a snapshot of the aggregate effect of vehicle pollutants upon air quality but lack the spatial diversity and are limited in modal variation. In addition, the pollutant mix cannot be attributed to a single vehicle

and only generalizations can be made about the aggregate fleet emissions, with vehicle distributions estimated through separate vehicle counts.

3.5.2 PEMS Studies

In recent years, the evolution of smaller and more mobile testing equipment have allowed for studies which use portable emission measurement systems (PEMS). PEMS instrumentation typically includes either sampling of ambient roadway air as a "chase vehicle" or the sampling of exhaust directly from the tailpipe of a test vehicle. These PEMS investigations have focused upon gaseous criteria pollutants (Frey et al. 2003; Coelho et al. 2009; Gierczak et al. 2006) as well as speciated exhaust elements (Truex et al. 2000; Jetter et al. 2000; Barth et al. 2006; Collins et al. 2007; Li et al. 2008). One study using PEMS found significantly higher NOx emission factors for diesel passenger vehicles from real-world driving compared to modeled results derived from dynamometer testing (Kousoulidou et al. 2013). Recent testing of ultra-low emission vehicles (ULEV) and partial zero emission vehicles (PZEV) using PEMS showed average running emissions for CO and NO_x were low with high emission events attributed to real-world, transient high-power demand (Barth et al. 2006; Collins et al. 2007). In another PEMS study, Frey et al. (2003) demonstrated that average emission rates for HC and CO_2 were 5 times greater, and that those of NOx and CO were ten times greater during accelerations compared with idle modes for ten gasoline-fueled vehicles.

PEMS studies involving LDV HEVs have been limited. Duarte et al. (2014) showed lower battery state of charge (SOC) between 40% and 50% in a MY 2011 Prius resulted in reduced periods of ICE-off operation and higher emission rates for carbon dioxide, carbon monoxide and nitrogen oxides compared with higher SOC operation (70% - 80%). Studies using PEMS which have focused upon the particulate emissions have been varied. These have focused upon examination of particle number distribution (Gouriou et al. 2004; Robinson and Holmén 2011; Huang et al.

2013), PM emission rates of HDDVs (Durbin et al. 2008; Zheng et al. 2014), and effects of bio-diesel (Tan et al. 2014). Robinson (2011) demonstrated significant effects of HEV re-starts upon particulate emissions, finding that average particle number concentrations (#/cc) of a 2010 Hybrid Toyota Camry were twice those of a conventional Camry for city driving conditions.

The use of disaggregate data from on-board instrumentation studies can be an important source for understanding emissions behavior of modern vehicles in greater spatial and temporal granularity. Studies have shown the importance of roadway design such as grade and curvature (Jackson and Aultman-Hall 2010; Boriboonsomsin and Barth 2009), the impact of driver behaviors (De Vlieger 1997; Ericsson 2001; Larsson et al. 2012) and other real-world driving considerations not replicated in laboratory testing. As LDVs become increasingly more sophisticated with greater reliance upon hybrid technologies, it is imperative to understand the transient operation in finer temporal scale with an aim to reduce high emissions associated with short duration events which cannot be discerned through aggregate methods.

Given the variability of HEV ICE operation, characterization of PN emission patterns from HEVs remains particularly challenging and has largely been confined to aggregate analysis. Furthermore, the high frequency of HEV RIEVs near intersections and under urban low speed conditions are of interest to further understanding of levels of pedestrian exposure to roadside particle concentrations, particularly in hot-spot locations. While aggregated emissions data from bag analysis and road side studies may be adequate for estimating pollution inventories of the on-road fleet at the local, regional, or national level, greater temporal and spatial resolution is desired with the evolution and increasing penetration of alternatively fueled vehicles. In this study, the use of the Total On-board Emissions Measurement System (TOTEMS) provides a disaggregate analysis of PN emissions for one 2010 Toyota Hybrid Camry under varying road features,

operating modes and traffic conditions. In this study, the data collected on tailpipe PN emissions under real-world driving conditions is unique because it compares emissions from a conventional vehicle to its HEV counterpart of identical make and model.

3.6 Vehicle Specific Power

Vehicle Specific Power (VSP) is a commonly accepted measurement of the instantaneous power required of a vehicle to overcome internal and external resistances of forward propulsion (Zhai et al. 2008). These resistance loads are categorized into four components, consisting of kinetic, potential, rolling resistance and aerodynamic resistance as seen in Figure 3 below. VSP is the sum of these four instantaneous resistive loads (in kW) normalized by mass (metric tons) to units of kilowatts per ton (kW/ton). VSP is largely dependent upon speed and acceleration. The concept of VSP was developed by Jimenez (1999) as a means to categorize vehicle operating parameters for different vehicle models during vehicle emissions measurement. This VSP parameter was later used by the EPA to standardize mobile source emissions estimation (Koupal et al. 2005).

In the basic derivation of the governing equation of VSP from Jimenez, the instantaneous power produced from the propulsive agents of the vehicle – for an HEV, the ICE and/or the EM while for a CV, solely the ICE – is equal to the four component forces shown in Figure 3. In the generalized Equation 3.3 below, instantaneous power from the propulsive forces (the ICE and/or the EM) are balanced by a) changes in the vehicle's potential energy (PE) and kinetic energy (KE) and b) resistive forces (aerodynamic drag and internal rolling resistance) multiplied by vehicle velocity of the vehicle.

$$VSP = \frac{\left(\frac{d}{dt}KE + \frac{d}{dt}PE\right) + (F_{RR} + F_{AD}) \times Vel}{m} \qquad \textit{Equation 3.3}$$

Where:

VSP = Vehicle specific power, kW/ton
KE = Kinetic energy, N·m
PE = Potential energy, N·m
F_{RR} = Rolling resistance force, N
F_{AD} = Aerodynamic drag force, N
Vel = Vehicle velocity, m/s
m = Vehicle mass, metric ton

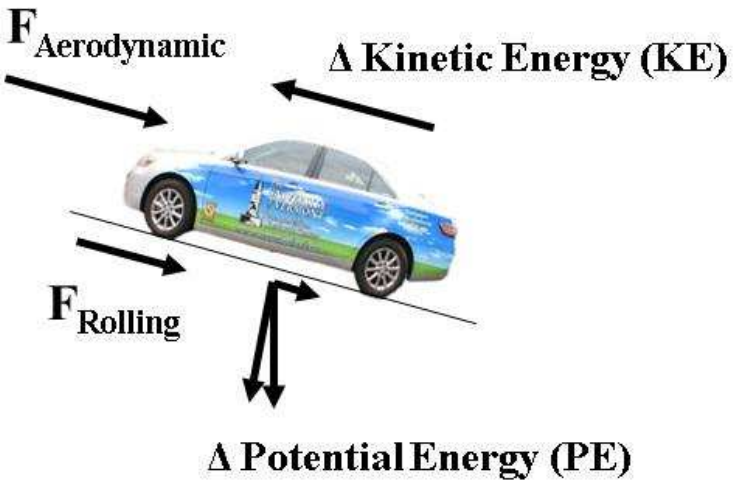

Figure 3. The basic forces acting on a vehicle in motion, adapted from Jimenez (1999).

3.7 ICE Operating Modes

The EPA has a developed a modelling framework called the Motor Vehicle Emissions Simulator (MOVES) which is used to estimate fleet emissions. This platform utilizes operating mode bins (OpModes) to categorize vehicle activity using a combination of ranges of vehicle specific power (VSP, kW/ton) and three tiers of vehicle speed (in mph) (Koupal et al. 2005). The binning method was achieved to optimize emissions and energy consumption modeling from wide

ranging vehicle data (Koupal et al. 2005). 0 shows the 23 bins for pollutant modeling purposes (EPA 2009).

While the operational mode methodology used by the EPA is useful for estimating and comparing pollutant emissions from a variety of vehicles, it is not ideally designed to incorporate hybrid vehicle modalities, with the contribution of electric assist and electric-only operation. Particularly, the division of MOVES OpModes into three speed categories does not take into consideration, or account for, the range of speeds for electric-only HEV operation in which emissions are effectively zero. While generalizations can be made to compare emissions and fuel consumption between HEV and CV vehicles at an aggregate scale, i.e. varying drive cycles, the modal operations require further refinement to allow for the differing demands placed upon the HEV ICE under varying road loads.

3.8 Road Typology

Many studies have shown that vehicle operation has significant impact upon vehicle emission and energy consumption. Road typology is commonly associated with different driving conditions, yet these are difficult to generalize due to differences in road geometry, road surface conditions, speed limits, congestion, vehicle composition, intersection control and individual driving styles. One traditional categorization of roadways classified by the U.S. Federal Highway Administration (FWHA) as seen in Figure 4 below assigns roads as Local, Collector or Arterial based upon levels of mobility and accessibility (Federal Highway Administration 2014).

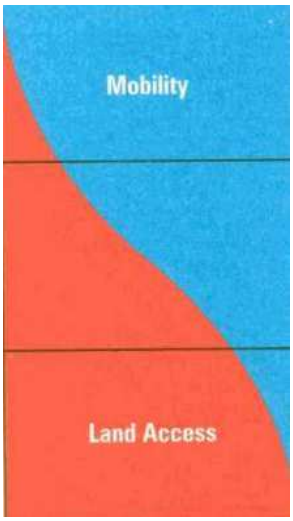

Arterials
High Mobility, Low Access

Collectors
Balance of Mobility and Access

Locals
Low Mobility, High Degree of Access

Figure 4. Classifications of Roadways: Collector, Local and Arterial. Source: FWHA, 2006.

This FHWA road classification is useful for travel demand modeling, but its utility for purposes of understanding differences in disaggregate vehicle operation are limited. Other simplified road categorization used by the EPA to compute CAFE fuel economy standards and emission factors for LDVs divides driving into 'city' and 'highway', defined by drive cycles which simulate typical vehicle operation along each road section. As a result of 2010 proposed Code of Federal Regulations (49 CFR Part 575), the EPA uses five drive cycles to compute the fuel economy of LDVs, two of which are shown in Figure 5 below – the 16.45 km Highway Fuel Economy Test Cycle (HWFET) and the 17.77 km Urban Dynomometer Driving Schedule (UDDS) otherwise known as Federal Test Procedure 75 (FTP-75) – as the basis for the fuel economy and emission factor derivations.

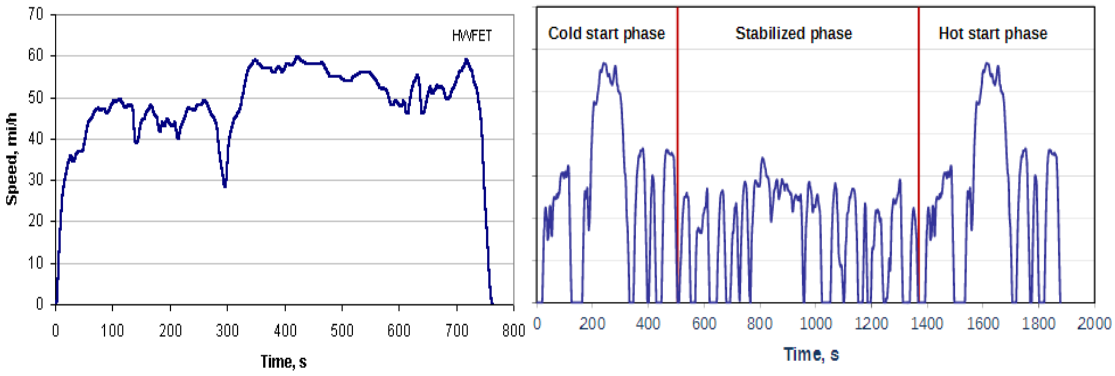

Figure 5. Highway Fuel Economy Test (HWFET, left) and Urban Dynomometer Driving Schedule (UDDS, right) drive cycles.

Numerous drive cycles such as those shown in Figure 5 above have been generated in the U.S., Europe and Asia to simulate different driving conditions and vehicle types for the purpose of comparing emissions and fuel consumption. Some authors have used simplified road classifications based upon speed and levels of congestion to urban, rural and highway or 'ring' road driving (De Vlieger 1997; Lenaers 1996). Generally, urban roadways are characterized by grid configurations with regular intersections and lower overall speed limits, with driving conditions consisting of frequent accelerations and decelerations, periods of idle (zero speed) and relatively little steady speed operation. Rural road ways can be characterized by frequent changes in horizontal and vertical road geometry, two-lane configuration, infrequent/sparse intersections and low traffic volume, resulting in overall higher speeds than urban driving and relatively little idle periods. Freeway roadways, falling within the arterial classification, have restricted access, four- or greater lane configuration and high speed limits (55 – 75 mph in most cases). While variation in approaches to categorizing road sections exist, classification based upon distinct mean operational parameters such as speed and road load are important to understand the effect of generalized driving conditions upon vehicle emissions and fuel consumption. For the purposes

of this investigation, the driving route used for emissions measurement has been categorized based upon the three generalized road classes described above- freeway, urban and rural.

4 Research Questions and Hypotheses

With the emergence and expansion of light-duty hybrid-electric vehicle models and their increasing penetration into the U.S. market, further understanding is necessary to shed light upon the re-ignition phenomena and the impact upon health and environment. Much focus has been placed upon the fuel savings presented by HEVs compared to conventional vehicles (CVs), but new evidence of differences in HEV emissions patterns as shown in the background sections above suggests further research is required. Specifically, examination of Particle Number (PN) emissions (in light of potentially more stringent regulation) in real-world sampling conditions with on-board portable instrumentation is useful to inform the emissions modelling community of the new advanced technologies found in gasoline HEVs. Consequently, the following research questions and hypotheses are presented here to address gaps in the literature.

1. **How do VSP and road section affect HEV ICE Operational Mode Distribution? What effect does vehicle speed have upon RIEV frequency?**

   Research shows that vehicle operational parameters for conventional vehicles affect vehicle emissions. HEV technology significantly alters the patterns of ICE operation compared with that of the conventional ICEs, with frequent shutdown, off and re-ignition events. With this new technology, the characterization of re-ignition events is important to understanding the unique PN emission patterns of the HEV. Using a new ICE OpMode framework, it is hypothesized that operational distribution of four HEV ICE OpModes – shutdown, off, re-ignition, stabilized on – will be significantly different between four road categories. It also hypothesized that overall, mean VSP for each HEV ICE OpMode

will vary significantly. Additionally, a mathematical model to predict RIEV temporal frequency and spatial density based upon mean vehicle speed operation will be developed. The utility of such a model will generate future predictions of PN inventory from HEV fleets.

2. **What are the quantified PN emission rates (PNER) attributable to re-ignition Events (RIEVs) compared to stabilized HEV operation?**

   Considering the evidence that re-ignition events occurring following ICE-off operation in HEVs are unique phenomena not replicated in conventional vehicles, it is expected that these RIEVs have unique emission patterns as well. High Emission Events (HEEs) have been associated with frequent HEV on-off cycling. Here, it is hypothesized that mean PN emission rates (PNER) immediately following a RIEV will be significantly greater than mean emission rates under hot stabilized operation. To explore this quantification, a new HEV operational framework is developed to distinguish between the different modes of the HEV ICE, and the duration of the RIEV is associated with observable cyclical fuel enrichment patterns.

3. **What measurable on-board factors impact the *magnitude* of PN emission rates occurring during RIEVs?**

   Past evidence has shown that PN is impacted by ambient air conditions, engine load, catalyst temperature and stoichiometric conditions. During HEV re-ignition events, high magnitude PN emission events are known to occur, but little is known of the causes of variation in RIEV PN emission rates. In quantifying the mean RIEV PNER, different parameters that immediately precede each event are examined, including ambient air

temperature and humidity, tailpipe temperature, VSP, speed, acceleration and period of ICE-off leading up to the RIEV. Though ambient air temperature has been shown to impact hybrid ICE-off activity, it is hypothesized that its effect upon RIEV PNER will not be statistically significant. Increased values of VSP and acceleration prior to RIEVs are hypothesized to result in significantly increased RIEV PNER, while increased values of prior ICE-Off period are hypothesized to result in significant decreases in RIEV PNER.

4. **Are the energy saving benefits of HEVs compared to CVs similarly reflected in the PN emission rates under different road sections?**

   The evolution of hybrid gasoline electric vehicle technology has largely been for the purpose of increasing fuel economy by reducing overall on-board gasoline consumption compared with conventional vehicles. While the gains in HEV fuel efficiency compared to CVs are well documented, less is known about the benefits of hybrid technology in terms of particulate emission reductions. It is hypothesized that significant differences exist between an HEV and comparable CV in overall PN emission rates (PNER) for four different road sections, with PNER of the HEV predicted to exceed those of the CV in urban driving while no significant differences in PNER are predicted between vehicles for the rural and highway driving.

5 Methodology

5.1 Data Collection

5.1.1 Vehicle Description

Two vehicles were used in the development of the particle number emissions data set using the TOTEMS: a 2010 Toyota Camry XLE and a 2010 Toyota Camry Hybrid. The choice of the Camry model was based upon their physical similarity (described in more detail below) and the popularity of the Toyota Hybrid Synergy® Drive (HSD). The selection of the Toyota Camry for this study allowed for the best comparison between a CV and its HEV equivalent available in the U.S. passenger vehicle market due to their essentially identical chassis, emissions control system, and climate control, as pictured in Figure 6. The patented HSD® powertrain, in addition to being equipped on all Toyota family HEVs, is currently licensed to Nissan (Altima Hybrid) and more recently, Mazda (Car Mart 2014). HSD®-powered vehicles represented over 71% of all hybrid models on U.S. roads in 2011 (U.S. DOE 2014). A summary of the two vehicle specifications is shown in Table 2.

The significant differences between the vehicles lie in the transmission systems, with the HEV equipped with two electric motor/generators and operated on a continuously variable gear ratio, while the CV operates with a 6-speed automatic transmission. Other slight differences, however, exist between the two vehicles, most notably the overall curb weight, with the HEV being approximately 10% heavier than the CV (3680 lb v 3373 lb), attributable to the additional BES. Other differences include the emissions rating (Ultra Low Emitting for the CV vs. Advanced Technology-Partial Zero Emission for the HEV), the slight difference in drag coefficient (HEV = 0.27 and CV = 0.28) and the addition of the regenerative braking system on the HEV.

Table 2. Specifications of the 2010 Toyota Camry.

Specification	Conventional	Hybrid
Make/Model	Toyota Camry	Toyota Camry
Trim	XLE	Hybrid
Year	2010	2010
Engine	2.5-Liter 4-Cylinder	2.4-Liter 4-Cylinder
Transmission	6-speed Automatic	Continuously Variable
Horsepower (hp@rpm)	169 @ 6000	187 @ 6000
Torque (lb-ft@rpm)	167 @ 4100	138 @ 4400
Electric Motor		Permanent Magnet AC Synchronous Motor
Batteries		Sealed Nickel-Metal Hydride (Ni-MH) 40 hp 244.8V
Fuel Economy Combined (MPG)	26	34
City (MPG)	22	33
Highway (MPG)	32	34
Fuel Capacity (gal.)	18.5	17.2
Emission Rating	ULEV II	AT-PZEV
Brakes	Power-assisted ventilated front/solid rear discs	Power-assisted ventilated front/solid rear discs with integrated regenerative braking
Tires	All-Season P215/60R16	All-Season P215/60R16
Coefficient of Drag	0.28	0.27
Weight (lbs)	3373	3680
Climate Control	Dual zone CFC-free	Dual zone CFC-free

Source: Toyota, 2010.

Figure 6. Conventional (l) and Hybrid (r) 2010 Toyota Camrys.

The two vehicles were also equipped with different internal combustion engines. The HEV was equipped with a 147-horsepower, 2.4 liter gasoline powered ICE, assisted with a 105 kW electric motor. The CV was powered by a 169-horsepower, 2.5 liter gasoline ICE. Both ICEs operated with four cylinders, with the HEV ICE operating under the Atkinson cycle and the CV ICE operating under the Otto cycle (Muta et al. 2004). While both vehicles were initially acquired simultaneously new, they were operated for a break-in period before sampling regimes were begun. During sampling, mileage readings for both vehicles ranged between 3000 and 8000 miles. Each vehicle operated identical TWCs, with electrically heated oxygen (O_2) sensors to maintain thermal stability of the sensors (Toyota 2010a). According to Toyota, during cold starts electric heating of the oxygen sensors is run at 100% duty cycle, between 0% to 100% duty cycle during normal driving and 50% duty cycle during idling (Toyota 2010b).

5.1.2 TOTEMS Instrumentation

The Total On-board Tailpipe Emissions Measurement System (TOTEMS; see Holmén et al. 2009 and Holmén et al. 2014) in total consisted of 30 on-board instruments collecting real-time data in order to quantify gas-phase and particle number concentrations, exhaust flow and temperature, ambient and cabin temperature and humidity, vehicle operating parameters, geo-spatial locations and dashboard driving video at one hertz resolution. This PEMS system was entirely self-contained and completely powered by two on-board 12-volt Lifeline GPL-8DA absorbent glass mat lead-acid batteries, with 255 Amp-hour ratings. The DC voltage was converted to AC for use by the emissions equipment using a Vector 2500-watt power inverter, with an automatic transfer switch (GoPower) used to provide continuous electrical supply when transferring to and from grid power. Much of the work undertaken to design and test this system was completed earlier and documented in the 2010 Holmén et al. (2009) report to the UVM TRC. A complete list of the

TOTEMS instrument suite can be found in Table B1 of Appendix B see Holmén et al. 2014). For this thesis only particle number emissions were analyzed.

5.1.2.1 Exhaust Flow Measurement

One key element in quantification of emission rates is the measurement of tailpipe exhaust flowrate. The TOTEMS utilized a specially modified tailpipe adapter, seen in Figure 7 below, designed to fit both Camrys snuggly and allow for collection of a continuous exhaust sample as well as exhaust pressure and ambient air pressure. This adapter consisted of four ports for (1) a pitot tube attached to four differential pressure transducers, (2) a static pressure sensor line, (3) a thermocouple, and (d) an exhaust sampling probe. The thermocouple was used to measure the exhaust temperature (°C) while the four differential pressure transducers measured pressure differential across different ranges of sensitivity to exhaust flow. The voltages from these four transducers were later used to compute the second-by-second exhaust flowrate (see Section 5.3.1), while the static pressure sensor established the ambient air pressure to assure that sampling was conducted under normal atmospheric conditions. The exhaust sample was drawn into the vehicle through a heated line. Following each transfer of equipment between vehicles, the pitot tube, sensitive to minor adjustments, was calibrated to ensure consistent sampling. Details and further description of the Pitot tube operation and calibration are found in Holmén et al. (2014).

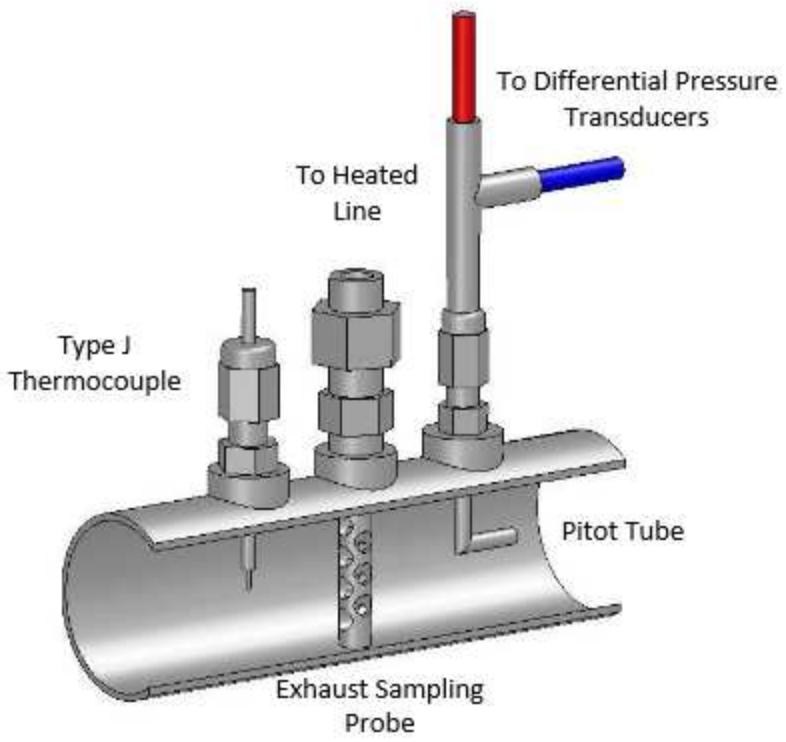

Figure 7. TOTEMS Specially Modified Tailpipe Adapter. Source: Holmén et al., 2014.

5.1.2.2 Particle Concentration Measurement Instruments

The TOTEMS instrument suite consisted of two particle measurement equipment: a TSI, Inc. Engine Exhaust Particle Sizer (EEPS) Model 3090 and a TSI, Inc. Ultrafine Condensation Particle Counter (UCPC) Model 3025A, both sampling at a rate of 1 Hz. The two particle instruments were used in tandem due to the complementary advantages and disadvantages of each. The EEPS counted particle number concentration distributions with ± 20% accuracy and sized particle diameter with ± 10% accuracy ranging from 5.6 to 562 nanometers in diameter. The EEPS detects and counts particles in 32 different diameter ranges, while the UCPC only counts total particles with diameter sizes 3nm to 3000nm. In the EEPS, particles greater than 562 nm were filtered out of the exhaust sample using a 1-micrometer cut cyclone attached to the inlet of

the EEPS. The advantage of the EEPS was its capability of measuring very high particle concentrations in excess of 1.0 x 10^7 particles per cubic centimeter (#/cc), while the UCPC was limited by an upper detection limit of 9.9 x 10^5 #/cc, thus making the EEPS ideal for measuring vehicular tailpipe exhaust emissions. The EEPS had lower accuracy at lower particle number concentration rates and had minimum detection limits for each diameter size due to electrometer noise, whereas the UCPC has no minimum detection limits and has a detection accuracy of 90% for all particles with diameters greater than 5 nm. The EEPS was much more susceptible to road vibrations and was mounted and secured to a platform containing 10 silicone gel mounts, effectively reducing electrometer noise during sampling an average of 64% (Holmén et al. 2014). These two particle detection instruments were found to track well during TOTEMS sampling (Robinson 2011).

The EEPS operates in principle on the theory of electrical mobility by separating particles in a disperse aerosol, whereby particles were first positively charged to both strip excessively negative charges on the particles and to minimize potential overcharging during the subsequent passage through negative charged electron cloud (TSI, Inc. 2010). Following the positive/negative charge regime, the particles entered an electrometer column containing 24 electrometer rings, 22 of which count particles and the top two which act as spacers. In the central column, a rod containing a reverse differential mobility analyzer (DMA) actively deflected the particles towards the 22 detecting rings. These 22 rings measured the discharged current from each of the 32 different particle diameter channels. While each channel is represented by the midpoint of the particle diameter range, a total count for all particles was derived by adding the count from all 32 particle channels. A description of the particle size ranges of each channel is shown in Table B2 of Appendix B .

Collection of all particle measurement data as well as other parameters was achieved using a Dell Optiplex GX620 using a Pentium D CPU. UCPC data was recorded using TSI AIM version 5.2.0 software, while the EEPS measurements were recorded using TSI EEPS version 3.1.0 software.

5.1.2.3 On-board Exhaust Collection and Sampling

As the exhaust sample was continuously drawn into the vehicle through the heated line (set at 191 °C to prevent water condensation), the raw tailpipe gas was divided into two streams, one to the gas-phase instrumentation and one to the particle detection instrumentation. Due to the high magnitude of particle concentrations found in tailpipe exhaust, dilution of the sample was required before analysis. This was achieved in a two-stage dilution system using a Rotating Disk Mini-Diluter (Matter Engineering MD19-2E) and an Air Supply Evaporation Tube (ASET 15-1). Though the MD-19 was capable of sampling dilution levels required for tailpipe exhaust analysis, it was limited by its output flow rate to 5 lpm, whereas the EEPS and UCPC required inputs of 10 lpm and 1.5 lpm respectively. Due to the output limitation of the MD-19, the ASET was coupled in line to provide greater flowrate output capable of supplying both particle instruments with a total of 11.5 lpm of diluted exhaust.

One lpm of sample exhaust was first drawn into the MD-19, and then using a 10-cavity disc , a heated portion of dilution air (80 °C to reduce condensation) was introduced into the sample for an initial exhaust dilution ratio of 15.23. In the second stage, 1.5 lpm of first stage diluted exhaust was drawn through an evaporation cell set to 50 °C to minimize the effect of different particle types reacting to the temperature gradient within the instrumentation. This second stage achieved a dilution ratio of 7.1, and the total dilution ratio of raw exhaust to dilution air was computed as 1:108 (the product of 7.1 and 15.23). Further description of the TOTEMS dilution system is found in Holmén et al. (2014).

5.1.3 Data Collection Phases

The vehicles were stored in an unheated laboratory in Perkins Hall on the University of Vermont campus when not in use. During each sampling event or run, a set of standard operating procedures were followed in phases to collect quality assurance data. To establish proper operation of on-board equipment prior to and following driving data collection, 10-minute *instrument blanks* and *tunnel blanks* were collected to determine background measurements of the instrumentation and to assess potential equipment malfunction. There were five driving phases during which the vehicle was in mobile operation, known as the W*arm-Up (3), Outbound (4), Park-and-Ride (5), Inbound (6)* and *Post-Route (7) Phases*. Together with the pre- and post-tunnel blank and instrument blanks, a total of nine phases were conducted during each run, shown in Table 3 below. Typically, the total duration for all nine phases was between four and six hours.

Table 3. TOTEMS Sampling Phases.

Phase Number	Phase Identification	Description
1	Pre-Run Instrument Blank	Pre-sampling emissions instrumentation zero
2	Pre-Run Tunnel Blank	Pre-sampling ambient background measurement with vehicle off
3	Warm-Up Driving	Journey to gas station and engine warm-up
4	Outbound Phase	Stabilized data collection: Burlington city loop to Richmond via I-89
5	Park-and-Ride	Idle at Richmond Park-and-Ride for at least one minute
6	Inbound Phase	Stabilized data collection: Richmond to Burlington via state and local roads
7	Post Route Travel	Votey Hall to gas station and back
8	Post-Run Tunnel Blank	Post-sampling ambient background measurement with vehicle off
9	Post-Run Instrument Blank	Post-sampling emissions instrumentation zero

The pre-instrument blanks were used to compute Instrument Detection Limits (IDLs) for the EEPS, which is explored further in the Section 5.3.3.1. The *Warm-Up phase* (2.5 mi /4km), beginning at Perkins Hall parking lot, allowed for operation of both vehicles sufficient to raise the temperature of the engine coolant to within normal range (80°C - 90°C), to top off the fuel tank and to assess any possible instrument issues before driving data collection. All TOTEMS on-board data collection was initiated during this phase. The *Outbound phase* (17mi /27 km) consisted of city driving within Downtown Burlington, VT and freeway driving southbound

along Interstate I-89 from Exit 14 to Exit 11. The *Park-and-Ride phase* was a short equipment operation check with the vehicle in park at the Williston Park-and-Ride parking lot. The *Inbound phase* (14mi /23 km) consisted of rural driving through Richmond and Williston and urban driving returning to Burlington and terminating at Votey Hall. The *Post-Route* phase allowed for stoppage of data recording systems and top-off of fuel before returning to Perkins Hall. A map of the route is seen in Figure 8.

During all sampling runs, the vehicle climate control was set to 70 °F to control for effects of auxiliary power demand from heating and cooling loads. For the purposes of particle emissions analysis in this work, only data collected during the *Outbound* and *Inbound* (sampling) phases was used. Total sampling time for these two phases was between 70 and 90 minutes for all runs.

5.1.4 Vehicle Operating Parameters from the Electronic Control Unit

Vehicle operating parameters (Table 4) were recorded using Toyota Techstream software (version 6.01.021) through a Mongoose scantool device (Drew Technologies). The scantool device was connected to the vehicle electric control unit (ECU) via the OBD-II port under the steering column, with data recorded to the Dell Optiplex CPU. A series of engine and vehicle operational parameters were collected at 3 Hz or greater for the entire duration of Outbound and Inbound phases. Typical parameters useful in explaining the vehicle operation and tailpipe emissions were collected where available for each vehicle and are in non-italicized in Table 4 below. These include engine speed (RPM), vehicle speed (kph), calculated engine load (% of maximum), engine coolant temperature (°C), ambient temperature (°C), and sample time.

Due to differences in the transmission of each vehicle, certain parameters were unavailable for collection in both vehicles. While *mass air flow, fuel injection volume, catalyst temperature* and *air-to-fuel ratio* parameters were collected in the CV, these were not simultaneously available in

the HEV when collecting parameters related to the hybrid BES operation. Conversely, unique HEV parameters collected are shown as italicized in Table 4 such as *electric motor* and *generator torque* and *speed, regenerative brake torque,* and *battery state-of-charge (SOC).*

Table 4. Conventional and Hybrid Operation Parameters from Scantool (Source: Sentoff, 2013)

Conventional Vehicle		Hybrid Vehicle	
Parameter	**Unit**	**Parameter**	**Unit**
Sample Time	MM:SS.mmm	Sample Time	MM:SS.mmm
Vehicle Speed	km/h	Vehicle Speed	km/h
Engine Speed	rpm	Engine Revolutions	rpm
Calculated Load	%	Calculated Load	%
Coolant Temperature	°C	Engine Coolant Temperature	°C
Ambient Temperature	°C	Ambient Temperature	°C
Run Distance	km	Run Distance	km
Mass Air Flow	gm/s	*Motor Revolution*	rpm
Fuel Injection Volume	ml	*Motor Torque*	Nm
Air to Fuel Ratio Lambda	Dimensionless	*Generator Revolutions*	rpm
Catalyst Temperature Sensor 1	°C	*Generator Torque*	Nm
Catalyst Temperature Sensor 2	°C	*Regenerative Brake Torque*	Nm
		State of Charge (All Batteries)	%
		Acceleration Sensor	%
		Maximum Chargeable Power to HV Battery	W
		Maximum Chargeable Power Out of HV Battery	W

5.1.5 Route Description

As discussed earlier, the sampling phases – Outbound and Inbound – consisted of mixed driving through urban, rural and freeway facilities. This closed 50-km loop route, shown in Figure 8 below, was designed to provide a range of driving conditions of a reasonable duration within the limits of the independent power source and reasonable instrument sampling durations. To ensure that the exact route was followed for each run, specific driving instructions were followed, beginning and ending at the Votey Hall parking lot entrance, via a complete set of turn directions, a copy of which is shown in Table A1 of Appendix A.

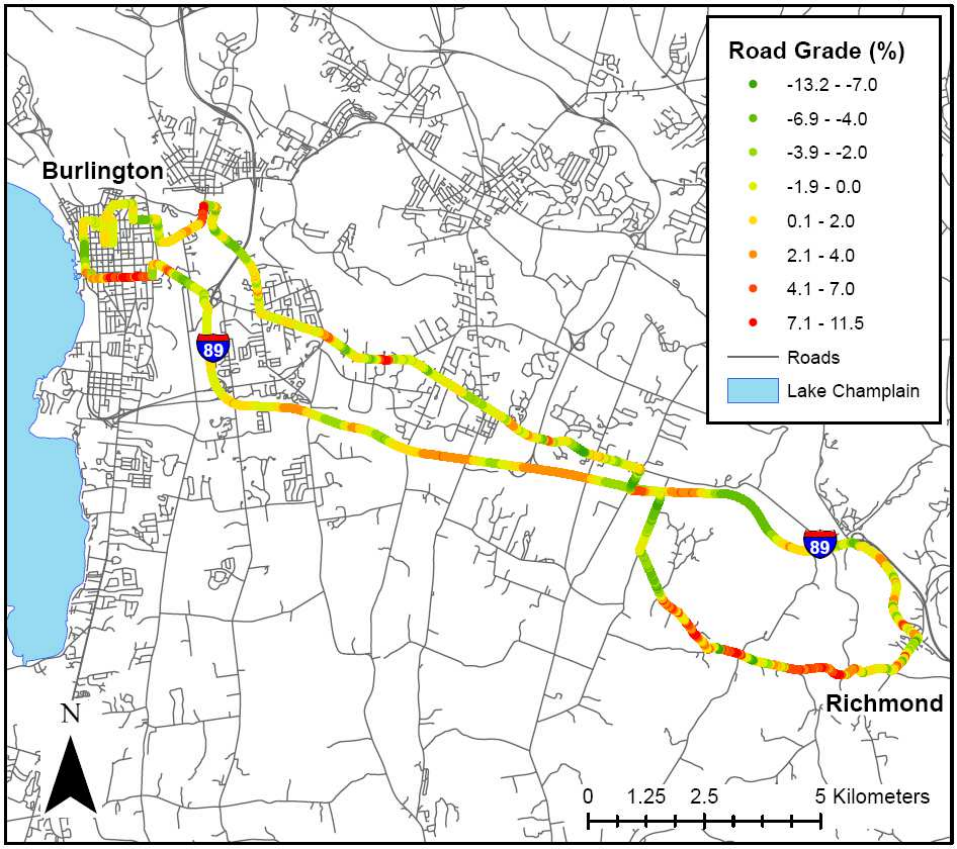

Figure 8. TOTEMS driving route with road grade. (Source: Holmén et al, 2014)

A single driver (Graduate Research Assistant Karen Sentoff) was used in all sampling runs as an intentional study design in an attempt to create similar driver behavior across the varying road conditions for each run. The driver observed the posted speed limit during all sampling periods.

5.1.5.1 Road Sections

To facilitate analysis of emissions and vehicle operation, the sampling phases were categorized by road sections. This categorization was achieved by dividing the route by continuous sections based upon changes in speed limit and frequency of intersection control. The Outbound phase was thus divided into two sections, Urban (I) and Freeway, while the Inbound phase was divided into a Rural and second Urban (II) section. The typical vehicle speed profile for each road section is shown for a typical run in Figure 9 below.

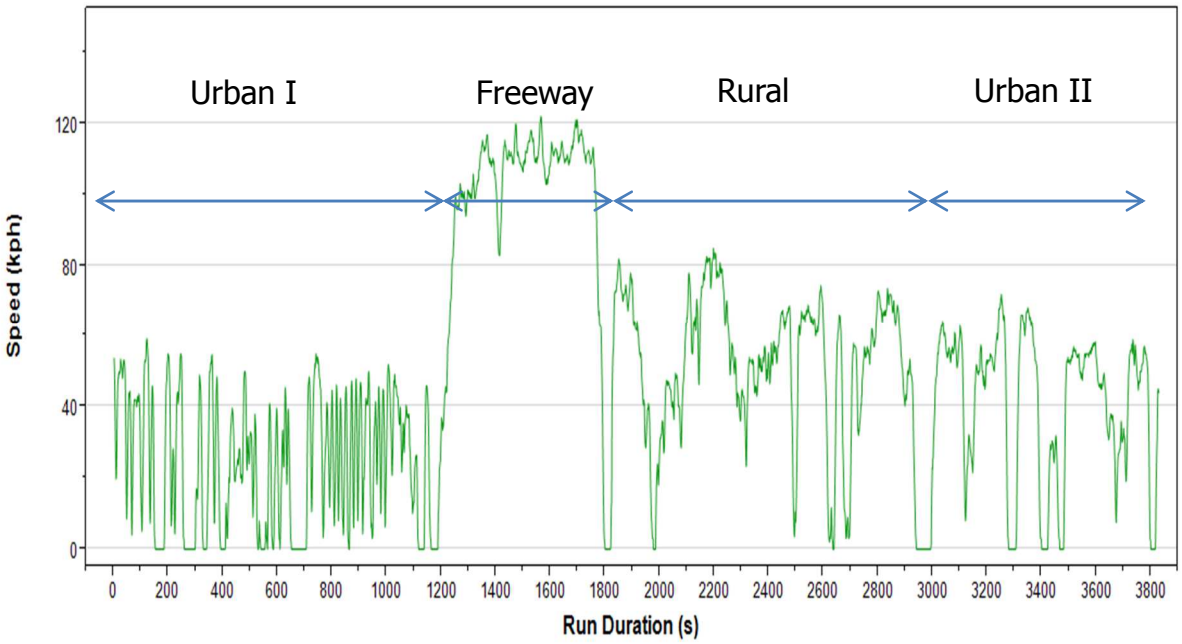

Figure 9. Sample speed profile for each road section along an entire run.

5.1.6 Ambient Conditions and Vehicle Position

In addition to the internal temperature measurement from the scantool device, temperature (°C) and relative humidity (%) recordings were made independently inside and outside the vehicle cabin. This was achieved through two HOBOware pro loggers (v2 U23-001), mounted in the rear seat and to the cabin roof via a magnetic mount. This data was recorded at 1 Hz through the use of Labview software and stored on the Dell Optiplex CPU.

In order to facilitate spatial analysis of vehicle operation and to identify road network characteristics of the sampling data, vehicle location along the route was collected at 1 Hz. This was achieved using two GPS devices in tandem: a Garmin Model GPS16-HVS and a Geologger V4.8. The Garmin data was recorded directly to the Dell in real time using Fugawi software, while the Geologger data was later downloaded following the completion of each run. Each

vehicle collected two-dimensional Cartesian coordinates as well as the speed of the vehicle each second.

The assignment of a single spatial location to each 1Hz temporal data point involved a quality control process. First, using ArcGIS 10.0 a 25-m buffer was created around the spline fit representation of the driving route (see Section Road Grade Measurement below), and all GPS data points from both the Geologger and the Garmin which fell outside within this buffer were filtered out. Excluded from spatial assignment (and thus analysis) were data from unanticipated construction detours, run abandonment and from non-sampling phases. A single, best fit Cartesian longitude and latitude was assigned to each temporal data point depending upon the presence of GPS measured locations. If both GPS instrument measurements were present, then an average of both locations was used, and if only one GPS instrument measurement was available then it was used solely. If both GPS instrument measurements were missing, then a scantool speed-based interpolation of position was estimated for a period of up to 15 seconds. All temporal data with GPS instruments measurement missing for a period of greater than 15 seconds were not assigned Cartesian locations. 95% of the entire sampling phase data set (287,698 s) was assigned a spatial location with only 5% location loss to GPS instrument failure.

5.1.7 Road Grade Measurement and Road Chainage

A critical component of the road network was the measurement of road grade at each vehicle location along the sampling route. This was achieved in three steps. First, road grade measurements (%) were collected along the entire route using the Vermont Department of Transportation's Automatic Road Analysis Network (ARAN) at spatial resolution between 2.2 and 3.3 meters and grade resolution of 0.1%. Secondly, to facilitate the joining of grade to each data point collected during on-board sampling, the entire path driven by the ARAN vehicle was discretized to a spline-fit polyline of 1-m point resolution (approximately 50,771 points covering

the Inbound and Outbound travelled route) with Cartesian latitude and longitude coordinates, generated by Resource System Group Inc. (RSG). Lastly, a discrete road grade value from the 1-m database was spatially joined to each of the temporal TOTEMS 1-s data using ArcGIS 10.0 software 'Near' tool.

In addition to Cartesian location and grade data, a sampling distance parameter was computed for each temporal datum. This parameter, *Chainage*, was computed as the cumulative distance driven from the start of the sampling route (along Colchester Avenue at the entrance Votey Hall). *Chainage* was measured as the one-meter spatial identifier of the RSG generated spline-fit poly line, with a minimum of 0 m and a maximum of 50,771 m (at the termination of the sampling route, again along Colchester Avenue at Votey Hall entrance).

5.2 Data Quality Control

A total of 75 runs were conducted between February 2010 and August 2011 (43 HEV and 32 CV), consisting of 287,698 data records for the sampling run phases (Outbound / Inbound). Attempts were made to conduct sampling at varying times of day to represent varying levels of traffic congestion travel patterns during daylight hours, with sampling time of day ranging from 8:00 AM to 8:00 PM. As a safety precaution to protect against possible accidental instrument damage and researcher injury, TOTEMS data collection runs were only conducted during dry road conditions and during daylight hours.

5.2.1 Data Exclusion

Despite the quality assurance measures, several runs were affected by instrument failure or malfunction, causing loss of data or compromise of data fidelity. For this analysis, four instruments were essential – the EEPS, the dilution system, the GPS units and the scantool device. To assure quality of data against instrument failure and operator error, a subset of the runs and sections were removed from analysis based upon the following criteria. For the EEPS, any run in which the Instrument Detection Limits (IDLs, see Section 5.3.3.1) for total particle concentration exceeded 5000 #/cc was excluded (runs 22 and 70; see Table B3 of Appendix B). Additionally, due to a malfunction in the peristaltic pump of the dilution system, runs 37 through 45 were excluded. Lastly, all road sections with greater than 5% missing data for either the GPS units or the scantool were excluded. Of the 300 road section sample runs (75 runs x 4 road sections), 77 sections were excluded from analysis. A total of 76,133 s (26% of all data) were excluded from analysis. A summary of the total number of records selected for analysis is included in Table 5, and complete list of the run sections included and excluded from analysis is shown in Table 6 and Table 7.

Table 5. Summary of Data Analyzed for each Vehicle and Road Section.

	Freeway		Rural		Urban I		Urban II	
	Records (s)	No. Runs	Records (s)	No. Runs	Records (s)	No. Runs	Records (s)	No. Runs
CV	16024	27	28560	26	32287	26	22879	26
HEV	18623	31	32741	30	35883	29	24565	28

Table 6. Summary of Data Selected for Analysis

		Freeway			Rural			Urban I			Urban II		
RUN	Vehicle	EEPS	Scantool	Location	EEPS	Scantool	Location	EEPS	Scantool	Location	EEPS	Scantool	Location
5	CV	✓	✓	✓	✓	✓	✓	✓	✓	✓	✓	✓	✓
6	CV	✓	✓	X	✓	✓	X	✓	✓	X	✓	✓	X
7	CV	✓	✓	✓	✓	✓	✓	✓	✓	✓	✓	✓	✓
8	CV	✓	✓	✓	✓	✓	✓	✓	✓	✓	✓	✓	✓
9	CV	✓	✓	✓	✓	✓	✓	✓	✓	✓	✓	✓	✓
10	CV	✓	✓	✓	✓	✓	✓	✓	✓	✓	✓	✓	✓
11	CV	✓	✓	✓	✓	✓	✓	✓	✓	✓	✓	✓	✓
12	CV	✓	✓	✓	✓	✓	✓	✓	✓	✓	✓	✓	✓
13	HEV	✓	✓	✓	✓	✓	✓	X	✓	✓	✓	✓	✓
14	HEV	✓	✓	✓	✓	✓	✓	✓	✓	✓	✓	✓	✓
15	HEV	✓	✓	✓	✓	✓	✓	✓	✓	✓	✓	✓	✓
16	HEV	✓	✓	✓	✓	✓	✓	✓	✓	✓	✓	✓	✓
17	HEV	✓	✓	✓	✓	✓	✓	✓	✓	✓	✓	✓	✓
18	HEV	✓	✓	✓	✓	✓	✓	✓	✓	✓	✓	✓	✓
19	HEV	✓	✓	✓	✓	✓	✓	✓	✓	✓	✓	✓	✓
20	HEV	✓	✓	✓	✓	✓	✓	✓	✓	✓	✓	✓	X
21	HEV	✓	✓	✓	✓	✓	✓	✓	✓	✓	✓	✓	✓
22	HEV	X	✓	X	X	✓	X	X	✓	X	X	✓	X
23	HEV	✓	✓	✓	✓	✓	✓	✓	✓	✓	✓	✓	✓
24	HEV	✓	✓	X	✓	✓	X	✓	✓	X	✓	✓	X
25	HEV	✓	✓	✓	✓	✓	✓	✓	✓	✓	✓	✓	✓
26	HEV	✓	✓	✓	✓	✓	✓	✓	✓	✓	✓	✓	✓
27	HEV	✓	✓	✓	✓	✓	✓	✓	✓	✓	✓	✓	✓
28	HEV	✓	✓	✓	✓	✓	✓	✓	✓	X	✓	✓	✓
29	HEV	✓	✓	✓	✓	✓	✓	✓	✓	✓	✓	✓	✓
30	HEV	✓	✓	✓	✓	✓	✓	✓	✓	✓	✓	✓	✓
31	CV	✓	✓	✓	✓	✓	✓	✓	✓	✓	✓	✓	✓
32	CV	✓	✓	✓	✓	✓	✓	✓	✓	✓	✓	✓	✓
33	CV	✓	✓	✓	✓	✓	✓	✓	✓	✓	✓	✓	✓
34	CV	✓	✓	✓	✓	✓	✓	✓	✓	✓	✓	✓	✓
35	CV	✓	✓	✓	✓	✓	✓	✓	✓	✓	✓	✓	✓
36	CV	✓	✓	✓	✓	✓	✓	✓	✓	✓	✓	✓	✓
37	CV	X	✓	✓	X	✓	✓	X	✓	✓	X	✓	✓
38	CV	X	✓	✓	X	✓	✓	X	✓	✓	X	✓	✓
39	CV	X	✓	✓	X	✓	✓	X	✓	✓	X	✓	✓
40	CV	X	✓	✓	X	✓	✓	X	✓	✓	X	✓	✓

Note :A check mark for each box indicates the data from the instrument was suitable for analysis, while a 'X' with red shading indicates data from the instrument was missing or erroneous. Any run road section which included one or more 'X' was excluded from analysis.

Table 7. Summary of Data Selected for Analysis (continued).

		Freeway			Rural			Urban I			Urban II		
RUN	Vehicle	EEPS	Scantool	Location	EEPS	Scantool	Location	EEPS	Scantool	Location	EEPS	Scantool	Location
41	HEV	X	✓	✓	X	✓	X	X	✓	✓	X	✓	✓
42	HEV	X	✓	✓	X	✓	✓	X	✓	✓	X	✓	✓
43	HEV	X	✓	✓	X	✓	✓	X	✓	✓	X	✓	✓
44	HEV	X	✓	✓	X	✓	✓	X	✓	✓	X	✓	✓
45	HEV	X	✓	✓	X	✓	✓	X	X	✓	X	✓	✓
46	HEV	✓	✓	✓	✓	✓	✓	✓	✓	✓	✓	✓	✓
47	HEV	✓	✓	✓	✓	✓	✓	✓	✓	✓	✓	✓	✓
48	HEV	✓	✓	✓	✓	X	X	✓	✓	✓	✓	X	✓
49	HEV	✓	✓	✓	✓	X	✓	✓	✓	✓	✓	X	X
50	HEV	✓	X	X	✓	X	X	✓	X	X	✓	✓	X
51	HEV	✓	✓	✓	✓	✓	✓	✓	✓	✓	✓	X	✓
52	HEV	✓	✓	X	✓	✓	X	✓	✓	X	✓	✓	X
53	HEV	✓	✓	✓	✓	✓	✓	✓	✓	✓	✓	✓	✓
54	CV	✓	✓	✓	✓	X	✓	✓	✓	✓	✓	X	✓
55	CV	✓	✓	✓	✓	✓	✓	✓	✓	✓	✓	✓	✓
56	CV	✓	✓	✓	✓	✓	✓	✓	✓	✓	✓	✓	✓
57	CV	✓	✓	✓	✓	✓	✓	✓	✓	✓	✓	✓	✓
58	CV	✓	✓	✓	✓	✓	✓	✓	✓	✓	✓	✓	✓
59	CV	✓	✓	✓	✓	✓	✓	✓	✓	✓	✓	✓	✓
60	CV	✓	✓	✓	✓	✓	✓	✓	✓	✓	✓	✓	✓
61	CV	✓	✓	✓	✓	✓	✓	✓	✓	✓	✓	✓	✓
62	CV	✓	✓	✓	✓	✓	✓	✓	✓	✓	✓	✓	✓
63	CV	✓	✓	✓	✓	✓	✓	✓	X	✓	✓	✓	✓
64	CV	✓	✓	✓	✓	✓	✓	✓	✓	✓	✓	✓	✓
65	CV	✓	✓	✓	✓	✓	✓	✓	✓	✓	✓	✓	✓
66	CV	✓	✓	✓	✓	✓	✓	✓	✓	✓	✓	✓	✓
67	CV	✓	✓	✓	✓	✓	✓	✓	✓	✓	✓	✓	✓
68	HEV	✓	✓	✓	✓	✓	✓	✓	✓	✓	✓	✓	✓
69	HEV	✓	✓	✓	✓	✓	✓	✓	✓	✓	✓	✓	✓
70	HEV	X	✓	✓	X	✓	✓	X	✓	✓	X	✓	✓
71	HEV	✓	✓	✓	✓	✓	✓	✓	✓	✓	✓	✓	✓
72	HEV	✓	✓	✓	✓	✓	✓	✓	✓	✓	✓	✓	✓
73	HEV	✓	✓	✓	✓	✓	✓	✓	✓	✓	✓	✓	✓
74	HEV	✓	✓	✓	✓	✓	X	✓	✓	✓	✓	✓	X
75	HEV	✓	X	✓	✓	✓	✓	✓	X	✓	✓	✓	✓
76	HEV	✓	✓	✓	✓	✓	✓	✓	✓	✓	✓	✓	✓
77	HEV	✓	✓	✓	✓	✓	✓	✓	✓	✓	✓	✓	✓
78	HEV	✓	✓	✓	✓	✓	✓	✓	✓	✓	✓	✓	✓
79	HEV	✓	✓	X	✓	✓	✓	✓	✓	X	✓	✓	✓

Note :A check mark for each box indicates the data from the instrument was suitable for analysis, while a 'X' with red shading indicates data from the instrument was missing or erroneous. Any run road section which included one or more 'X' was excluded from analysis.

5.2.2 Temporal Alignment

Temporal alignment between the EEPS, pitot tube differential pressure sensors, scantool and GPS data streams was necessary for each run to create an aggregated second-by-second data set. A temporal lag is defined as the difference in time (s) between associated events in two instruments. The combination of multiple instruments collecting temporal data in real time represented a significant challenge, as each of the instruments had a unique time stamp associated with the initiation of sampling, and considerable effort was required to most accurately align each instrument data set into a consistent time. Calculation of second-by-second tailpipe pollutant emission rates posed a unique challenge in terms of aligning instantaneous vehicle operation parameters with associated emission events. One example was the lag between the recorded particulate exhaust sample and the engine event associated with the emission. An inherent delay between the time the ECU would record an engine event (e.g., change in RPM) and the corresponding 'downstream' flow rate measurement from the differential pressure sensors, and yet again another delay as the exhaust sample travelled through the dilution system and ultimately recorded in the EEPS. Thus lag 'adjustments' were required to bring each instrument data set 'in line' as a result of a) physical flow lag of the exhaust between the engine and tailpipe, b) physical flow lag of exhaust sample between tailpipe and the particle measurement instruments, and c) variable instrument response lag.

Lag adjustments for all instruments to create a consistent temporal data set were achieved in a multi-step process. Because the GPS instruments were continuously recording throughout each of the nine phases, the GPS time stamp was established as the true temporal datum to which all other instruments were adjusted. Because the scantool was re-initiated for the Inbound phase at the Park-and-Ride stop, the temporal lag adjustment process for all instruments was conducted twice for each run - for both Inbound and Outbound phases. The temporal alignment of the all

instruments for the entire data set was previously performed by Sentoff (2013). Sentoff (2013) identified pairs of instruments used to perform the adjustments in steps: the "stationary" instrument, or instrument whose timestamp would remain fixed, and the moving or "lag-adjusted" instrument, or instrument that was to be temporally adjusted (see Table 8). Each step resulted in a temporal shift of the "lag-adjusted" parameter ranging from 0 seconds to 119 seconds (see Appendix G of Holmén et al. 2014).

Using Matlab 7.10.0, Sentoff (2013) first generated a *n* x 241 matrix, with n being the number of second-by-second records for each outbound and inbound phase of each run. The 241 data points for each row *n* consisted of the records of the "lag-adjusted" (or moving) parameter - 120 seconds before and 120 seconds after as well as the original recorded parameter. Sentoff (2013) subsequently computed Pearson's correlation coefficients between the "stationary" parameter (variable measured by the stationary instrument) records and each of the 241 moving parameter records, corresponding to a temporal lag ranging from -120 to 120 seconds. The temporal shift (in seconds) with highest value Pearson's correlation coefficient was then chosen thus applied to each record of the moving variable within the phase. Table 8 below shows the three steps taken to compute the lag adjustments between the instruments used for analysis here. Relative humidity and temperature sensor measurements were temporally joined to the primary Labview (L1) device associated with differential pressure sensor recordings. Further detail of the complete list of run and phase temporal lags computed for the TOTEMS data set can be found in Sentoff's 2013 Thesis (2013) and the report by Holmén et al. (2014).

Table 8. Sequential Lag Adjustment Parameters based upon Pearson's Correlation Coefficients (from Sentoff, 2013)

Step	Stationary Instrument	Stationary Parameter	Lag-Adjusted Instrument	Lag-adjusted Parameter
1	GPS	Vehicle Speed (kph)	Scantool	Vehicle Speed (kph)
2	Scantool	Engine Speed (RPM)	Differential Pressure Sensors	Computed Exhaust Flowrate (lpm)
3	Scantool	Calculated Load (%)	EEPS	Total PN concentration (#/cc)

5.3 Parameter Calculations

5.3.1 Computed Exhaust Flow Rate

As part of the TOTEMS data compilation, one method of computation of second-by-second exhaust flow rate ($Q_{exhaust}$) was through the differential pressure sensor instrumentation. Prior to each of the on-board installations of TOTEMS instrumentation and equipment, flow rate measurements (liters per minute, or lpm) were calibrated using customized flow calibration apparata (see Holmén et al. 2014). A total of six calibrations were conducted before each vehicle instrumentation installation (three CV, three HEV). The runs were consequently arranged into six run groups according to these calibrations, including CV-I (Runs 5-12), CV-II (Runs 31-36), CV-III (Runs 54-67), and HEV-I (Runs 13-18), HEV-II (Runs 46-53) and HEV-III (Runs 68-79).

From the six separate calibrations, voltage data was collected from each of the four differential pressure sensors as well as the voltage from a Sierra 620S flow meter. Voltage readings from the Sierra 620S flow meter were then converted to a flow rate (lpm) using the original calibration data from the manufacturer. A regression of flow rate using a square fit and forcing through zero intercept was thus developed from the voltages of each of the four differential pressure sensors

(see Holmén 2014). Sensor number four was the most sensitive (and best suited for lower flow rates) while sensors three, two and one were successively less sensitive (and suited for the highest flow rates). Additional sequential logic was developed to identify the most accurate sensor based upon its range of voltage, and a single sensor was thus chosen for each second of sampling. From this single sensor, using the square fit regression, the chosen flowrate was computed. A summary of the four equations used to compute $Q_{exhaust}$ and the logic used for selection are provided in Appendix C

5.3.2 Flow Rate Estimation

While the above mentioned flow rate computation was successfully computed for much of the sampling runs, some runs were problematic due to faulty operation of the secondary battery which charged the differential pressure sensor system. In addition, the sensitivity of the fourth (and most sensitive) sensor appeared to result in susceptibility to erratic readings, especially during the low engine idle of the CV and the engine on and off events of the HEV. To overcome these irregularities and to simplify the calculation of flow rate, a regression estimating exhaust flow rate was developed for each vehicle based upon scantool measurements. This choice was based upon the consistency and fidelity of the ECU data collected through the scantool. Correlation matrices (see Appendix C) showed that mass air flow (MAF) in the CV and engine speed (RPM) in the HEV had the highest correlation of the engine parameters with the computed flow rate described in Section 5.3.1, noting that MAF was not collected in the HEV (see table E1 and E2). To generate estimated flow rate regressions for each vehicle, a subset of data was selected from of the installation phases described in Section 5.3.1. The run from each installation phase with the highest Pearson's correlation between a) $Q_{exhaust}$ and MAF for the CV and b) $Q_{exhaust}$ and RPM for the HEV was selected (See Figures . A best fit linear regression for CV and

a second-order regression for HEV were subsequently developed to form an *Estimated Flowrate* parameter, seen in Figure 10 below.

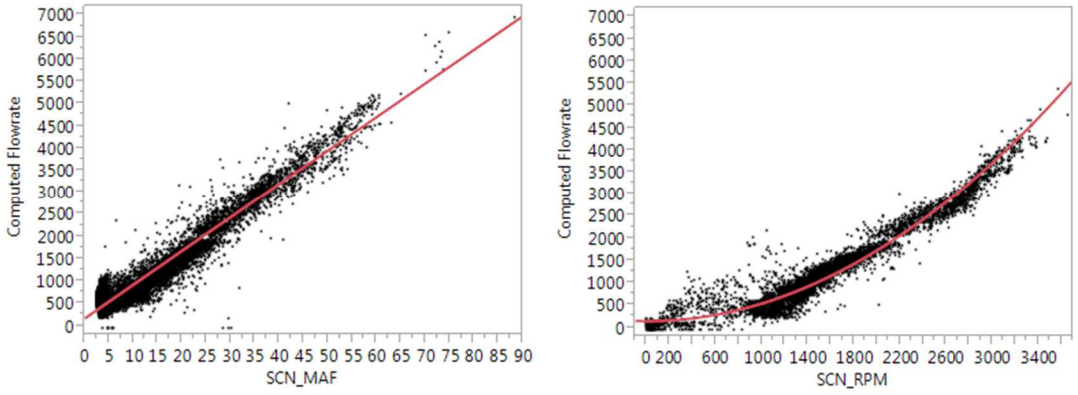

Figure 10. Scatterplot of Mass Air Flow (g/s) v. Computed Flow Rate (lpm) for CV (left) and RPM v. Computed Flow Rate (lpm) for HEV (right). Linear regression of CV Mass Air Flow (SCN_MAF) and second order regression of HEV Engine Speed (SCN_RPM) are shown in red.

The regression equations to estimate tailpipe exhaust flow rate developed from the subset of data ($R^2_{CV} = 0.94$ and $R^2_{HEV} = 0.96$) are shown for each vehicle in Equations 5.1 - 5.3:

$$Q\_EST_{CV} = 170.16 + 75.67\ (MAF_{CV}) \qquad \textit{Equation 5.1}$$

When $RPM_{HEV} > 0$,

$$Q\_EST_{HEV} = 145.36 + 0.000397\ (RPM_{HEV})^2 \qquad \textit{Equation 5.2}$$

When $RPM_{HEV} = 0$

$$Q\_EST_{HEV} = 0 \qquad \textit{Equation 5.3}$$

Where:

Q_EST_{cv} = Estimated Tailpipe Exhaust Flowrate of the Conventional Vehicle, in lpm
Q_EST_{HEV} = Estimated Tailpipe Exhaust Flowrate of the Conventional Vehicle, in lpm
MAF_{CV} = Mass Air Flow of the Conventional Vehicle, in g/s
RPM_{HEV} = Engine Speed of Hybrid Electric Vehicle Internal Combustion Engine, in rpm

5.3.3 Emission Rates

5.3.3.1 EEPS Total PN Concentration Corrections

For this analysis, EEPS raw total particle number emission rates (PNER) were corrected for instrument electrometer noise based upon the 10-minute tunnel blank sampling prior to each run. EEPS total particle concentration (#/cc) instrument detection limits (IDLs) were computed for each run as the pre-run mean tunnel blank concentration plus three standard deviations ($\mu + 3\sigma$) of pre-run tunnel blank data (Eq. 5.4).

$$IDL_{EEPS} = TB_{\mu} + 3\,TB_{\sigma} \qquad \textit{Equation 5.4}$$

Where:

TB_{μ} = Run Mean EEPS Pre-Tunnel Blank Total PN concentration, in #/cc
$TB\sigma$ = Run Standard Deviation of EEPS Pre-Tunnel Blank Total PN concentration, in #/cc

Raw 1 Hz EEPS total PN concentration ($EEPS_{raw}$) data were corrected by subtracting these IDL values, or when the IDL concentration exceeded the raw concentration the IDL was used as the corrected measurement. Thus the computation of the corrected EEPS total PN concentration ($EEPS_{corr}$) is shown in Equations 5.5 and 5.6:

$$EEPS_{corr} = EEPS_{raw} - IDL_{EEPS} \text{ when } EEPS_{raw} > IDL_{EEPS} \qquad \textit{Equation 5.5}$$

$$EEPS_{corr} = IDL_{EEPS} \qquad \text{when } EEPS_{raw} \leq IDL_{EEPS} \qquad \textit{Equation 5.6}$$

5.3.3.2 Exhaust Flow Rate Temperature Correction

Exhaust flowrates computed from Equations 5.1 - 5.3 required further adjustment due to sensitivity of the pitot tube to temperature. During some sampling, faulty thermocouple function required estimates of exhaust temperature, and regressions were developed based upon scantool parameters (Holmén et al. 2014). Exhaust temperature measured at the tailpipe or estimated ($T_{exhaust}$,°C) was converted to degrees Kelvin, and the second-by-second estimated temperature-compensated exhaust flow rate (Q_{TC}) was computed for both vehicles as shown in Equation 5.7:

$$Q_{TC} = Q\_EST \times \frac{(T_{exhaust}+273.15)}{298.15} \qquad \textit{Equation 5.7}$$

Where:

Q_{TC} = Temperature-compensated exhaust flow rate, lpm

$T_{exhaust}$ = Temperature of exhaust, °C

$Q\_EST = Q\_EST_{CV}$ or Q_EST_{HEV} [Eqs. 5.1 – 5.3]

5.3.3.3 Second-by-Second EEPS Total Concentration Emission Rate Computation

Development of second-by-second PN emission rates (PNER) in total particles per second (#/s) were computed based upon the EEPS PN concentration (#/cc) corrected for tunnel blank measurements, the estimated tailpipe exhaust flowrate in lpm, and the exhaust dilution factor:

$$\text{PNER} = EEPS_{corr} \left[\frac{\#}{cc}\right] x\ Q_{TC} \left[\frac{L}{min}\right] x \left[\frac{1000cc}{L}\right] x \left[\frac{1\ min}{60\ sec}\right] x\ DF \qquad \textit{Equation 5.8}$$

Where:

PNER = Total Particle Number Emission Rate, #/second
$EEPS_{corr}$ = Corrected EEPS Total Particle Number diluted concentration, #/cc
Q_{TC} = Temperature Corrected Exhaust Tailpipe Flow Rate, lpm
DF = exhaust dilution factor = 108

5.3.3.4 High Emission Event Records (HEERs)

To better understand the relative magnitude of the PN emissions from RIEVs compared to stabilized operation, a High Emission Event Record (HEER) parameter was developed. While High Emission Events (HEEs) have been mentioned in previous literature (Robinson 2011), it is important to clarify the temporal characteristics of such events. Typically, a High Emission Event involves a period of significantly increased pollutant emission rates occurring during transient activity, with an associated peak magnitude. Figure 11 demonstrates a 150-s driving sample showing PN emission rates and RPM for both vehicles (CV Run 11, top and HEV Run 16, bottom). In this figure, two CV HEEs are shown occurring at t~10 s and t~110 s, and two HEV HEEs are shown occurring at t~50 s and t~130 s. For this analysis, a High Emission Event Record

(HEER) is defined as any second with a PNER exceeding the 95th percentile of all CV and HEV records during engine-on operation, for all road sections combined. For the subset of data analyzed in this thesis, this HEER threshold was computed as 9.3 x 10^{10} particles per second, and this value is indicated in Figure 11 by a dashed black line. As can be seen in Figure 11 a High Emission Event may include more than one HEER.

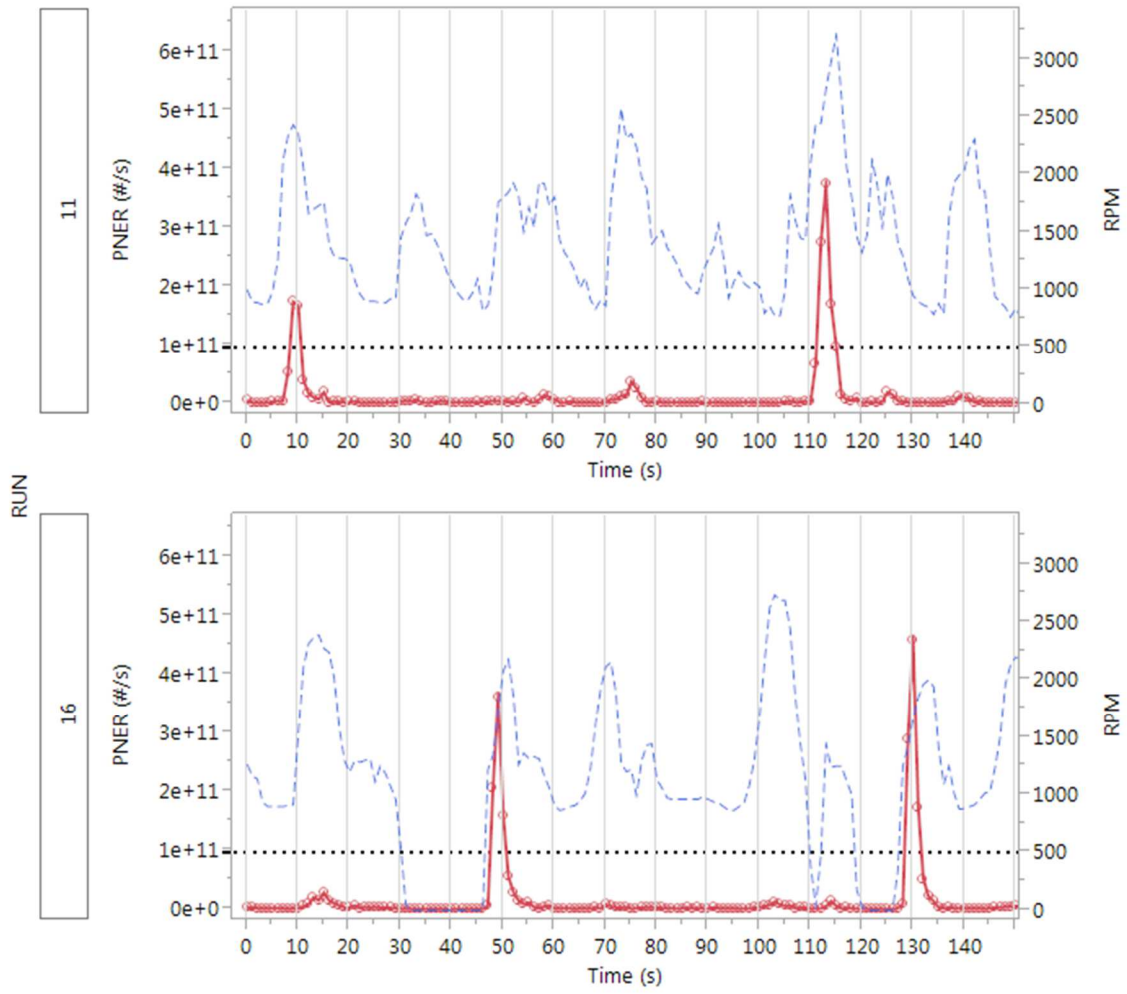

Figure 11. Time series sample of PNER (red solid) and RPM (blue dashed) for CV Run 11 (top) and HEV Run 16 (bottom).

5.3.3.5 EEPS PN Emission Factor Computations

PN Emission Factors (EF) are a measure of the total particles emitted over a defined distance of travel, typically in number per mile or number per kilometer (#/km). PNEF is an aggregate measure of particulate emissions compared to the instantaneous particulate emissions expressed through PNER. Regulation of tailpipe PN emissions in Europe is measured in the spatial context (#/km) while in the U.S., regulation of tailpipe particle matter is measured in mass per mile (g/mi). For the analysis conducted here, the entire sampling route (50.7 km) is categorized into 100-m chainage bins. While other smaller bin sizes of 50-m and 20-m were considered, a choice of 100-m bins was made based upon a minimum length of roadway in which at least two seconds of data was recorded in each road section. For each 1-s record, the chainage value (in meters) is rounded to the nearest nominal 100 meters using JPM 10.0 rounding function. The chainage bins were designated solely upon this nominal chainage identification and were independent of any other roadway characteristics such as intersections or changes in road grade. The first and last 100-m bin of each road section was excluded from analysis, as these bins tended to be underpopulated when rounding above and below the nominal 100-m chainage value. The total PN emitted within the chainage bin is computed by integrating the PN emission rate across the duration of activity within the bin. Here, PNEF (#/km) is computed as the total PN emitted within each 100-m chainage bin divided by distance the vehicle travelled within the bin (nominally 0.10 km) as shown in Equation 5.9.

$$PNEF_N = \frac{\sum_{t=1}^{t=max}(PNER_t \times 1\ sec)}{Dist_N} \qquad \textit{Equation 5.9}$$

Where:

$PNEF_N$ = Particle number emission factor of chainage bin *N*, #/km

$PNER_t$ = Particle number emission rate at second *t*, #/s

t = Elapsed time of travel along 100 m chainage bin *N*, seconds

t_{max} = Total duration of vehicle travel within 100 m chainage bin *N*, seconds

$Dist_N$ = Total distance vehicle traveled along 100 m chainage bin = 0.10 km

5.3.4 Vehicle Specific Power

To make comparisons of emission patterns between the vehicle types, vehicle specific power (VSP), or the instantaneous force required of the vehicle to overcome all road loads, measured in kilowatts per metric ton or kW/ton, was computed for each second of data. Based upon the generalized VSP Equation 3.3, VSP was calculated (see Equation 5.10 below) for both vehicles based on measured vehicle speed, acceleration, road grade and a combination of measured and calculated vehicle parameters with assumed values for vehicle constants (Jimenez 1999). See Holmén et al. (2009) for more information.

$$VSP = Spd\left[1.1Acc + g\left(\frac{Gr}{100} + C_R\right)\right] + \frac{1}{2}\rho_a\left(\frac{C_D \times A}{m}\right) Spd^3 \qquad \textit{Equation 5.10}$$

Where:

VSP = Vehicle Specific Power, kW/ton

Spd = Vehicle speed, m/s

Acc = Vehicle acceleration computed from the scantool speed (see Eq. 5.11 below), m/s^2

g = Gravitational constant (9.81 m/s^2)

Gr = Road grade (%)

C_R = Dimensionless coefficient of rolling resistance = 0.0135

ρ_a = Air density, kg/m^3

C_D = Coefficient of aerodynamic drag, unitless

A = frontal area of the vehicle, m^2

m = Vehicle mass fully instrumented, kg

Second-by-second vehicle acceleration *Acc* (m/s^2) is computed based upon vehicle speed measured from the scantool speeds, as shown in Eq. 5.11 below:

$$\text{Acc} = \left(\frac{Spd_t - Spd_{t-1}}{\Delta t}\right) \times \frac{1000\ m}{3600\ s} \qquad \textit{Equation 5.11}$$

Where:

Acc = Vehicle acceleration at time t, m/s^2
Spd_t = Vehicle Speed at time t, kph
Δt = Change in time = 1 sec

Air density ρ_a (in kg/m^3) was computed in Equation 5.12 below:

$$\rho_a = \frac{P_a}{R_a \times (T_a + 273.15)} \quad [\text{ in kg/m}^3] \qquad \textit{Equation 5.12}$$

Where:

P_a = Atmospheric Pressure (1.01325*10^5 N/m^2)
R_a = Gas constant for air (287.058 N·m/kg·K)
T_a = Ambient air temperature, °C

5.3.5 Estimated Fuel Rate and Fuel Consumption

In order to provide an additional comparison of vehicle performance, second-by-second fuel rate was computed using scantool records. In the CV, fuel rate (ml/s for cylinder 1) was directly measured (see Eq. 5.13 below), but in the HEV it was not recorded due to limitations in the Controller Area Network (CAN) configuration of the Toyota Techstream software. To overcome

this deficiency, a regression of HEV fuel rate was developed using the data collected from a single run using the HEV engine CAN. From this single run, HEV fuel rate (ml/s for cylinder 1) was recorded at 3 Hz and models were developed using other engine parameters available during normal HEV sampling. Linear and quadratic models were tested using engine speed (RPM) and calculated load (%), with a final selection of quadratic model using calculated load due to its high coefficient of determination ($R^2 = 0.82$), indicating that 82% of the variation in measured fuel rate could be explained by the model. Estimations of HEV fuel rate are shown in Equations 5.14 and 5.15 below.

$$FR_{CV} = FR_{SCN} x\ 4 \qquad \textit{Equation 5.13}$$

$$FR_{HEV} = 0.42 + 1.486\ x\ 10^{-4}(Calc\_Load_{HEV})^2 \quad \text{when RPM} > 0 \qquad \textit{Equation 5.14}$$

$$FR_{HEV} = 0 \qquad \text{when RPM} = 0 \qquad \textit{Equation 5.15}$$

Where:

FR_{CV} = Fuel rate of Conventional Vehicle, ml/s
FR_{HEV} = Fuel rate of Hybrid Vehicle, ml/s
FR_{SCN} = Fuel rate of cylinder 1 of Conventional Vehicle (from scantool), ml/s
$Calc\_Load_{HEV}$ = Percent Calculated Load of Hybrid Electric Vehicle (from scantool), unitless

To compute the vehicle normalized fuel consumption (FC) for each 100-m chainage bin, an equation for each vehicle, similar to 5.9 above, is used.

$$FC\_CV_N = \frac{\sum_{t=1}^{t=max}(FR\_CV_t \times 1\ sec)}{Dist_N} \times \frac{L}{1000\ ml} \times 100 \qquad \textit{Equation 5.15}$$

Where:
FC_CV_N = Conventional Vehicle Fuel Consumption of each 100-m chainage bin *N*, in L/100 km
FR_CV_t = Conventional Vehicle Fuel Rate at second *t*, ml/s
t = Elapsed time of travel along chainage bin *N*, seconds

t_{max} = Total duration of vehicle travel within 100 m chainage bin *N*, seconds

$Dist_N$ = Total distance vehicle traveled along 100 m chainage bin N = 0.10 km

And

$$FC\_HEV_N = \frac{\sum_{t=1}^{t=max}(FR\_HEV_t \times 1\ sec)}{Dist_N} \times \frac{L}{1000\ ml} \times 100 \qquad \textit{Equation 5.16}$$

Where:
FC_HEV_N = Hybrid Vehicle Fuel Consumption of each 100-m chainage bin *N*, in L/100 km
FR_HEV_t = Hybrid Vehicle Fuel Rate at second *t*, ml/s
t = Elapsed time of travel along chainage bin *N*, seconds

t_{max} = Total duration of vehicle travel within 100 m chainage bin *N*, seconds

$Dist_N$ = Total distance vehicle traveled along 100 m chainage bin N = 0.10 km

The relative difference between vehicle fuel consumption for each road section is computed using the following equation:

$$Relative\ Difference\ in\ FC = \frac{FC\_CV - FC\_HEV}{FC\_HEV} \times 100\% \qquad \textit{Equation 5.17}$$

5.4 Hybrid ICE Operational Mode

5.4.1 OpMode Framework

In order to facilitate the characterization of RIEVs, a new methodological framework is presented here to identify the operational modes of the HEV that are distinct from a CV. While traditional designation of operational modes has focused upon kinetic properties of the vehicle – idle, acceleration, cruise – a new framework for HEV "ICE operational modes" (ICE OpMode) is introduced to identify the state of transition of the ICE between off and on. The framework used is limited solely to the operation of the ICE, and does not include modes which distinguish the proportional contribution of the electric motor to propulsion of the vehicle, or a "hybridization factor" (Holder and Gover 2006). While the inclusion of such modes that quantify the proportional electrical assist from the battery electric system (a hybridization factor) may be useful for other types of emission analysis, the purpose of this framework is to simplify and characterize the exact second of re-ignition. The framework used to assign an ICE OpMode to each of the TOTEMS data points is presented in Table 9. During all CV operation, the ICE OpMode was assigned Stabilized On, as the engine was never shut down.

For the purpose of this new framework, five ICE OpMode states were categorized: Stabilized On, Off, Shutdown, Full Re-ignition (F-RIEV) and Partial Re-ignition (P-RIEV). Without a priori knowledge of the ICE shutdown and re-ignition trigger points, or thresholds in real-time (a fuzzy logic process guided by solely by the ECU), a proxy for these events was established based on measured engine speed (RPM) and a set of prior conditions (see Table 9). As all sampling data was tabulated at 1Hz frequency, the discrete measurement of each state's duration was based upon one-second increments.

ICE-Off state was identified as any record with an engine speed equal to 0 RPM. To determine a nominal threshold between the remaining four states (On, Shutdown and F- and P-RIEVs), an HEV ICE idling event criterion was established. During sampling, most standstill (zero speed) operation the HEV ICE would turn off, yet in some circumstances (typically low SOC) the HEV ICE was observed to 'idle' temporarily between approximately 900 - 1100 RPM. To mark the transition from ICE-On to ICE-Off, an engine speed threshold of 800 RPM was therefore established, a value conservatively selected slightly below the measured HEV ICE idle range.

Three generalized conditions were thus established to categorize the ICE OpMode: RPM equal to zero, RPM less than or equal to 800 but greater than zero, and RPM greater than 800. Table 9 includes an additional set of prior conditions necessary to categorize every record within the HEV data set for each RPM range. An ICE-Shutdown was identified when RPM $\leq$ 800 and the change in RPM is negative ($RPM_t - RPM_{t-1} < 0$), indicating the engine speed is approaching zero (ICE-Off).

During some driving regimes, especially congested, low speed driving, rapid changes in power demand resulted in frequent ICE on and off cycling. Under these conditions, some Shutdown events were not followed by a distinct ICE-Off state – that is, engine speed did not reach 0 RPM – but instead was followed by an increase in engine speed. A Partial Re-ignition event (P-RIEV) was thus defined by an engine speed greater than 0 RPM at time *t* and a Shutdown (RPM < 800) state at time *t -1*. A Full Re-ignition event (F-RIEV) was defined by an engine speed greater than 0 RPM at time *t* and an Off (RPM = 0) state at time *t -1*.

A 3-s period following the initial record of P-RIEV and F- RIEV (as defined above) was identified as the post-re-ignition state (see Table 9). This designation in effect defines a four-second re-ignition event (1-s re-ignition record and 3-s of post re-ignition records), over which

the RIEV associated emissions were quantified. (Further explanation of the 4-s RIEV period is provided in Section 5.4.2.) In some instances, this 3-s post re-ignition period was interrupted by a Shutdown state, thus reducing the total RIEV duration to 3-s, 2-s or 1-s. By process of elimination, all remaining HEV ICE operation with engine speed greater than 800 RPM and not meeting any of the prior conditions describe in Table 9 was designated as Stabilized On.

Table 9. HEV ICE OpMode Framework Logic

RPM state at time *t*		Prior Condition	Current OpMode Assignment
$RPM_t = 0$		None	*OFF*
$RPM_t \leq 800$	**a**	OpMode $_{t-1}$ = *OFF*	*F-RIEV*
	b	$(RPM_t - RPM_{t-1}) < 0$	*SHUTDOWN*
	c	$(RPM_t - RPM_{t-1}) \geq 0$	*P-RIEV*
$RPM_t > 800$	**d**	OpMode $_{t-1}$ = *P-RIEV* **or** OpMode $_{t-1}$ = S*HUTDOWN*	*P-RIEV*
	e	OpMode $_{t-2}$ = *P-RIEV* **or** OpMode $_{t-2}$ = S*HUTDOWN* **and** OpMode $_{t-1}$ = *P-RIEV*	
	f	OpMode $_{t-3}$ = *P-RIEV* **or** OpMode $_{t-3}$ = S*HUTDOWN* **and** OpMode $_{t-2}$ = *P-RIEV* **and** OpMode $_{t-1}$ = *P-RIEV*	
	g	OpMode $_{t-1}$ = F-RIEV **or** OpMode $_{t-1}$ = *OFF*	*F-RIEV*
	h	OpMode $_{t-2}$ = *F-RIEV* **or** OpMode $_{t-2}$ = OFF **and** OpMode $_{t-1}$ = *F-RIEV*	
	i	OpMode $_{t-3}$ = F-*RIEV* **or** OpMode $_{t-3}$ = OFF **and** OpMode $_{t-2}$ = *F-RIEV* **and** OpMode $_{t-1}$ = *F-RIEV*	
		None of the above	*STABILIZED ON*

Figure 12 shows a time series plot of the HEV operation for Run 16 along a portion of the Urban I road section. Ten RIEVs are depicted (blue asterisks) along with vehicle speed (red) and ICE engine speed (green). Nine F-RIEVs are shown to occur as well as one P-RIEVs (occurring at t~ 260-s).This distinction between the two types of re-ignition events here accounted for potential effects of incomplete fuel combustion occurring during partial engine shutdown and associated impacts upon resulting PN emissions.

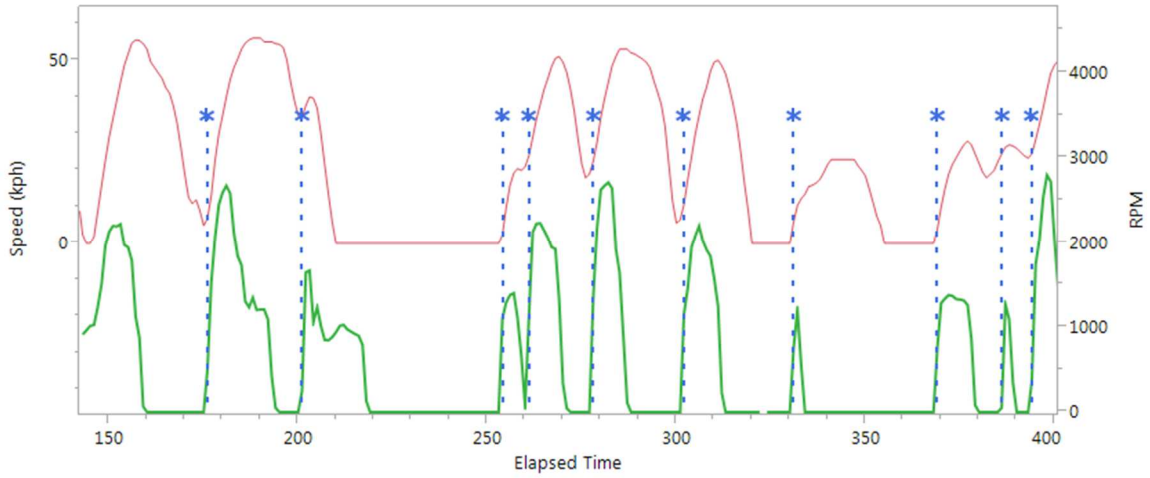

Figure 12. Time series plot of HEV speed (red), RPM (green) and times of RIEVs (blue asterisk).

5.4.2 RIEV Duration Rationale

In exploring the comparison of emissions between the HEV and CV, it was important to note that the uniqueness of HEV ICE operation, with five observed states, created a challenge in the quantification of associated emissions. While a re-ignition was triggered by RPM thresholds, the emissions resulting from such an event were not necessarily constrained to the single 1-sec record, but instead were observed to be spread over several records. To better understand the

unique combustion conditions during a HEV re-ignition event, ICE operating parameters that could not be collected during regular HEV data collection due to scantool limitations (see Section 5.1.4) were measured for a single run (as described in Section 5.3.5), with the scantool collecting a different set of engine parameters at a temporal resolution of 3 to 4 Hz.

During this separate HEV sampling, the air-to-fuel ratio (A/F) and fuel rate (ml/s) scantool data were collected, and a unique pattern of enleanment/enrichment during 184 RIEVs was shown to recur in each of the events as seen in Figure 13. An A/F of 14.7 indicates the stoichiometric ratio between fuel and air for complete combustion of gasoline, while enleanment is characterized by excess air (lean burning) and enrichment characterized by excess fuel (rich burning).

Shown in Figure 13 are mean engine speed (blue, top), fuel injection rate in ml/s (red, middle), and mean normalized air-to fuel ratio parameter Lambda (green, bottom; see Section 3.4.2). Note that the elapsed time along the x-axis includes negative values, which indicates the period of engine off leading up to the RIEV. The vertical dashed black line at t = 0.0 s indicates the re-ignition point.

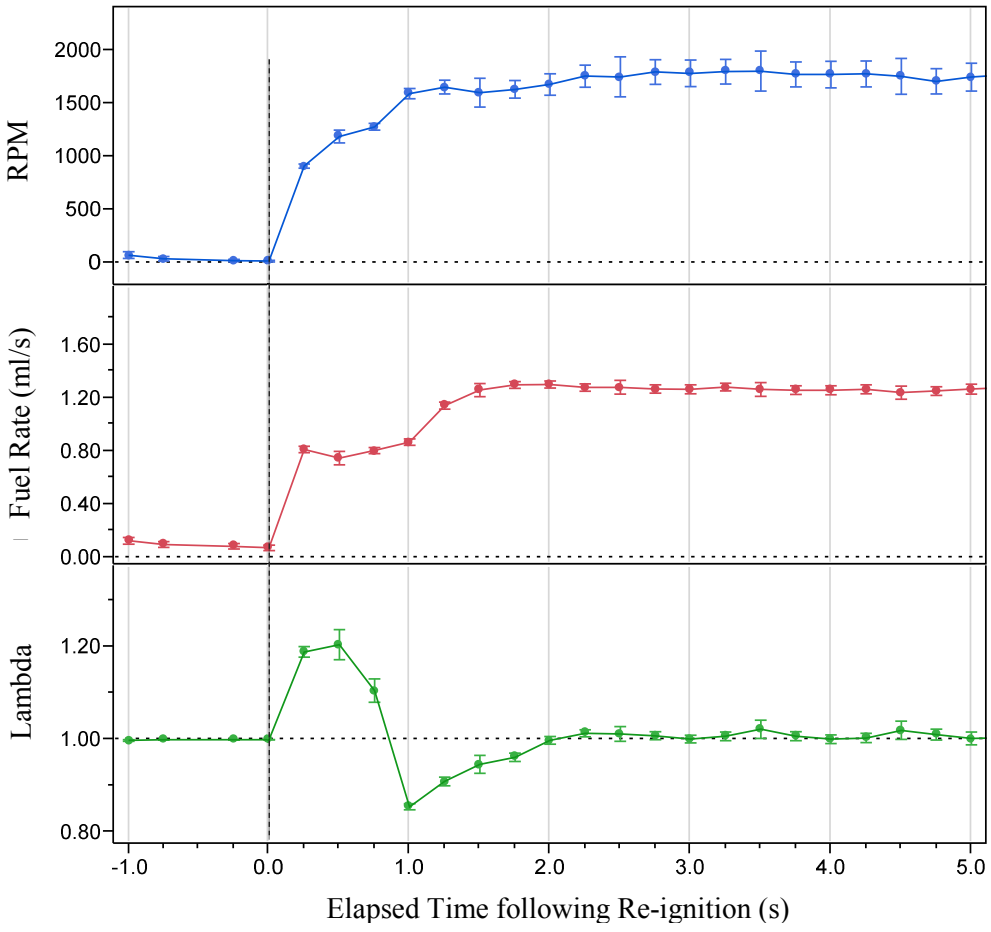

Figure 13. Time series plots of RPM (top), fuel rate (middle) and Lambda (bottom) for 184 Re-ignition events over one run.

As observed in earlier literature, enrichment conditions ($\lambda < 1$) typically lead to an increase in particle emissions (Kittelson 1998). Enrichment conditions were observed during each of the 184 RIEVs. For this analysis, the average period (in seconds) required for the A/F ratio to return to stoichiometric conditions ($\lambda = 1$) after re-ignition was used to establish a basis for the duration of the RIEV. As shown by the bottom plot of λ in Figure 13, this period was determined to be, on average, 2.0 seconds following re-ignition. Assuming some dispersion effects as a result of the

exhaust travelling through the tailpipe, this 2-s RIEV period was doubled to 4-s to establish the temporal basis for computation of PN emissions associated with each re-ignition event. While typical RIEV operation was identified based upon the four-second duration, as mentioned above a RIEV was "truncated" in some instances by ICE shutdown occurring before the full four second period, and in these instances, the RIEV operation was identified using the truncated duration of between 1-s and 3-s.

PNERs were quantified for every second of data from the EEPS. In addition, the peak $PNER_{RIEV}$ was the highest PNER value that occurred during the 4-s (or less during truncated events) event duration. In addition to computing the second-by-second PN emission rate, the cumulative PN inventory (#) for each road section was computed by summing all the second-by-second PNER over each road section.

5.5 Analysis Methods

For the purpose of organizing and reporting data, performing statistical analyses, generating graphical plots, generating modal coding and performing quality control processes, various methods and software platforms were used. As earlier described, much of the data acquisition and recording, lag adjustment and temporal tabulation of run data was performed in earlier work by Sentoff (2013). In this work, post processing of the temporal data set was primarily achieved exclusively using SAS Institute JMP versions 10.0 and 11.0 statistical software. For spatial joins of route grade data to the second-by-second on-board vehicle data, and for the filtering of GPS erroneous records to fit a 25-m buffer around the travelled route, Esri, Inc. ArcGIS version 10.0 was used. In the following Results and Discussion section (Section 6), the products of these analyses to address research questions within this thesis are presented in full detail.

The original full and entire data set, including 32 CV and 43 HEV runs (287,698 s of Outbound and Inbound data), including records from each instrument, was compiled (per time alignment and lag adjustment computations) by Sentoff (2013) using Matlab 7.10.0. Road section divisions described in Section 5.1.5 were achieved using the chainage parameter developed through JMP 10.0. Calculated parameters detailed in Section 5.3 were coded, computed and compiled using JMP 10.0. Using JMP *Round* tool, the 100-meter chainage bin parameter were computed by rounding each chainage value (in meters) to the nearest nominal 100 m value.

All graphical presentation of trends in data and relationships between variables, as well as all initial tabulations were performed using *Analyse* and *Graph* toolboxes in JMP 11.0. Pearson's correlation coefficients were performed using the Restricted Maximum Likelihood method, while all linear and quadratic regressions were performed using JMP 11.0 *Analyze>Model* tool. The one-way analysis of variance (ANOVA) and t-tests detailed throughout Section 6 were conducted

using the *Analyze>Fit Y by X* tool in JMP 11.0 performed using an alpha of 0.05 for all tests in order to address the thesis hypotheses questions pertaining to PN emission rates and emission factors presented earlier in Section 4 of this thesis.

6 Results and Discussion

6.1 Data Summary

To establish that the driving conditions for each vehicle were similar, a comparison of the total sampling time, ambient conditions and vehicular kinetic operation experienced across the selected subset data (See Section 5.2.1) for the two vehicles is shown in Table 10 below. Data collection from six different run groups (CV- I, CV-II, CV-III and HEV-I, HEV-II, HEV-III; see Section 5.3.1) was conducted over an 18-month period. For all sections, total sampling time was 12% greater for the HEV (111,812 s) compared with the CV (99753 s) for the final analysis data subset. Mean ambient temperatures for road sections were slightly lower in the CV (16.0°C – 17.1 °C) compared with the HEV (17.5 °C – 19.2 °C) with an overall range of -7°C to 35°C for the CV and -4°C to 34°C for the HEV. Mean road section relative humidity (%) was nearly identical between vehicles except for Freeway with a 6% difference, with overall ranges of 26% - 80% for the CV and 19%-82% for the HEV. Mean vehicle speed for each run is shown in Figure 14 with Freeway (blue), Rural (red), Urban I (purple) and Urban II (green) road sections. Figure 15 shows box plots speed for each of the six run groups and each road section.

Table 10. Summary of Run Statistics for CV and HEV for all Runs by Road Section.

		Freeway		Rural		Urban I		Urban II	
		CV	HEV	CV	HEV	CV	HEV	CV	HEV
Speed	Mean	**101.6**	**99.2**	**53.7**	**53.1**	**23.7**	**22.9**	**38.8**	**38.2**
(kph)	Std. Dev.	19.1	20.5	19.1	19.9	16.7	17.0	20.2	20.7
VSP	Mean	**8.41**	**7.47**	**3.34**	**3.18**	**1.44**	**1.40**	**1.82**	**1.74**
(kW/ton)	Std. Dev.	11.97	10.25	10.03	9.33	7.28	7.03	6.79	6.35
Outside rH	Mean	**48.0**	**45.3**	**49.5**	**48.9**	**46.6**	**45.0**	**47.3**	**47.0**
(%)	Std. Dev.	9.0	10.7	10.3	12.1	9.2	9.9	9.7	10.2
Outside Temp.	Mean	**16.0**	**17.5**	**16.2**	**17.8**	**16.6**	**17.6**	**17.1**	**19.2**
°C	Std. Dev.	11.1	11.5	11.3	10.9	11.0	11.0	11.6	11.1
Total Sampling Time (s)		**16024**	**18623**	**28560**	**32741**	**32287**	**35883**	**22882**	**24565**
Number of Runs		**27**	**31**	**26**	**30**	**26**	**29**	**26**	**28**

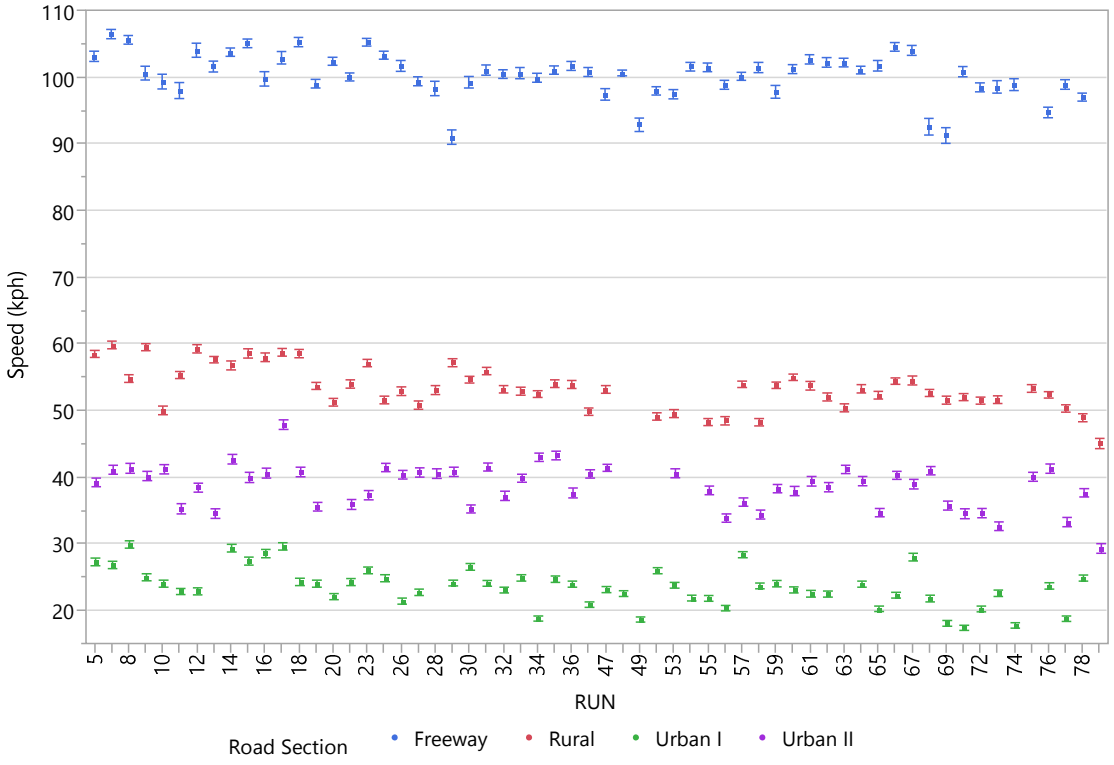

Figure 14. Mean road section vehicle speed (kph) by run. One standard error bars shown.

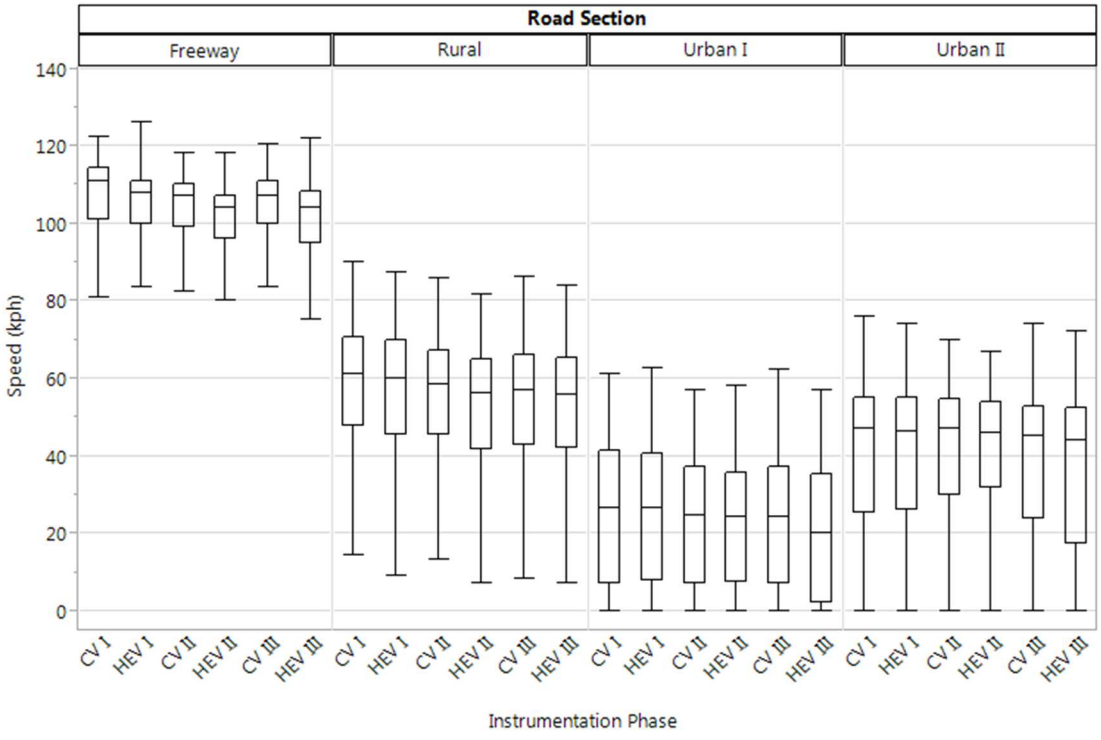

Figure 15. Box plots of vehicle speed (kph) for each road section by Run Group.

Using t-tests (α = 0.05), overall comparison of speed (kph) by vehicle type revealed statistically significant differences in means, with CV means greater than HEV means for each of the road sections. The overall percent differences between vehicle mean speed for each road section, however, were quite small, ranging from 1% to 3%. Figure 15 shows box plots of speed for each vehicle (CV=blue, HEV=red) for each road section.

T-tests (α = 0.05) of mean vehicle VSP showed significantly different means between vehicles for Rural and Freeway sections, but no significant difference between vehicle means for Urban I and Urban II. T-tests showed significant differences between each road section mean VSP and speed for each vehicle. Figure 17 shows the mean VSP for each road section by the six run groups.

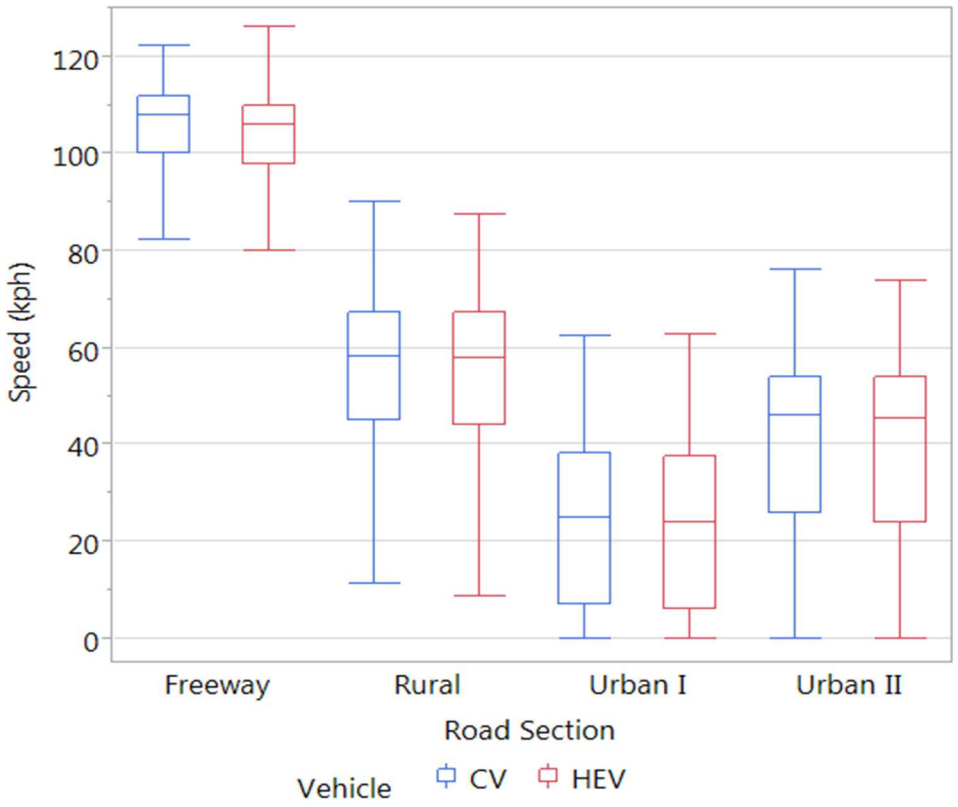

Figure 16. Box Plots of speed by road section for each vehicle (CV = blue, HEV = red).

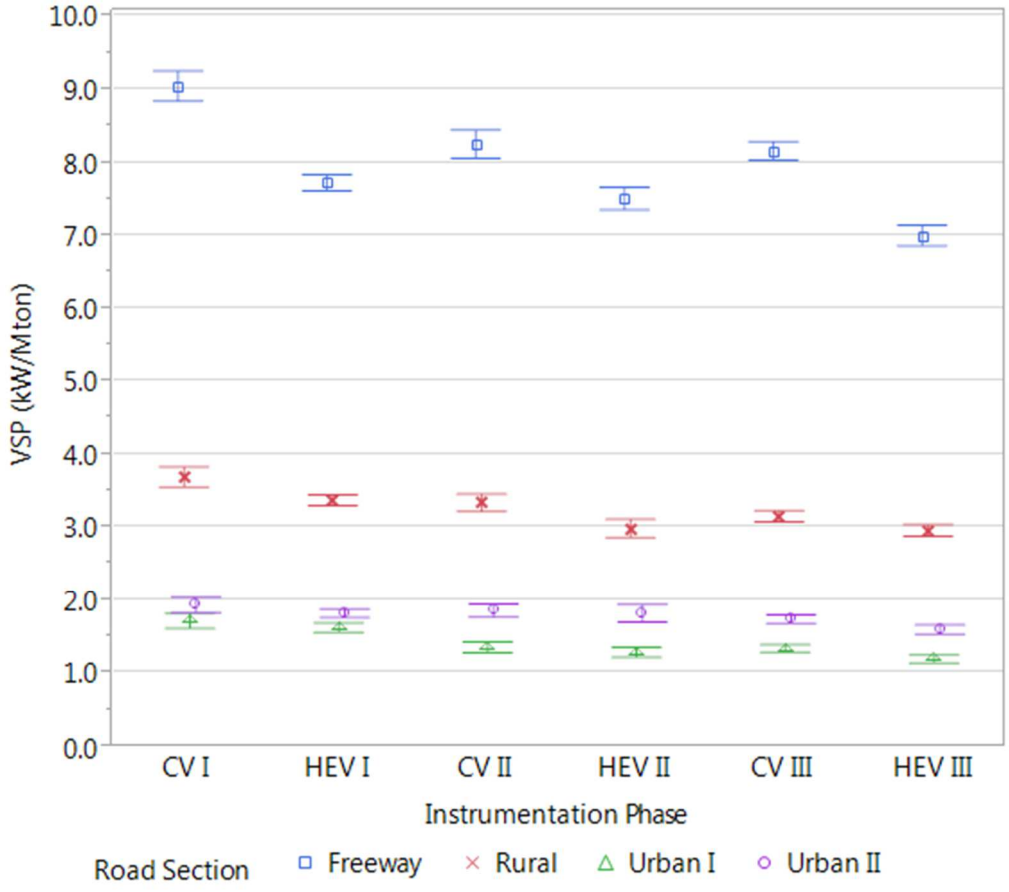

Figure 17. Mean VSP (kW/ton) for each road section by Run Group. Error bars are one standard error.

While driving conditions differed from run to run due to differences in time of day and seasonal traffic variation, every attempt was made by the driver to maintain the same driving style throughout the 18-month sampling period. Overall differences in VSP between vehicles were expected due to the 10% greater mass in the instrumented HEV, having the effect (despite slightly lower coefficient of drag and frontal area) of lowering HEV VSP compared with that of the CV. Other differences in kinetic operation were observed as well. There does appear, from

examination of Figure 14 and Figure 15, to have been a trend in decreased speed over the entire sampling period (Run 5 to Run 75) for both vehicles. This is most notable in the Rural mean speed, and to a lesser extent Freeway mean speed. Examination of the mean VSP over each run group showed a more pronounced declining trend over time within Freeway sections and, to a lesser extent, Rural sections.

Though there were no obvious measurable explanations for the observed change in speed over time, one likely explanation is presented. It is likely that the driver may have become accustomed to the driving route over the course of 75 repeated runs, and as a result may have adopted less aggressive driving habits, resulting in a decrease in overall power demand. In addition, the change in co-pilot after the first two run groups (CV-I and HEV-I) may have had an impact upon the driving style of the driver. Figure 18 shows the standard deviation of VSP for each road section across the six run groups by vehicle. In all but CV Freeway driving, standard deviation of VSP was higher in the first run group compared to the last two, indicating more aggressive driving tactics in the early CV and HEV sampling.

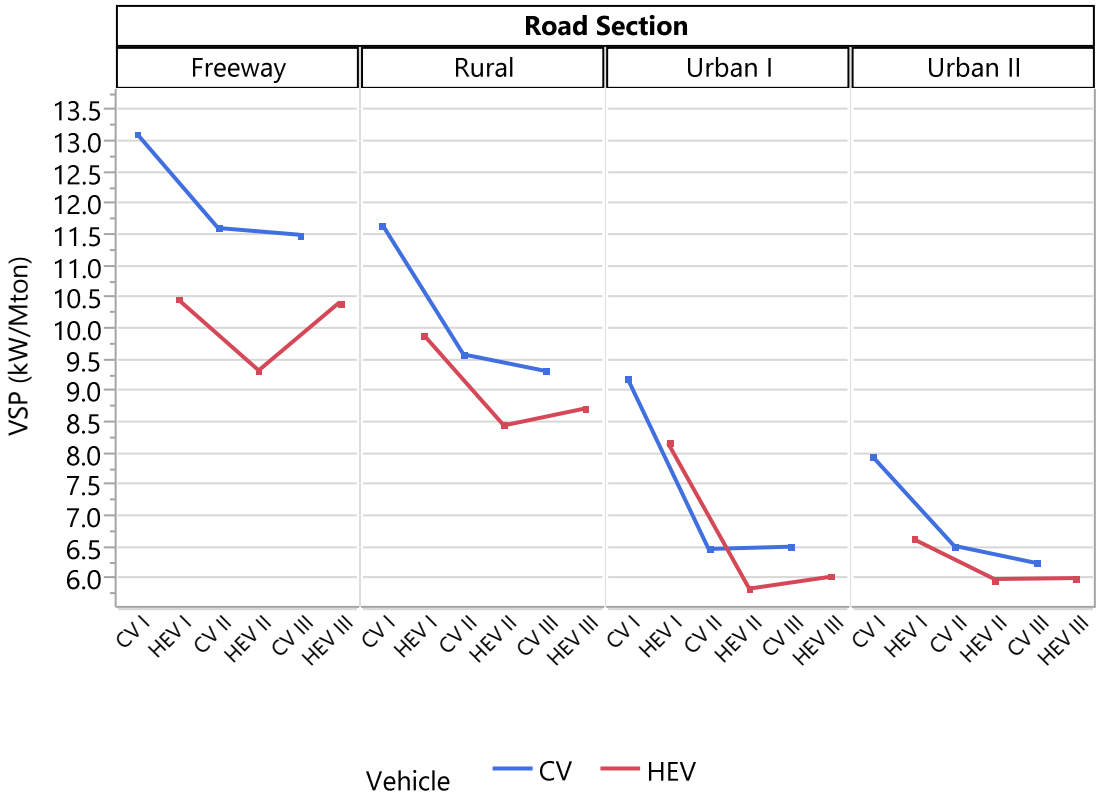

Figure 18. Standard Deviation of each vehicle VSP by Road Section and Run Group.

Mean VSP as computed here does not reflect the hybridization effect, or proportion of propulsion provided by the electric motor, and is thus not necessarily a good indicator of HEV ICE activity and associated emissions. VSP was instead used to compare the similar operation of the two vehicles. For the subset of data analyzed, 99% of all VSP activity for both vehicles ranged between -21.0 and 29.6 kW/ton. For all analysis here, the 1% of VSP outliers (0.5% above and below) were removed from the data set (see Appendix F for more details). Distribution of sampling across this VSP activity range (-21.0 and 29.6 kW/ton) is shown for each road section and vehicle in Figure 19. As can be seen in Figure 19, the distribution of activity differs between each road section.

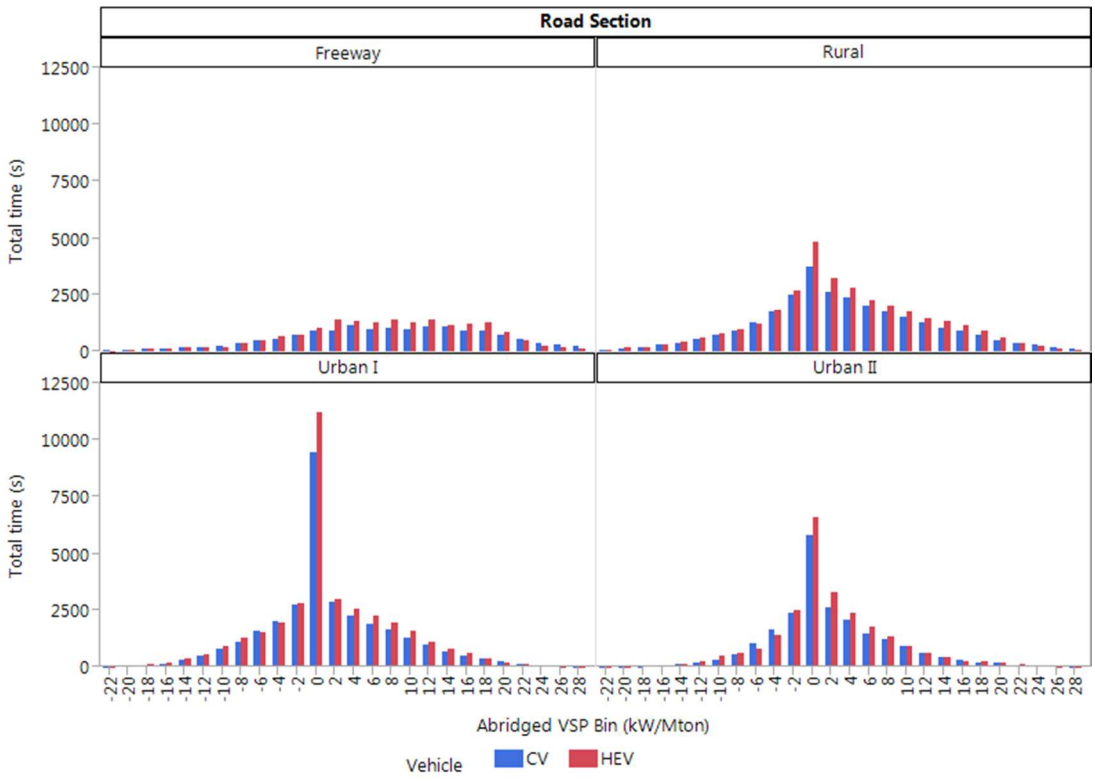

Figure 19. Total time (sec) of vehicle activity in each VSP bin by Road Section for subset of data analyzed.

Overall, the distinctive distribution spread of speed for each road section as demonstrated in Figure 16 as well as the VSP distributions across the four road sections shown in Figure 19 illustrate the representation of each road section as a separate drive cycle (see Figure 9). Each road section had varying ranges of road grade, speed limits, intersection-control and traffic volume. A summary of the characteristics of each road section are given in Table 11 below. The lower maximum speed limits and higher density of intersection control under Urban road sections (4.6 and 1.3 intersections per km for Urban I and II sections, respectively) contrast with the higher maximum speed limits of Rural and Freeway sections with relatively lower intersection

control (0.4 and 0.0 controls per km for Rural and Freeway, respectively). The Freeway road section included both an on-ramp and off-ramp portion. These differences between each road section were the basis for comparative analysis of vehicle activity and emissions.

Table 11. Road Section Summary.

	Grade (%)		Posted Speed Limit (mph)		Average Annual Daily Traffic [A]		# Intersections		Total Distance
	Min	Max	Min	Max	Min	Max	**Stop**	**Signal**	**(km)**
Freeway	-6.25	4.1	55	65	13395	22015	1	0	17.1
Rural	-13.05	9.7	30	45	1550	7230	3	4	16.6
Urban I	-6.4	10.7	30	35	2500	41810	17	21	8.2
Urban II	-7.4	11.1	30	40	6000	19840	1	11	9.6

A. Average Annual Daily Traffic values gathered from 2005-2010 Automatic Traffic Recorder counts. Source: CCRPC, 2012.

6.2 Comparison of Vehicle Activity

Vehicle engine speed varied significantly between the two vehicles across all four road sections, as can be seen by the box plots and mean of RPM for both vehicles in Figure 20. This result is expected for two reasons. First, during low speed and low power demands, HEV ICE was frequently shutdown (RPM = 0), while in the CV, the ICE operated at idle engine speed or greater (RPM > 600). Secondly, though not measured directly in this work, the contribution of electrical power from the BES to propel the vehicle during acceleration was assumed to result in lower HEV ICE power required, compared with the CV ICE under similar driving conditions. T-tests showed that mean vehicle engine speeds were statistically different ($\alpha = 0.05$) for each road section. Overall mean and standard deviations of CV engine speed under Urban I and Urban II were nearly identical (1302 ± 513 and 1362 ± 449, respectively) as were mean HEV engine speeds and standard deviations (656 ± 797 and 650 ± 816, respectively). Under combined Urban I and II driving, CV engine speed was approximately twice that of HEV, due to the significant ICE-Off (0 RPM) activity of the HEV (see Section 6.3). Under Rural road section driving, overall engine CV engine speeds were 1.4 times higher than HEV (1581 ± 523 and 1121 ± 905), while under Freeway driving, where the HEV was rarely off (see Section 6.3) the CV and HEV engines speeds were similar (2112 ± 428 and 1839 ± 812). For each road section HEV standard deviations were greater than CV despite the CV lower overall means, indicating a much greater variation in HEV engine activity.

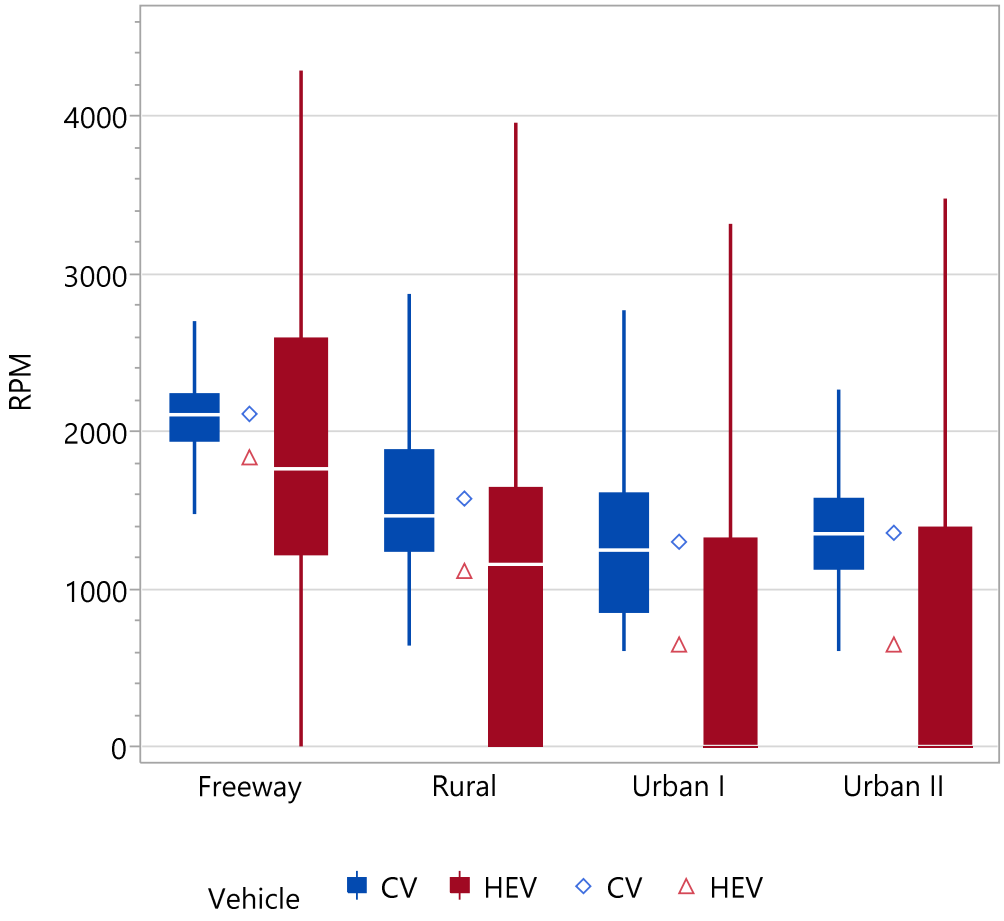

Figure 20. Box plots and mean of RPM by road section (blue = CV, red = HEV).

To demonstrate the typical difference in operation between the two vehicle types, a graphical comparison of RPM, vehicle speed, VSP and PNER is shown in Figure 21 for a 2000m subset of the Urban I driving route. Shown along the x-axis in Figure 21 are the chainage locations (in meters from the beginning of the route) of each vehicle for one run, and, for the HEV, the location of RIEVs are indicated by vertical green hash marks. The vehicle speeds are similar spatially across the driving sample that includes nine intersections, yet the engine speeds are

significantly different due to the HEV ICE on-off cycling. Characteristically, the HEV ICE shutdown occurs as the vehicle slows down to a stop, and the HEV ICE remains off while the vehicle is stationary as well as in the first moments of acceleration from stop. In this driving sample, ten shutdowns and eleven RIEVs are shown. Eight of the ten shutdowns occurred during deceleration to a stop while two occurred during higher speed, low load operation (chainage ~ 1240m and 2150m). Of the eleven RIEVs, ten were Full (occurring after at least 1 second of ICE-Off activity) and one was Partial (at chainage ~ 2240m, occurring immediately following a shutdown, with no prior ICE-Off activity), as indicated at the top of Figure 21.

The HEER threshold was computed to be 9.3 $x10^{10}$ particles per second (see 5.3.3.4) and is indicated by the dashed horizontal line in the PNER plot of Figure 21. In the final analysis data set, 76.4% of all HEERs were emitted by the HEV. Of the 3212 RIEVs, 2117 (65.7%) contained at least one HEER. In the HEV urban driving sample shown in Figure 21, ten HEER instances were observed, nine of which occurred during a RIEV, with two HEERs occurring during one RIEV at chainage ~ 1600. For the same stretch of roadway, only four CV HEER instances were observed. In the HEV, a pattern of negative VSP prior to each RIEV is observed (see bottom plot of Figure 21), and each of the 10 RIEVs occurred as VSP surpassed the 0 KW/ton value. Seven of the eleven RIEVs occurred during acceleration from an intersection control. This sample serves to illustrate the high proportion of HEERs associated with RIEVs under urban driving, where stops and low speed accelerations result in frequent engine off and on cycling.

A similar comparison of activity for Freeway driving is seen in Figure 22, showing a sample of 14,000 m of operation. The differences seen here from the Urban driving sample are a lack of ICE-Off and RIEV activity due to the high speeds (> 70 kph), and VSP is generally above 0 kW/ton. PNER in the CV appear to generally exceed the HEER threshold during increases in

engine speeds above 2500 to 3000 RPM, while similar increases in HEV RPM typically do not appear to result in similar HEERs, with the exception at chainage ~ 15500 m. Overall, the HEV PNER appears to be generally lower than CV PNER across all but the highest road loads during high speed (>80 kph) Freeway driving.

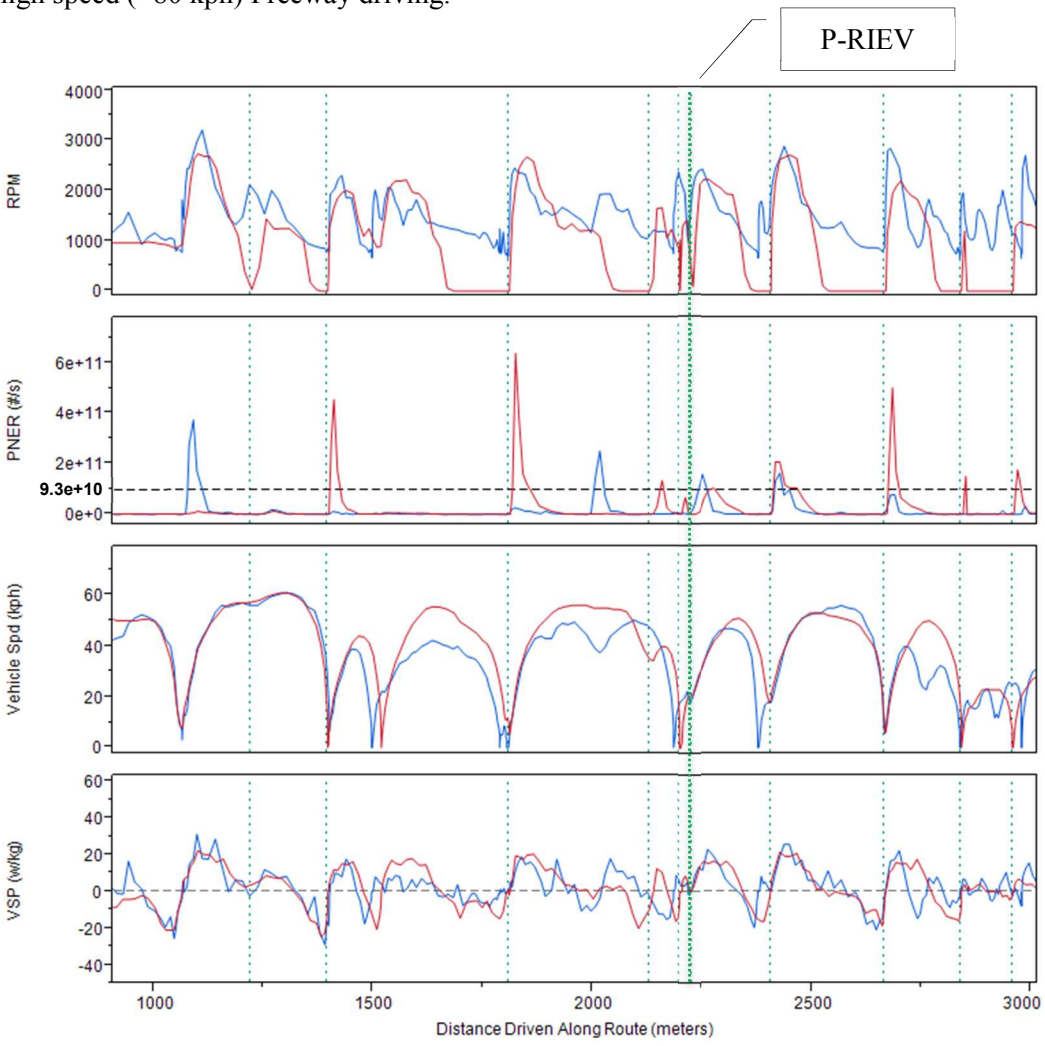

Figure 21. Sample comparison of vehicle operation during Urban I driving for the CV (blue, Run 11) and HEV (red, Run 16), from top to bottom: RPM, PNER (#/s), vehicle speed (kph) and VSP (kW/ton). Vertical dashed green lines indicate Full RIEVs with the heavier vertical dashed green line indicating a Partial RIEV. Horizontal black dashed line at PNER = 9.3 x 10^{10} indicates HEER threshold.

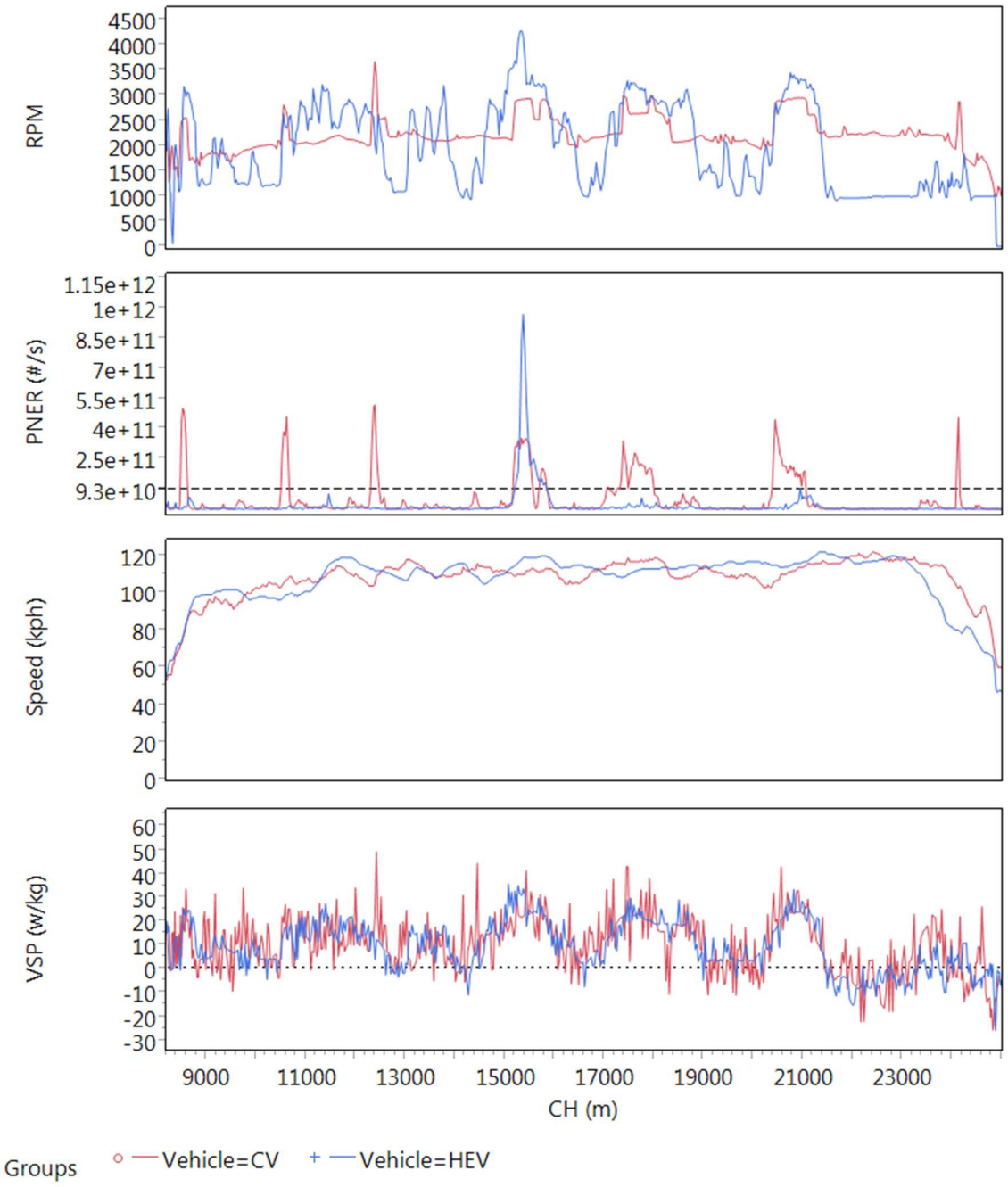

Figure 22. Sample comparison of vehicle operation during Freeway driving for the CV (blue, Run 11) and HEV (red, Run 16), from top to bottom: RPM, PNER (#/s), vehicle speed (kph) and VSP (kW/ton). Horizontal black dashed line at PNER = 9.3 x 10^{10} indicates HEER threshold.

6.3 HEV ICE Operation Characterization

The primary difference between the on-board activity of the two vehicles is demonstrated by ICE shutdown and re-ignition events of the HEV contrasting with the continuous ICE operation of the CV. As expected, overall HEV ICE OpMode distribution varied considerably between Rural, Freeway and Urban driving. Shown in Figure 23 are the relative frequencies of the HEV ICE OpModes within each road section for each HEV run (top) and bar graphs of the overall mean relative frequency of four ICE OpModes within each road section (bottom). The four OpModes shown include the Partial and Full RIEVs (green), Stabilized On (blue), Off (green) and Shutdown (purple) modes. (Note that while in the top plot the total distribution of the four OpModes equals 100%, in the bottom plot of mean relative frequencies of all four OpModes the total is not necessarily 100%. This is because the computation of each OpMode average frequency is independent.) Urban I and II driving were very similar in OpMode distribution, with 49% to 52% of average run operation in Off mode and 14% of average run operation in RIEV mode. However on average, 11% of Rural and only 1% of Freeway driving was spent in RIEV mode. In runs 17 and 47, Urban I driving resulted in much lower than average Off mode frequency. While it is not clear why Urban runs 17 and 47 resulted in such low Off mode frequency, these two run temperatures were lower than average (3 °C and 1 °C, respectively), and the Urban I road section is the first section sampled. It is likely that the combination of cold temperature and the fact that Urban I road section is the first of the four road sections driven indicates that the HEV may have been insufficiently warmed up compared to other runs, as these low ICE-Off frequencies (compared to mean road section values) did not occur in other warmer runs or in other road sections, specifically Rural and Urban II. Runs 17 and 47 values were included in average frequency computations for Urban I driving.

Figure 23. Relative frequency of ICE OpModes of all 33 HEV runs by road section (top) and Run mean percent time of each OpMode by road section (bottom). Error bars (bottom) are one standard error.

On average, Freeway driving involved 1.6 and 3.1 times more Stabilized mode driving than that of Rural and combined Urban driving, respectively. For all HEV activity, the top speed observed in ICE-Off mode was 65 kph (40 mph), thus providing explanation for the high proportion of Freeway activity spent in ICE Stabilized On mode.

One parameter potentially useful in predicting the relative frequency of the HEV off-on activity is the occurrence of idle speed events. Here, an idle speed event is defined as any period where scantool vehicle speed was less than 2.0 kph. For each HEV run and road section, the mean percent of total operational time spent at idle speed was computed. A scatterplot of mean HEV ICE-Off time vs. mean percent speed idle is shown in Figure 24. Note that Freeway data is excluded from this analysis due to its relatively low ICE-Off activity.

The positive relationship between overall road section speed idle time and HEV ICE-Off is as expected, with a coefficient of determination (R^2) of 0.516. Though speed idling explains nearly 52% of the variation in HEV ICE-Off at the road section level, a significant proportion of ICE-Off activity remains unexplained. Figure 25 shows the mean ICE-Off activity during speed idle and non-speed idle (scantool speed $\geq$ 2 kph) for all HEV data for each road section. On average across the three road sections (excluding Freeway), the ICE was off between 87% and 98% of the time during speed idle activity, while the ICE was off between 24% to 45% during non-speed idle activity. Overall road section differences in the effect of non-speed idle upon ICE-Off indicate that additional characteristics of the driving conditions experienced within each road section have an impact upon ICE OpMode.

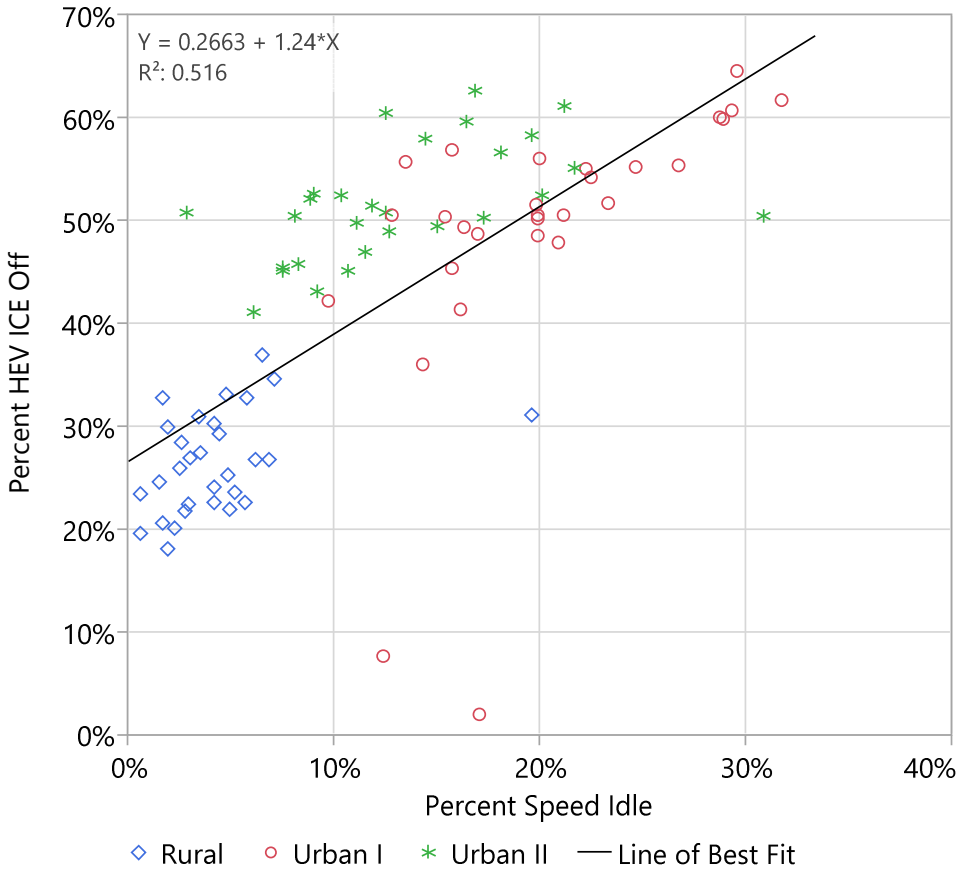

Figure 24. Scatterplot of percent ICE-Off time vs. percent speed idle time for each HEV run by Rural (blue), Urban I (red) and Urban II (green) road sections. Black line shows the linear regression with the equation shown.

Disaggregate effects of activity upon HEV ICE-Off mode are shown in Figure 26. Plots of mean percent ICE-Off for all HEV activity by binned vehicle speed (nearest 5 kph) demonstrate some differences between the road sections. Again, Freeway sections have been removed from analysis.

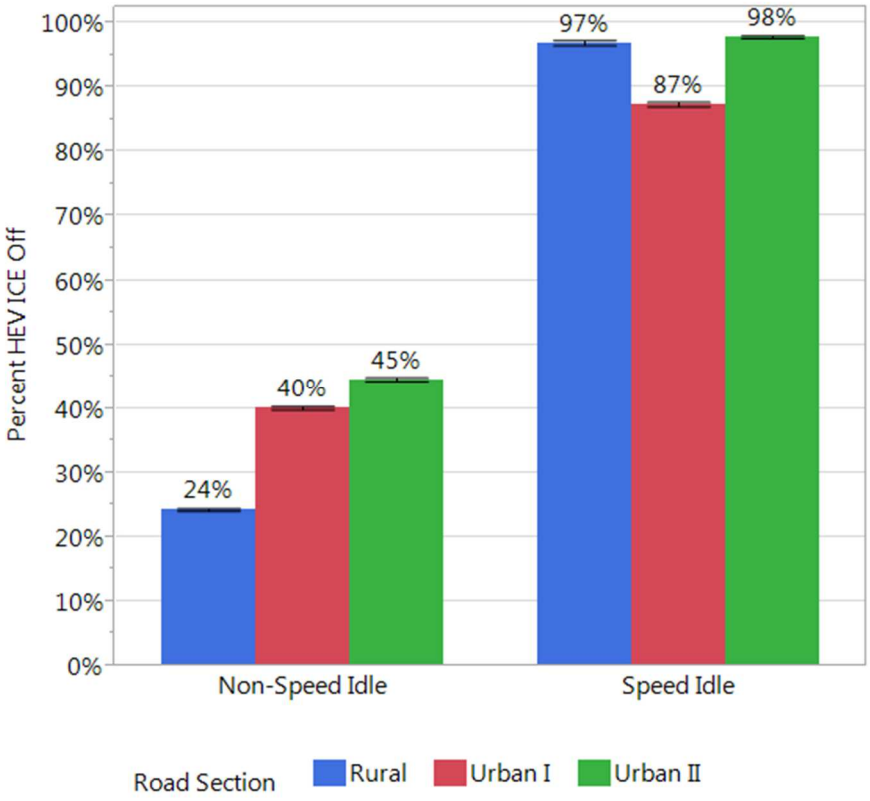

Figure 25. Bar graphs of mean run percent HEV ICE-Off mode for all HEV data during Speed Idle and Non-Speed Idle for three road sections. Error bars are one standard error.

For vehicle 0 to 65 kph speed bins, each road section showed a general trend of decreasing percent of ICE-Off with increasing speed. As mentioned previously, the observed maximum speed while in ICE-Off mode was 65 kph. Analysis of means using t-tests (alpha = 0.05) showed statistically significant differences in percent ICE-Off mode between road sections for each of the 0 to 65 kph speed bins. It is likely that this variation in percent time in ICE-Off mode between road sections is partly explained by differences in the road load (VSP) between road sections occurring within each activity bin. Figure 27 shows bar graphs of mean vehicle acceleration and mean VSP by 5kph speed bin for each road section. In Figure 27, differences in acceleration are

obvious between road sections within each bin, and mean VSP varies considerably as well between road section within each bin.

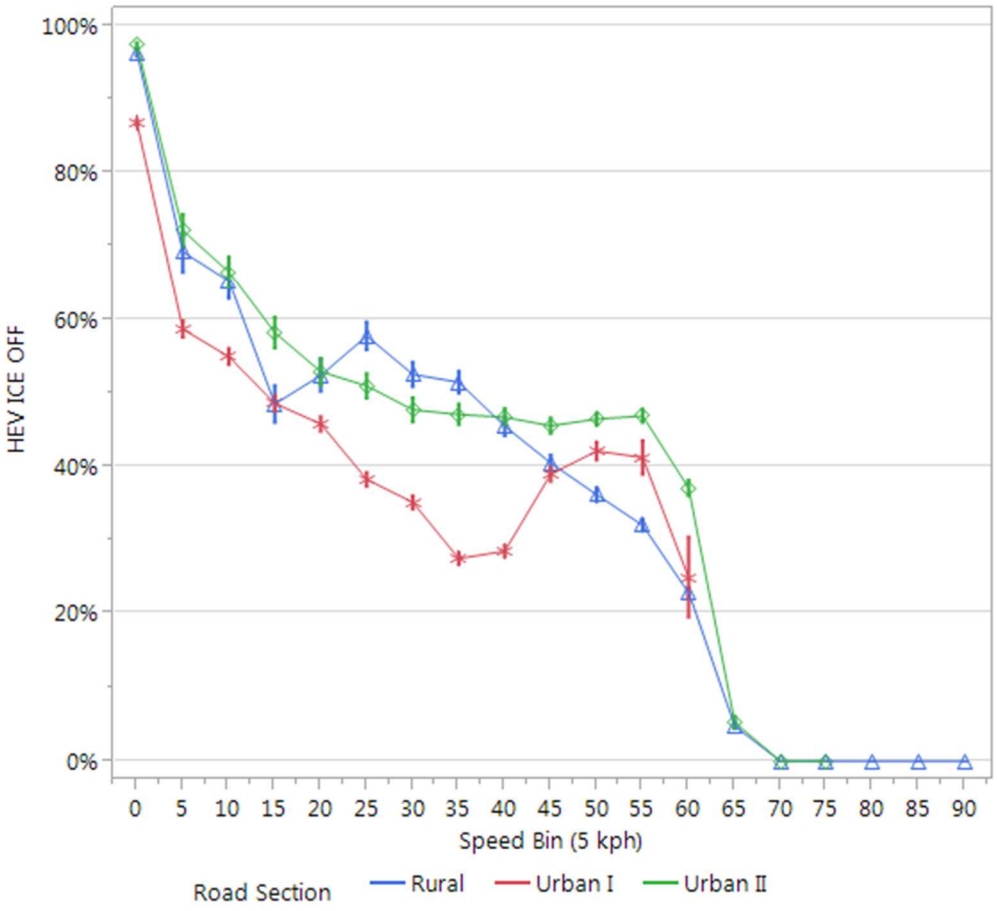

Figure 26. Mean percent time for all HEV data in ICE-Off mode by speed bin (rounded to nearest 5 kph, top) for three road sections. Error bars are one standard error.

Figure 28 shows plots of mean percent HEV ICE-Off and mean vehicle speed by binned VSP (nearest 2 kW/ton) with Freeway driving excluded. This plot shows obvious differences in mean

vehicle speed between the three road section across all VSP bins, with the highest speeds in Rural followed by Urban II and Urban I mean speeds. Differences between Rural road section mean percent HEV ICE-Off and Urban I and Urban II percent HEV ICE-Off are seen in VSP bins < 0, but in VSP bins 0 – 10 the differences between road sections were minimized. Lower Rural road section percent HEV ICE-Off values compared to Urban I and II values in VSP bins < 0 are likely the result of higher overall Rural speeds, which potentially exceeded the 65 kph maximum ICE-off threshold. The larger error bars in the negative VSP bins are attributable to smaller sample sizes within these bins compared with higher magnitude bins. While percent HEV ICE-Off remained relatively unchanged in negative VSP bins, VSP bin 0 kW/ton is shown to be the break point in HEV ICE-Off activity, with a decreasing trend in HEV ICE-Off from VSP bin 0 to 10. Above VSP bin 10, the proportion of HEV ICE-Off operation diminished to zero for all three road sections. Figure 27 and Figure 28 serve to highlight the variation in speed, grade and acceleration between road sections for each VSP bin. Given that the HEV ICE operation is controlled by a sophisticated fuzzy logic system which takes into consideration multiple parameters, it is likely that these variations in speed, grade and acceleration within the same VSP bin across road sections can have an impact upon the HEV OpMode distribution, especially in VSP bins below 0 kW/ton.

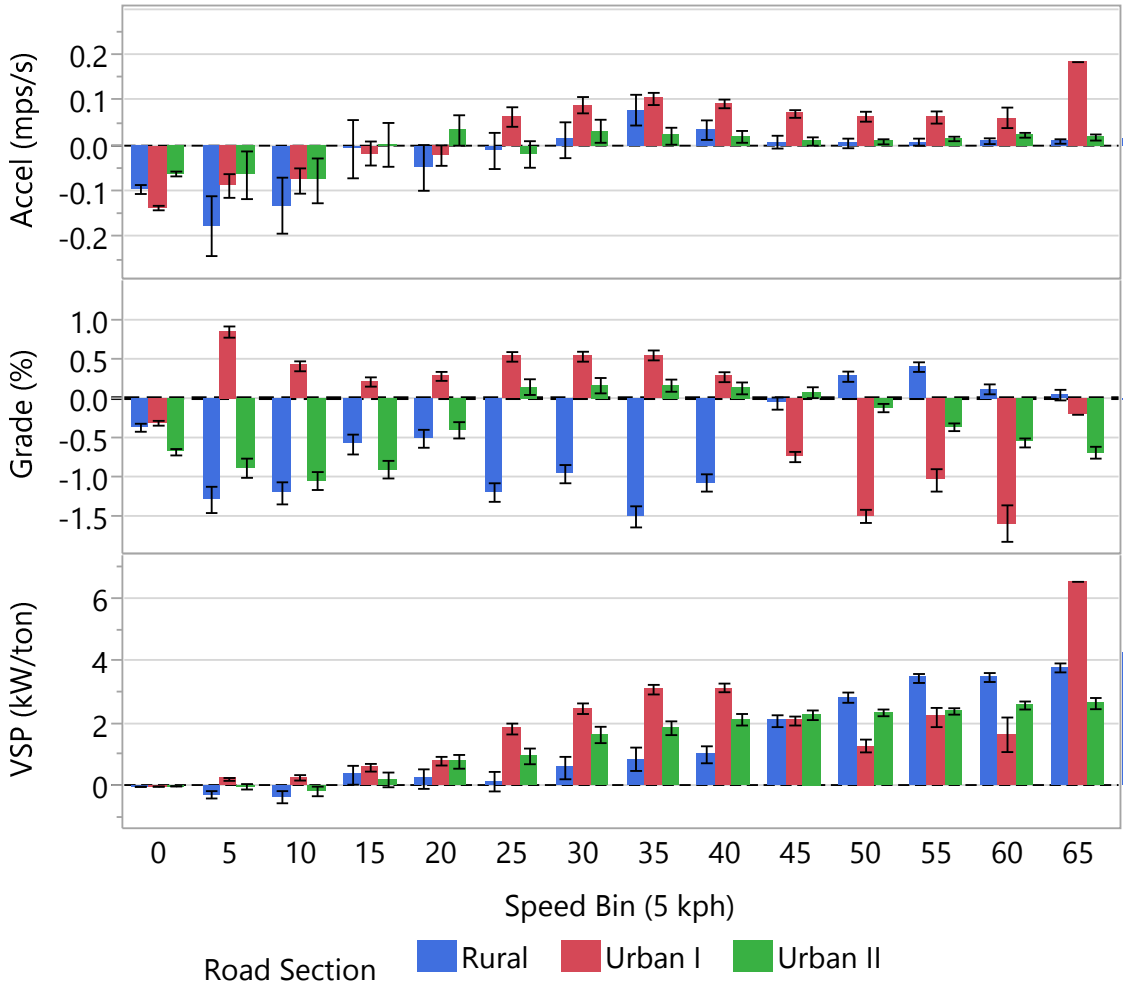

Figure 27. Bar graphs of acceleration (mps/s, top), road grade (percent, middle) and VSP (kW/ton, bottom) for speed bins 0 kph through 65 kph for all HEV data except Freeway driving. Error bars are one standard error.

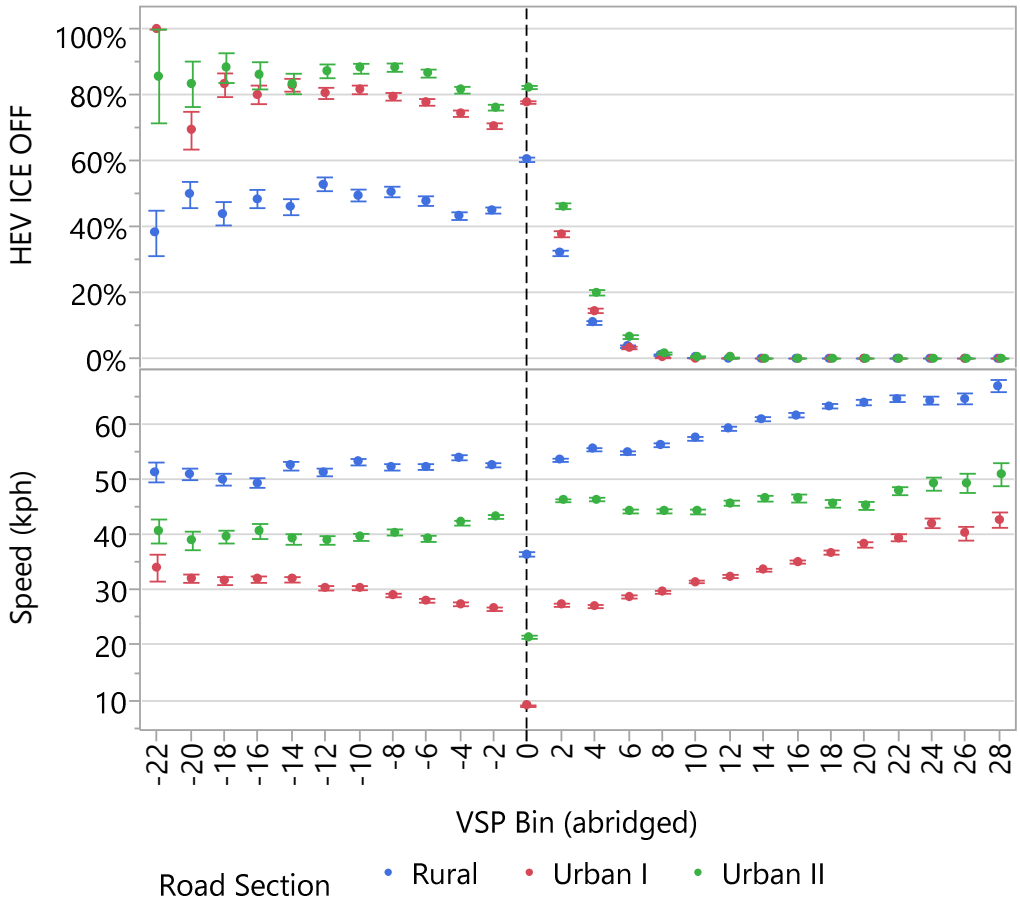

Figure 28. Mean percent time spent in HEV ICE-Off mode (top) and mean speed (bottom) by VSP bin (rounded to nearest 2 kW/ton, bottom) for three road sections. Error bars are one standard error.

Further examination of the distribution of ICE OpModes (combined Shutdown and Off, RIEV and Stabilized) by VSP bin is shown in Figure 29, with the two Urban road sections combined to a single category. Freeway driving is shown to have very little RIEV operation within any VSP bin, attributable to RIEVs being limited to the on-ramp and off-ramp. For Rural and Urban driving, as the combined ICE Shutdown and Off Mode share diminished above VSP bin 0

kW/ton, RIEV mode operation increased and was highest (~23% for Rural and ~41% for Urban) between VSP bin 4 and 6. RIEV mode share above these maxima diminish for both Rural and Urban driving. Of note is the small increase in RIEV mode share at ~bin 26, which consists of a small population (130 records) with RIEV activity in the second, third and fourth second of duration (see Section 5.4.2). This small phenomenon indicates that the first second of RIEVs generally occur at lower VSP, while successive seconds of the RIEV duration (t=2s through t=4s) can occur during higher VSP. This is further explored in Section 6.6.6 below.

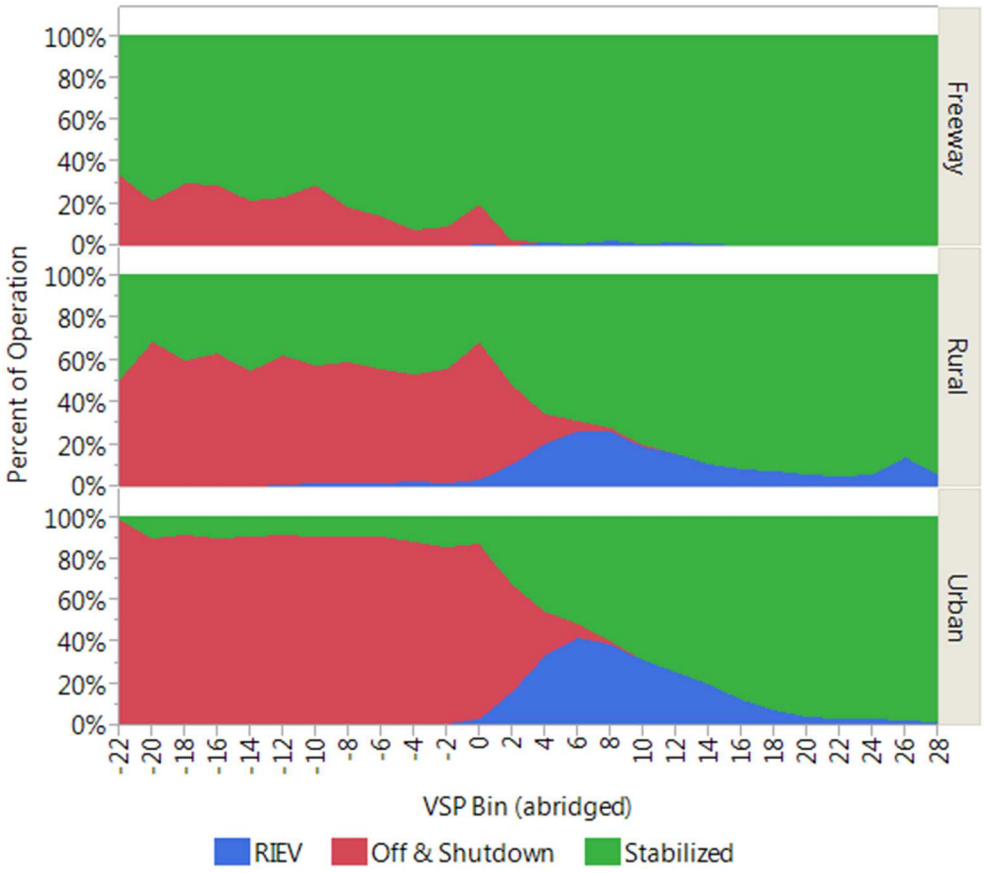

Figure 29. Distribution map of HEV ICE OpModes RIEV (blue), Off and Shutdown (red) and Stabilized (green) by VSP Bin for three road sections.

6.4 RIEV Characterization

6.4.1 RIEV summary

Over the course of 31 HEV runs encompassing 118 road sections of data collection, a total of 3212 RIEVs were recorded and are summarized in Table 12. (See Table H1 in Appendix H for a full summary of RIEVs by run.) Overall, the RIEV frequency (#/hr) was highest during Urban I (133/hr) and Urban II (131/hr) driving, followed by Rural (103/hr) and Freeway (11/hr) driving. Examination of the spatial density of RIEVs, measured as the number events per distance traveled (#RIEVs/km), showed greater differences between Urban I, Urban II and Rural road sections compared with RIEV frequency. Spatially, RIEVs occuring during Urban I driving (5.6/km) were on average 1.7 times more common than Urban II RIEVs (3.3/km) and nearly three times more common than Rural RIEVs (1.9/km). This pattern corresponds to increasing mean speed from Urban I, Urban II an Rural driving and a corresponding decrease in intersection density (see Table 11). Again, all of the 55 RIEVs observed along the Freeway section occurred during either on-ramp (during congested conditions) or off-ramp (deceleration to a stop) driving. Figure 30 demonstrates the relationship between RIEV spatial density (#RIEVs/km) and percent speed idle for 87 road section samples (Freeway excluded). A linear regression ($R^2 = 0.56$) demonstrates the strength of the relationship between RIEV spatial density and percent idle time (%).

Table 12 and Figure 30 demonstrate the relationship between driving conditions and the frequency of RIEVs. The road section with the highest intersection density, Urban I (4.6 intersections per km) had the greatest RIEV mean spatial density (5.61 ± 1.7 #/km) but also considerably greater variation compared with Urban II (1.3 intersections/ km, 3.33 ± 0.71 RIEVs/km) and Rural (0.24 intersections/km, 1.88 ± 0.26 RIEVs/km). While RIEV density appears to correspond with mean speed, other factors which may potentially affect RIEV spatial

density include traffic congestion, where greater volume of vehicles cause more frequent stop and go conditions.

Table 12. Summary of RIEVs by road section.

	Total # RIEVs[A]	Total Time (s)	Total Distance (km)	RIEV Spatial Density Mean and S.D. [B] (#RIEVs/km)	RIEV Frequency Mean and S.D. [A] (#RIEVs/hr)	Intersection Density (# Int./km)
Freeway	55	18623	530.1	0.12 ± 0.07	11.2 ± 4.2	0.06
Rural	938	32741	498.0	1.88 ± 0.26	102.9 ± 23.1	0.24
Urban I	1324	35883	237.8	5.61 ± 1.7	133.8 ± 34.2	4.6
Urban II	895	24565	268.8	3.33 ± 0.71	131.3 ± 28.9	1.3

A. Includes Full and Partial RIEVs.
B. of RIEV spatial density and frequency mean and standard deviation computed from each run (see Table H1 in Appendix H)

One measure of aggregate PN activity is the Total PN emitted, or PN inventory within each road section. PN inventory (#) is computed by integrating PNER across the entire duration of the road section (see Table H2 and Table H3 of Appendix H). One additional measure of the impact of RIEVs upon PN emissions is the proportion of the PN inventory attributable to RIEV activity. In Figure 31, box plots of the portion of PN inventory (as a percent of total) emitted during each HEV road section attributable to RIEV operation are shown. Values for HEV Stabilized On portion of PN inventory, not included in Figure 31, make up virtually all remaining total road section PN. During Urban I driving, with a mean of 5.6 RIEVs/km, an average 60% of the total PN inventory was attributable to RIEV operation. In contrast, under Freeway driving, with an average of 0.1 RIEVs/km, only 5% of total PN inventory was attributed to RIEV operation. These comparisons underscore the general impact of RIEV frequency upon PN emissions and how road type and driving conditions affect HEV PN emissions.

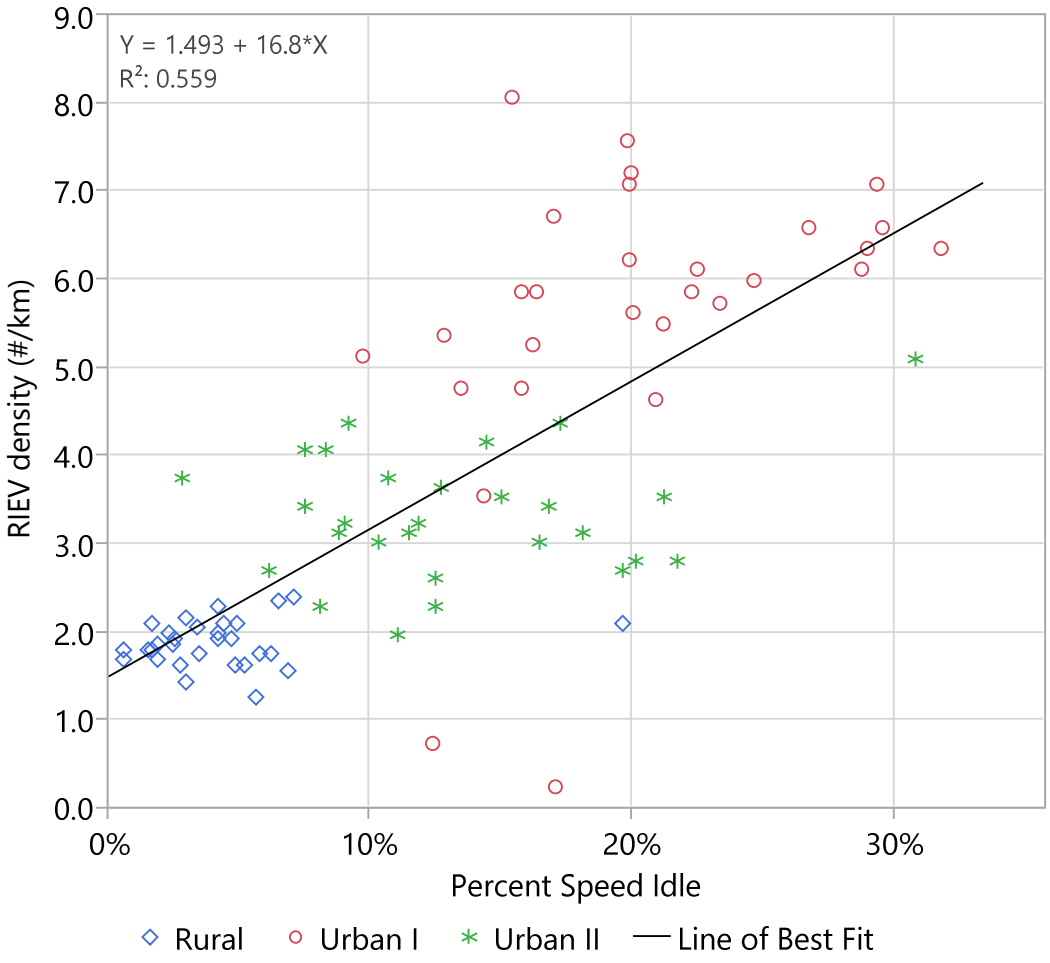

Figure 30. Scatter plot of RIEVs spatial density (#/km) by percent speed idle (Freeway excluded) for 87 road section samples. Line of fit (black line) also shown.

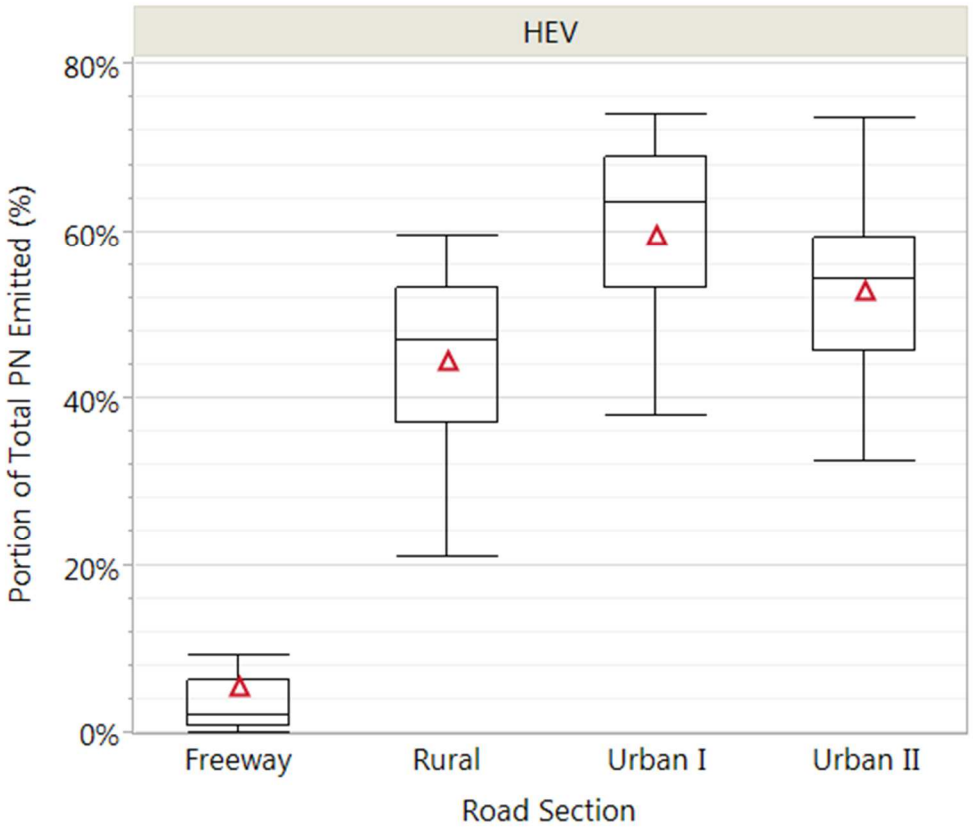

Figure 31. Box plots of portion of PN inventory (% of total) emitted during each HEV run attributable to RIEV operation, by road section. Red triangles indicate the mean RIEV proportion of total PN inventory. N= 31 for Freeway, N = 30 for Rural, N=29 for Urban I and N=28 for Urban II road sections.

6.4.2 Particle Number emissions during RIEVs

A graphical sample of second-by-second HEV PNER for Urban I driving is shown in Figure 32. This time series plot of RPM and PNER shows approximately 140-s of operation and includes eight RIEVs. PNER is represented by the red line and RPM is represented by the blue dotted line. PN emissions attributed to the RIEVs – based upon a four-second duration – is indicated by the vertical green lines under the red PNER trace. Figure 32 demonstrates that HEV RIEV mode

operation is typically associated with high magnitude PNER (HEERs) compared with Stabilized On PNER. Also shown in Figure 32 is a large variation in the magnitude of each RIEV-associated peak PNER in this 140-s sample. Though six of the eight RIEVs had peak PNER magnitude above the $9.3x10^{10}$ HEER threshold, two RIEVs did not result in a HEER. In this example, RIEV peak PNER ranged from $0.25x10^{11}$ to $4.7x10^{11}$ #/s.

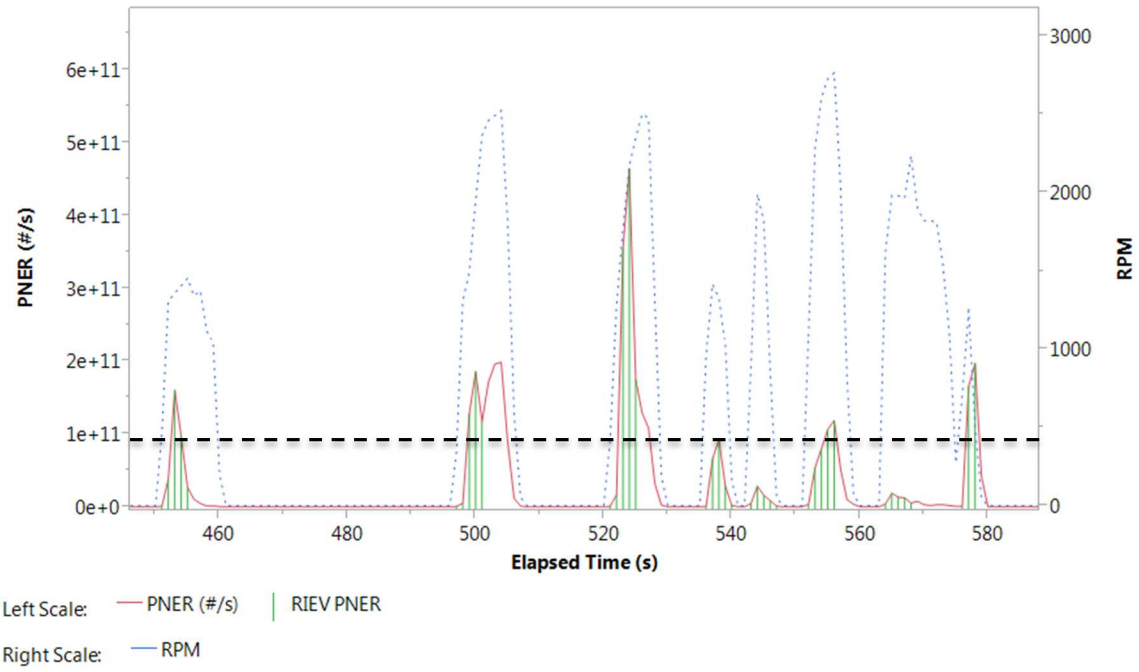

Figure 32. Time series plot during Urban I driving of HEV PNER (red continuous line), RIEV mode operation (green vertical lines) and RPM (blue dotted). HEER threshold of $9.3x10^{10}$#/s indicated by black dashed line.

Examination of the typical PN emissions during RIEVs reveal similar patterns for all road sections. Shown in Figure 33 are box plots of PNER for each second succeeding a re-ignition for all 3212 RIEVs (both Full and Partial). Second zero (t=0) represents the record immediately

preceeding the RIEV. Shown in Figure 33 are the first four seconds (t=1 to t=4) which represent the RIEV- attributed emissions, and an additional six seconds of Stabilized On operation (t=5 to t=10) following a RIEV for comparison of the two modes. Note that the post-RIEV period shown in Figure 33 (t = 5 to t = 10) only includes ICE Stabilized On activity, thus ICE Shutdown or Off modes are excluded. In some RIEV instances, the ICE Shutdown occured before a full four-seconds had transpired. Approximately 87% of all RIEVs reached full four-second duration, while 13% were cut short (truncated) by a shutdown at three, two or 1 seconds. Data from truncated RIEVs are excluded in Figure 33. The purpose of Figure 33 is to demonstrate PNER during typical RIEV activity and the transition to Stablized On activity.

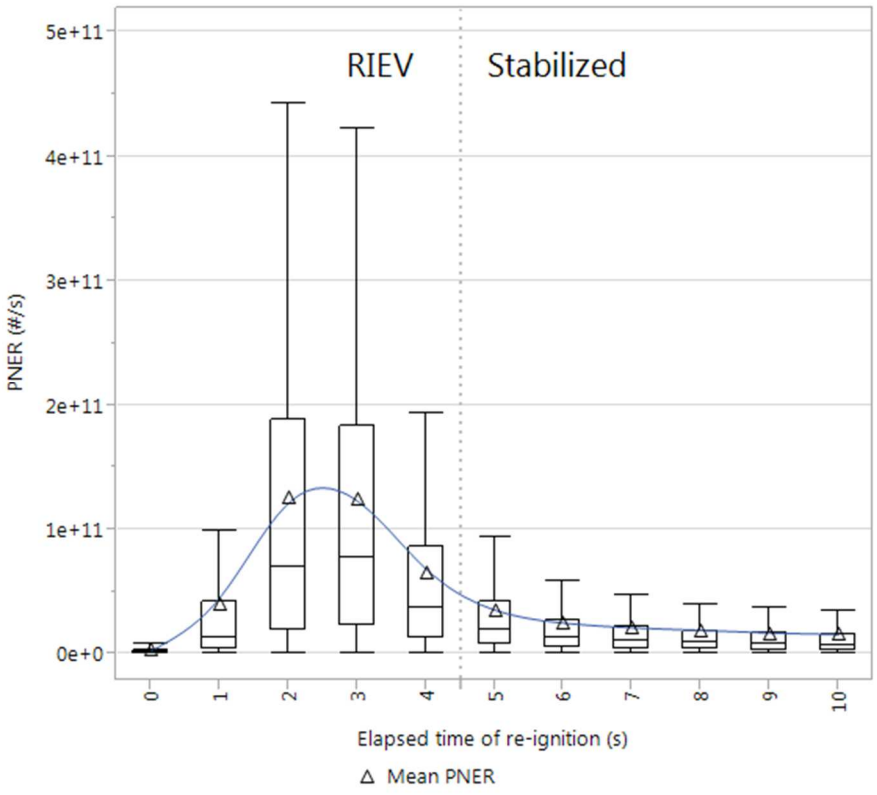

Figure 33. Box plots and means of PNER for each successive second following a typical RIEV.

Peak PNER during all RIEVs typically occurred between t = 2 s and t = 3 s as seen in Figure 33. Overall, mean peak RIEV PNER (1.57 ± 1.66 x10^{11} #/s) occurred at t = 2.5 s. PNER at t = 2.5 s was approximately twice that of t = 4 s (6.49 x10^{11} #/s) and approximately five times PNER at t = 7 s (2.15x10^{11} #/s). Of the 3212 RIEVs observed, approximately 17% were Partial (565) and the remainder Full (2647). A histogram and box plot of Peak PNER for all RIEVs is shown in Figure 34. Forty-eight percent of all RIEV peak PNER fell below the HEER threshold (shown by the red dashed line in Figure 34). Though 52% of RIEV peak PNER records were HEERs (and, as stated earlier in Section 6.2, approximately 65% RIEVs included at least one HEER), a significant proportion of RIEVs were not associated with high magnitude PNER. Further exploration of the factors affecting RIEV PNER and possible explanation for this variation is discussed in Section 6.5.

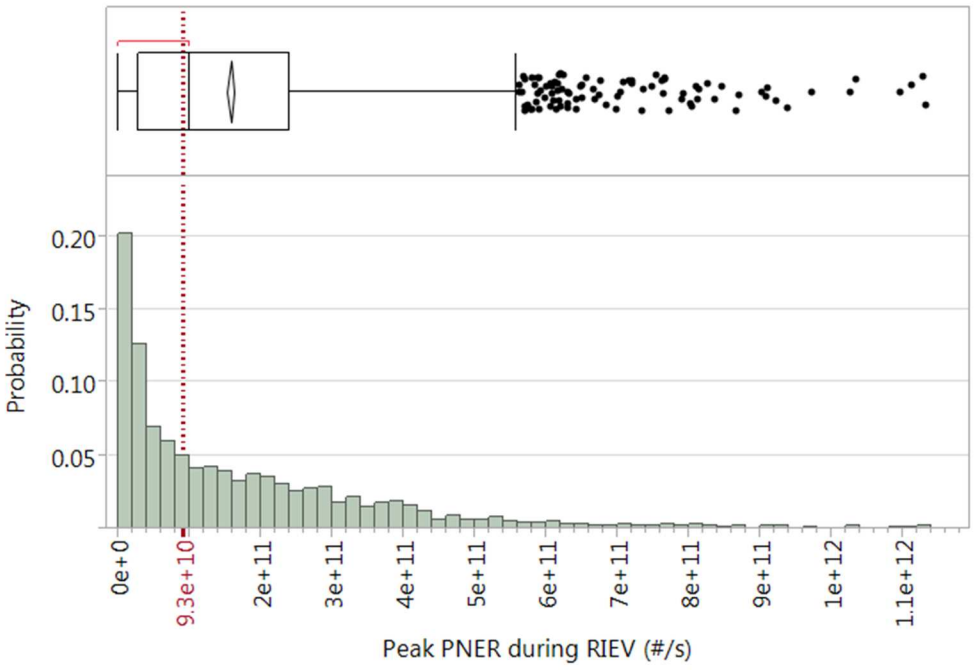

Figure 34. Box Plot and Histogram of Peak RIEV PNER (#/s). The HEER PNER threshold of 9.3x10^{10} #/s is indicated by the red dashed line.

6.5 Factors Affecting Magnitude of RIEV PN Emission Rates

Exploration of the factors affecting PN emission rates following re-ignitions was conducted for each of the 3212 events. As shown earlier, 52% of all RIEVs peak PNER resulted in a HEER, and attempts were made to explain the variation in magnitudes of these peak events. For each RIEV, the value of ambient temperature, ambient relative humidity, speed, acceleration, VSP, battery state of charge (SOC), duration of prior ICE-off time, and exhaust temperature were collected at the second immediately preceding the re-ignition (t = 0; see Section 6.4.2). Correlations between mean RIEV PNER (computed by integrating PNER over the duration of the event divided by the duration, ranging between 1 s and 4 s) and each of the variables listed above are shown in Table 13. (A correlation matrix of all the parameters is shown in Appendix F .) Of all the parameters, only exhaust temperature (p = 0.225) was shown to have a correlation coefficient greater than 0.20.

Table 13. List of parameters measured during each of the 3212 RIEVs and associated correlation coefficients.

Variable	Parameter	Pearson's correlation coefficient (r)
Mean RIEV PNER[A]	#/second	1.000
Speed	kph	-0.079
Acceleration	m/s	0.098
SOC	%	-0.095
Exhaust temperature	°C	0.225
VSP	kW/ton	0.020
Ambient temperature	°C	0.052
Ambient relative humidity	%	0.119
Prior ICE-Off duration	seconds	-0.062

A. Mean RIEV PNER is computed as the total PN (#) emitted divided by the duration of the RIEV (s).

A lack of strong correlation between any of the measured parameters and mean RIEV PNER indicates that there were other factors influencing the magnitude of PNER during RIEVs. One possible explanation is that fuel injected into the cylinders during ICE shutdown did not go through complete combustion, thus during the ICE shutdown process some fuel remained potentially unburned or partially combusted within the cylinders. Upon re-ignition, it is likely that this unburned and partially burned fuel was expelled from the cylinders and resulted in a short duration of high magnitude exhaust particle number concentrations. Further, the variation observed in the mean PNER during RIEVs could be potentially linked to variability in the number of fuel injection pulses executed by the ECU following the ECU 'decision' to shut down the ICE (Yu et al. 2008). Additionally, upon the ECU 'decision' to re-start the ICE, there was likely some variation in the number of strokes, and thus variation in the amount of incompletely combusted fuel injected into the cylinders, required before the re-ignition process was completed and the ICE was fully firing on all four cylinders (Yu et al. 2008). Any combination of these potential variations may have resulted in a quantity, however small, of unburned fuel expelled from the engine during RIEVs and resulted in a HEER. During normal sampling, fuel injection rate (ml/s) was not measured in the HEV, and furthermore, the potential variations in fuel injection described above likely occurred at the sub-hertz level, while this data set was aggregated to 1 Hz. While separate HEV fuel injection data was collected as described in Section 5.4.2, no concurrent PN data was measured. Though a model for HEV fuel injection was developed based upon RPM, it was assumed that this model was temporally too coarse (1 second aggregation) and hence not adequate to accurately represent the total fuel injected during brief shutdown periods. Thus, this lack of sufficient HEV fuel injection data prevents further investigation of these potential explanations of peak PNER during RIEVs.

Though no single variable showed strong correlation with mean RIEV PNER, additional investigation involved the computed variable *duration of ICE-Off prior to the RIEV (*prior duration). For all 3212 RIEVs, the computed prior duration ranged between 0 and 196 s with a mean of 12 s, and 99.5% of prior durations were less than 100 s. Shown in Figure 35 are, from top to bottom, a) a histogram of number of RIEVs, b) a scatter plot of exhaust temperature of RIEV (at t = 0; see Section 6.4.2) and c) a scatterplot of mean PNER of for each RIEV binned by 2-s prior durations under 100 s. The distribution of 2-s ICE-Off prior duration was right skewed, with 90% of all prior durations 32 s or less. As expected, exhaust temperature decreases with increasing prior duration bin, indicating a cooling of the tailpipe system.

While the correlation between mean RIEV PNER and prior duration was extremely weak (p = -0.06), an interesting phenomenon was observed at a finer scale. Figure 36 shows a) the percent frequency of RIEVs and b) the mean PNER for prior duration 32 sec and under. Notably, approximately 17% of all RIEVs were Partial (bin 0-s, effectively no prior ICE-Off duration) and the mean Partial RIEV PNER appears to be higher magnitude than PNER resulting from bins 1-s through 6-s. A unique non-linear trend was observed for prior ICE-Off durations ranging between 1 and 10-s. Mean RIEV PNER appears to reach a second maxima at around 10-s and then continues to decrease with greater ICE-Off duration beyond 10-s.

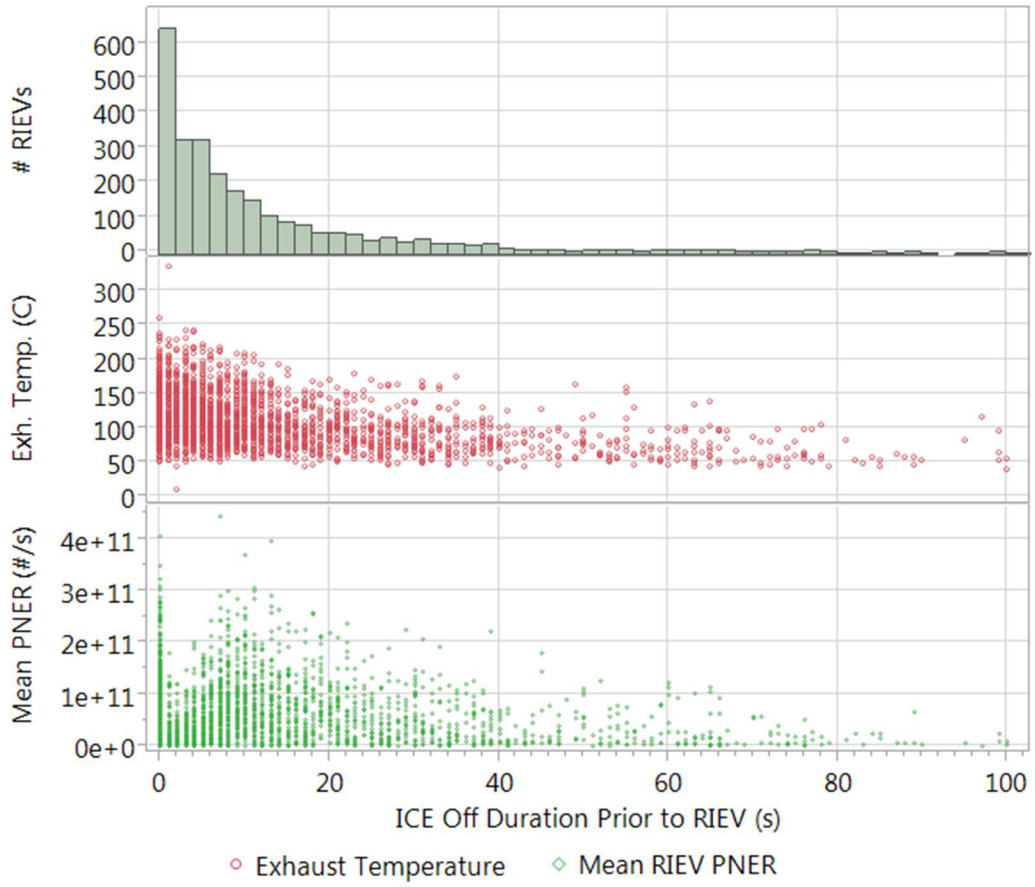

Figure 35. From top to bottom: a) Histogram of RIEVs , b) Scatter plot of exhaust temperature immediately prior to RIEV (°C), and c) Scatterplot of mean RIEV PNER (#/s), binned by prior ICE-Off duration (2 seconds). Note RIEVs with prior ICE-Off durations greater than 100 s are excluded.

The overall non-linear pattern described above - a high magnitude PNER for 0-s bin prior ICE shutdown, followed by a trough and second peak at ~ 10-s - suggests that specific ranges of ICE-Off duration are optimal for reduced PN emissions while others are not. Here, we see that partial RIEVs (representing 17% of all RIEVs), and the RIEVs with ICE-Off periods between 6-s and 15-s (representing 25% of all RIEVs), were in general high emitting (8.49 ± 7.08 x 10^{10} #/s and

8.15 ± 6.44 x 10^{10} #/s, repsectively), while RIEVs with ICE-Off prior duration ranging from 1-s and 5-s (30% of all RIEVs) had a mean PNER, on average, three to four times lower (2.41 ± 3.13 x 10^{10} #/s). Categorizing prior ICE-Off duration into four bin groups – 0-s, 1-s to 5-s, 6-s to 15-s, and greater than 16-s - student t-tests (alpha = 0.05) were computed between each pair of groups. A box plot of PNER for the four bin groups, each group mean and overall mean (5.7 x 10^{10} #/s) is shown Figure 37 as well as the t-test results, with a null hypothesis of unequal means between each pair of groups. Overlapping circles in Figure 37 indicate pairs of groups where the null hypothesis cannot be rejected. The results of these t-tests showed statistically different PNER means for three of the four groups (acceptance of the null hypothesis), with 0-s (Partial RIEVs) and the 6s - 15 s groups not being found statistically different from each other.

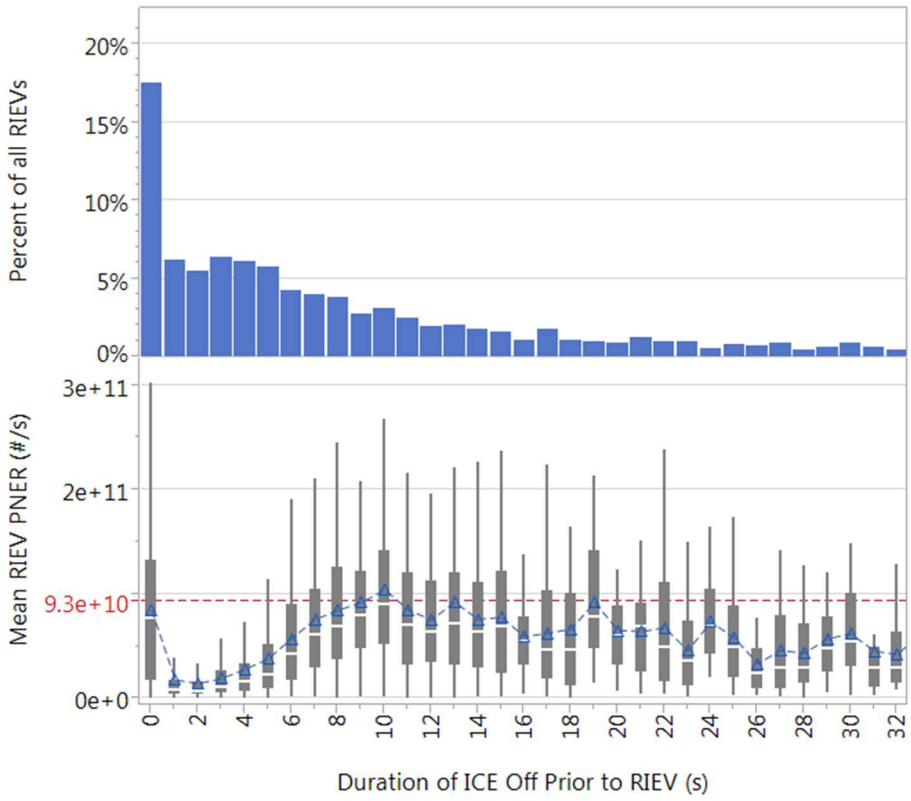

Figure 36. A) Percent of all RIEVs (top) and B) Box Plots of mean RIEV PNER (bottom) for each bin of ICE-off duration prior to RIEV (nearest 1-s). Note 1) HEER threshold of 9.3 x 10^{10} (#/s) is indicated by red dashed line, and 2) mean PNER for each prior duration bin indicated by blue triangle. Prior duration bins greater than 32 s are excluded.

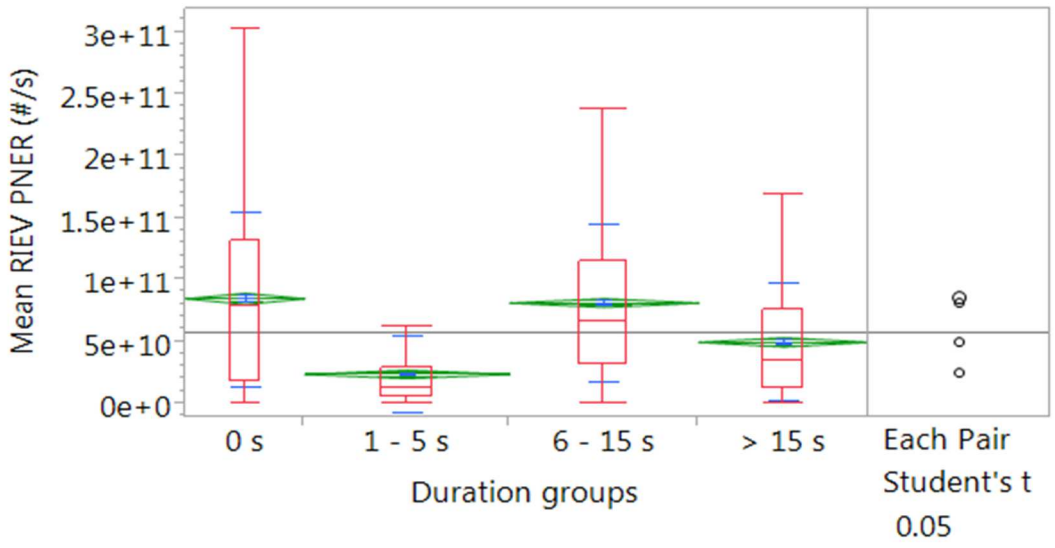

Figure 37. Box plots (red) of Mean RIEV PNER (#/s) by four groups of Prior Duration ICE-Off groups. Overall mean RIEV PNER of 5.72 x 10^{10} #/s indicated on plot by the black horizontal line, with blue hash marks indicating quartiles of each road section.

Note: Green diamonds and black circles show the range between upper and lower 95th percentile interval around the mean, with non- overlapping circles indicating significantly different means.

While the potential causes of the PNER pattern described above remain unexplored here and while this pattern may be unique to the Toyota Hybrid Synergy Drive system, it is clear that shifts in prior ICE-Off durations towards the 1-s to 5-s range could result in significant reductions in overall RIEV PN emissions. The fuzzy logic employed by the ECU to manage ICE operation is likely in part designed to optimize fuel conservation by extending ICE-Off duration for as long as possible during low road load demand and zero speed events. In the likely event that the U.S. EPA follows the European trend and eventually adopts particulate number tailpipe regulations, the evidence presented here of these patterns of high PNER during specific intervals of prior ICE-Off durations will be important in future design of hybrid technologies.

6.6 Comparison of Performance Between Vehicles

Overall comparisons between vehicles and between road section was conducted using mean emission factors as well as emission rate analyses by ICE OpMode and by VSP bins. For each run and road section, Total PN (#) and Fuel Consumption (ml) are tabulated in Table H1 and H2 in Appendix H

6.6.1 VSP , Engine Speed and Calculated Engine Loads

As reported earlier, VSP comparisons for overall operation found VSP_{CV} to be between 3% and 12% on average greater than the VSP_{HEV} (see Table 14), largely attributable to the greater mass (10%) of the HEV. Upon examination of HEV ICE OpModes, mean VSP during ICE Shutdown and ICE-Off modes occurred during negative power demand, ranging from -9.3 kW/ton (Freeway) to -1.1 kW/ton (Urban II). In comparison, HEV Stabilized and RIEV modes occurred at higher overall mean power demand, with similar mean VSP across all road sections (see Table 14). Freeway driving saw the highest power demand during RIEV and Stabilized modes (8.1kW/ton). VSP for RIEV and Stabilized modes for the remaining three road sections were on average lower and similar, with overall differences between modes no greater than 20%. In a comparison between vehicles, HEV Stabilized On showed greater power demand than CV Stabilized On (essentially all CV operation) in the three non-Freeway road sections. VSP was on average 2.0, 4.4 and 3.8 times greater during HEV Stabilized On operation than CV Stabilized On for Rural, Urban I and Urban II driving, respectively (see Table 14). During Freeway driving, where the HEV almost exclusively ran in Stabilized On mode, CV and HEV Stabilized On modes on average operated under similar road loads (8.4 kW/ton and 8.1 kW/ton, respectively).

Table 14. Summary of mean and standard deviation of VSP, RPM and PNER by ICE OpMode and Road Section.

Vehicle Specific Power (kW/ton)

ICE OpMode	Freeway	Rural	Urban 1	Urban II	All Sections
HEV Off	-5.6 ± 6.8	-3.2 ± 5.7	-2.5 ± 4.7	-1.8 ± 4.1	-2.4 ± 4.9
HEV Shutdown	-9.3 ± 9.9	-4.1 ± 9.9	-2.1 ± 4.2	-1.1 ± 4.1	-2.5 ± 5.7
HEV Stabilized On	8.1 ± 9.9	6.0 ± 9.6	6.4 ± 7.4	6.7 ± 6.5	6.8 ± 9.0
HEV RIEV	8.1 ± 4.9	6.7 ± 5.9	5.8 ± 4.1	6.0 ± 4.0	6.2 ± 4.7
HEV all operation	7.47 ± 10.2	3.18 ± 9.33	1.40 ± 7.03	1.74 ± 6.35	3.0 ± 8.5
CV all operation	8.41 ± 11.2	3.34 ± 10.0	1.44 ± 7.28	1.82 ± 6.79	3.2 ± 9.2

Engine Speed (RPM)

	Freeway	Rural	Urban 1	Urban II	All Sections
HEV Off	0	0	0	0	0
HEV Shutdown	247 ± 223	262 ± 237	268 ± 243	264 ± 240	264 ± 240
HEV Stabilized On	1931 ± 726	1656 ± 635	1532 ± 542	1601 ± 534	1713 ± 656
HEV RIEV	1453 ± 594	1400 ± 603	1270 ± 502	1320 ± 507	1325 ± 540
HEV all operation	1839 ± 812	1121 ± 905	656 ± 797	650 ± 816	988 ± 941
CV all operation	2112 ± 428	1582 ± 523	1302 ± 513	1362 ± 450	1526 ± 564

Particle Number Emission Rate (#/s x10^{10})

	Freeway	Rural	Urban 1	Urban II	All Sections
HEV Off	0	0	0	0	0
HEV Shutdown	0.35 ± 1.39	0.78 ± 2.28	0.57 ± 1.70	0.61 ± 1.55	0.64 ± 1.85
HEV Stabilized On	1.31 ± 2.35	1.89 ± 4.20	1.90 ± 3.81	2.53 ± 6.24	1.79 ± 3.99
HEV RIEV	5.50 ± 9.60	8.40 ± 13.4	6.90 ± 11.5	6.31 ± 10.2	7.15 ± 11.7
HEV all operation	**1.30 ± 2.56**	**2.04 ± 5.96**	**1.59 ± 5.36**	**1.61 ± 5.47**	**1.68 ± 5.23**
CV all operation	**3.16 ± 8.14**	**1.93 ± 6.19**	**0.70 ± 4.16**	**1.13 ± 1.10**	**1.55 ± 7.47**

6.6.2 Comparisons of PN Emission Rates by OpMode

PNER varied considerably across HEV ICE OpModes as seen in Table 14. As expected, mean PNER during off mode was zero (no exhaust flow was emitted when RPM was zero), while PNER during shutdown mode ranged between 0.35 and 0.78 x10^{10} #/s (see Table 14). Mean road section HEV Stabilized On PNER ranged from 1.31 to 2.53 x 10^{10} #/s and mean RIEV PNER ranged from 5.50 to 8.40 x 10^{10} #/s. On average, RIEV PNER was between 2.5 and 4.4 times greater than HEV Stabilized PNER for all road sections. A comparison of mean PNER for all records within each OpMode (Shutdown and Off are combined) across the four road sections is shown in Figure 38.

Overall differences in mean CV (Stabilized On) PNER by road sections was expected, as higher VSP in general is associated with increases in PNER. Mean CV PNER was greatest during Freeway driving (3.16 x 10^{10} #/s) followed by Rural driving (1.93 x 10^{10} #/s) and Urban I and II driving (0.70 and 1.13 x 10^{10} #/s, respectively). CV VSP was highest overall for Freeway, followed by Rural and Urban driving. This relationship, however, did not hold true for the HEV Stabilized On. HEV Stabilized On Freeway operation, with the highest VSP, showed the lowest PNER (1.31 x 10^{10} #/s), while Rural, Urban I and II operation, with the lower mean VSP, showed higher mean PNER (1.89 to 2.53 x 10^{10} #/s).

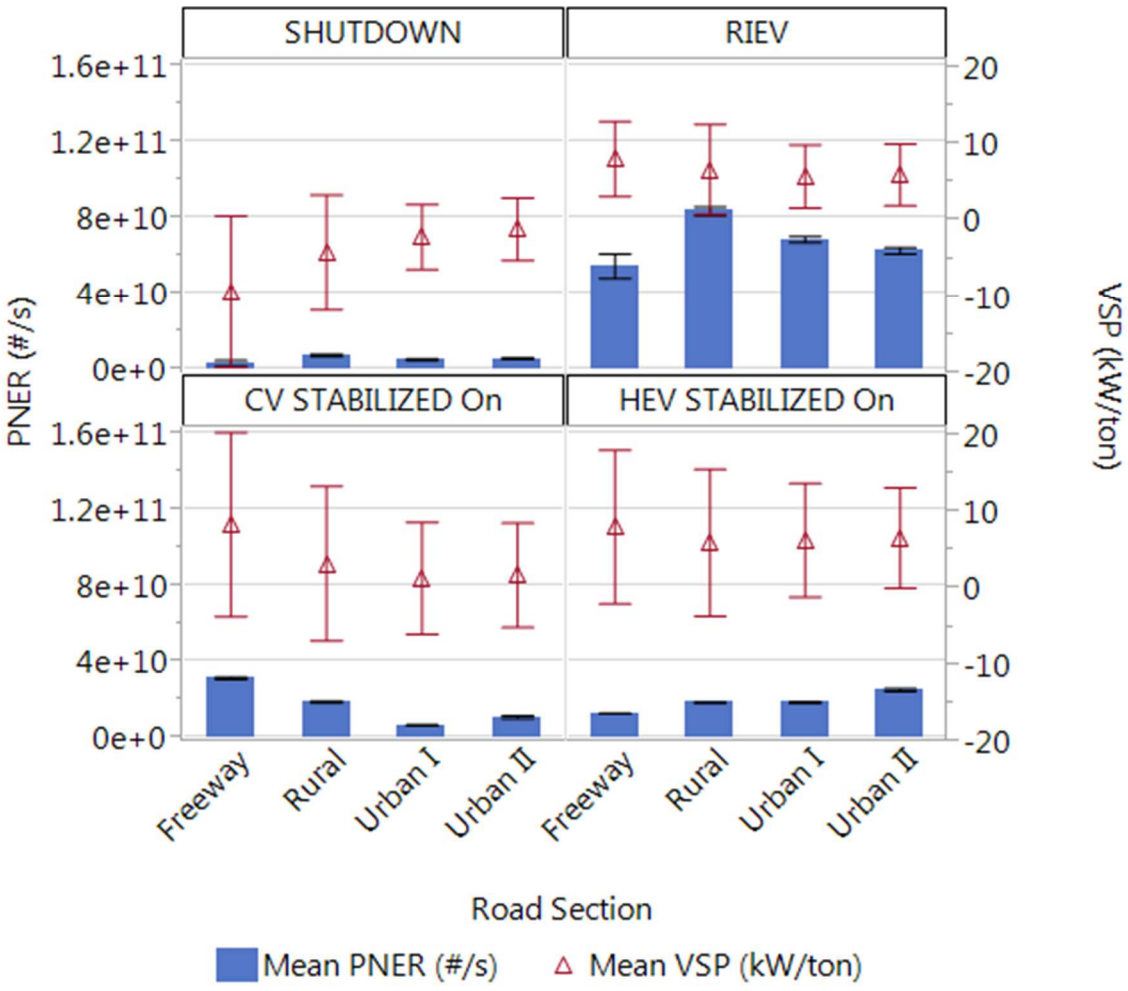

Figure 38. Bar graph of mean PNER (blue) and mean VSP (red triangle) by ICE OpMode for each road section. Standard error bars are shown for mean PNER in black and standard deviation bars are shown for VSP in red.

While further investigation of the causes in the unexpected relationship between VSP and PNER for the HEV Stabilized On operation is not conducted here, one possible explanation may be the amount of power supplied by the battery electric system (BES) to meet the instantaneous road load demands. While the quantity of power supplied by the BES remains unquantified, the Toyota

HSD® system uses the BES to supplement the ICE during accelerations (Kawahashi 2004), thus reducing the overall engine load required to meet the road load, creating a buffer effect. It is possible that the amount of buffering that occurred during different activity, such as high speed Freeway driving versus low speed Urban driving, was variable, and thus may have affected the actual engine load and, consequently, PNER. Thus, any significant modal comparisons between the vehicles while the ICE is on (both Stabilized on and RIEV) should involve an investigation into the quantification of the "hybridization factor" (Holder and Gover 2006).

6.6.3 Comparisons of overall vehicle mean PNER

Table 15 shows the results of the student t-tests with connecting letters report for PNER by road section (levels) for all operation in each vehicle. For the CV, significant differences in PNER means existed between all road sections, and for the HEV significant differences existed between all HEV means except between the Urban I and Urban II road sections.

Table 16 shows results of Student t-tests comparing means of each vehicle for each road section. CV PN emission rates were relatively greater than HEV during Freeway driving, with $PNER_{CV}$ on average 2.4 times greater than $PNER_{HEV}$. Under Urban I and Urban II driving, the relationship was reversed, with $PNER_{HEV}$ on average 2.4 and 1.4 times greater than $PNER_{CV}$, respectively. During Rural driving, PNER was similar between vehicles (CV =1.93 x 10^{10} #/s, HEV= 2.04 x 10^{10} #/s).

Table 15. Connecting letters report of student t-tests (alpha=0.05) comparing PNER means of each Road Section (levels) for the CV (top) and the HEV (bottom).

CV Road Sections	Connecting Letters[A]	Mean PNER (#/s)
Freeway	A	3.16e+10
Rural	B	1.93e+10
Urban II	C	1.13e+10
Urban I	D	6.95e+09
HEV[B] Road Sections	**Connecting Letters**	**Mean PNER (#/s)**
Rural	A	2.04e+10
Urban II	B	1.61e+10
Urban I	B	1.59e+10
Freeway	C	1.30e+10

A. levels (road sections) not connected by same letter have significantly different means.

B. HEV activity includes all OpModes.

Table 16. Student t-test results comparing vehicle PNER means for each road section. (alpha = 0.05).

Road Section	t-ratio	Prob. > |t|	Overall PNER Difference[A]	Relative PNER Difference[B]
Freeway	-29.49	<0.0001	-1.86e+10	-59%
Rural	2.20	0.028	1.08e+09	6%
Urban I	24.02	<0.0001	8.90e+09	78%
Urban II	6.14	<0.0001	4.88e+09	70%

A. Overall PNER difference equals mean CV all operation PNER subtracted from mean HEV all operation PNER (#/s) from Table 15.

B. Relative PNER difference equals the Overall PNER difference divided by the mean CV PNER multiplied by 100%.

For all operation during each road section, as seen in Table 14 the PN emission benefits of the HEV during Freeway driving, where the HEV acts most like a conventional vehicle, are attributed here to the relative lack of re-ignition events and power obtained from the HEV BES. During Urban driving the HEV PN emission benefit is lost, however, despite the significantly large portions of ICE-Off activity with no PN emitted. During Urban I and II driving, the relatively greater average PNER of the HEV compared to the CV is attributable to the frequent RIEVs with HEERs. Rural driving, overall, as expected, seems to straddle the relative PNER difference between vehicles of the Freeway (-59%) and Urban I and Urban II road sections (78% and 70%, respectively). only 6% greater overall CV PNER compared to that of the HEV difference between each vehicle (see Table 16). The difference in vehicle PNER means (all operation) was statistically significant for road sections (see Table 16).

6.6.4 PN Emission Factors

Table 17 and Figure 39 show the comparison of overall PN emission factors (PNEF) and fuel consumption (FC) by vehicle and road section. (Note both PNEF [#/km] and FC [L/100 km] are computed based upon 100-m chainage bins; see Equations 5.15 and 5.16.) While PNER allows for comparison of disaggregate temporal activity, PNEF and FC provide comparisons of aggregate activity in a spatial context. Though the independence of data aggregated within each 100-m chainage bin is in question due to the repeated across all runs, it is assumed here that activity in every 100-m chainage bin are sufficiently independent from all other 100-m bins. Plots of mean vehicle PNEF for each 100-m chainage bin are shown for each road section in Appendix I

Overall road section mean PNEF (#/km) for the CV ranged from 1.02 to 1.28 x 10^{12} #/km while that of the HEV ranged from 0.46 to 2.36 x 10^{12} #/km. Comparisons between vehicles by road section, as expected, reflected similar PNEF relationships as observed for the PNER comparison

between vehicles. During Freeway, driving mean $PNEF_{CV}$ as 2.4 times greater than that of mean $PNEF_{HEV}$, while during Urban I and Urban II driving the relationship was reversed, with mean $PNEF_{HEV}$ 2.3 times and 1.4 times greater than that of mean $PNEF_{CV}$, respectively. By comparison, overall mean Rural PNEF (CV=1.28 x 10^{12} #/km, HEV=1.34 x 10^{12} #/km) were relatively similar between vehicles.

Table 17. Mean and One Standard Deviation of PN Emission Factors and Fuel Consumption for each vehicle by road section.

		Freeway	Rural	Urban I	Urban II
PN Emission Factor ($x10^{12}$ #/km)	CV	1.09 ± 2.59	1.28 ± 3.15	1.04 ± 2.84	1.02 ± 7.27
	HEV	0.46 ± 0.75	1.34 ± 2.62	2.36 ± 3.53	1.45 ± 3.18
Fuel Consumption[A] (l/100km)	CV	4.23 ± 2.27	6.21 ± 4.21	11.4 ± 8.48	6.94 ± 6.51
	HEV	3.95 ± 1.30	5.10 ± 2.92	7.28 ± 5.26	4.38 ± 4.06

A. Fuel consumption here is computed using Equations 5.15 and 5.16.

Differences existed, however, in the comparison of PNEF between road sections for each vehicle. Figure 39 shows the overall mean PNEF and FC for each vehicle across each road section. Student t-tests (alpha = 0.05, see Connecting Letters report in Table 18) showed no significant difference in pairs of PNEF means for CV Urban I, Urban II and Freeway driving, with an overall relative difference (computed as the absolute value of the range of all means divided by the smallest mean multiplied by 100%) of 17% between means for all road sections. In contrast, Student t-tests for the HEV showed significant means between all pairs of road sections except Rural and Urban II, with an overall relative difference of 413% in means between all road sections. These results suggest that CV PN emission factors are less sensitive to differences in

road typology and overall speed as compared to those of the HEV. This is not surprising, as the CV ICE power output is designed to accommodate all road loads, while the HEV ICE is coupled with the BES to optimize energy management within different driving conditions.

Table 18. Connecting letters report of Student t-tests (alpha=0.05) comparing PNEF means of each Road Section (levels) for the CV (top) and the HEV (bottom).

CV Road Sections	Connecting Letters[A]	Mean PNEF (#/km)
Rural	A	1.28e+11
Freeway	B	1.09e+11
Urban I	B	1.04e+11
Urban II	B	1.02e+11
HEV Road Sections	**Connecting Letters[A]**	**Mean PNEF (#/km)**
Urban I	A	2.36e+11
Urban II	B	1.45e+11
Rural	B	1.34e+11
Freeway	C	0.45e+11

A. levels (road sections) not connected by same letter have significantly different means.

As expected with the ULEV and SULEV emission ratings of the 2010 Camry CV and HEV, the total range of PNEF for both vehicles across all road sections (0.45 to 2.36 x10^{12} #/km) appears to be 1 to 2 orders of magnitude lower than those of one 1998 highway investigation of road-side measurements (10^{13} to 10^{14} #/km) for purely CV traffic, including a small but not insignificant proportion (5%) of high-emitting diesel trucks (Jamriska and Morawska 2001). The range of PNEF for the CV and HEV in this study also show the two vehicles to be within one order of magnitude of the proposed 2016 European LDV regulations of 6 x 10^{11} #/km. While measured

PN emission factors may vary significantly depending upon the testing equipment and methods, the results from this study suggest that the impact of re-ignitions upon overall HEV PNEF must be taken into consideration under future regulatory schemes.

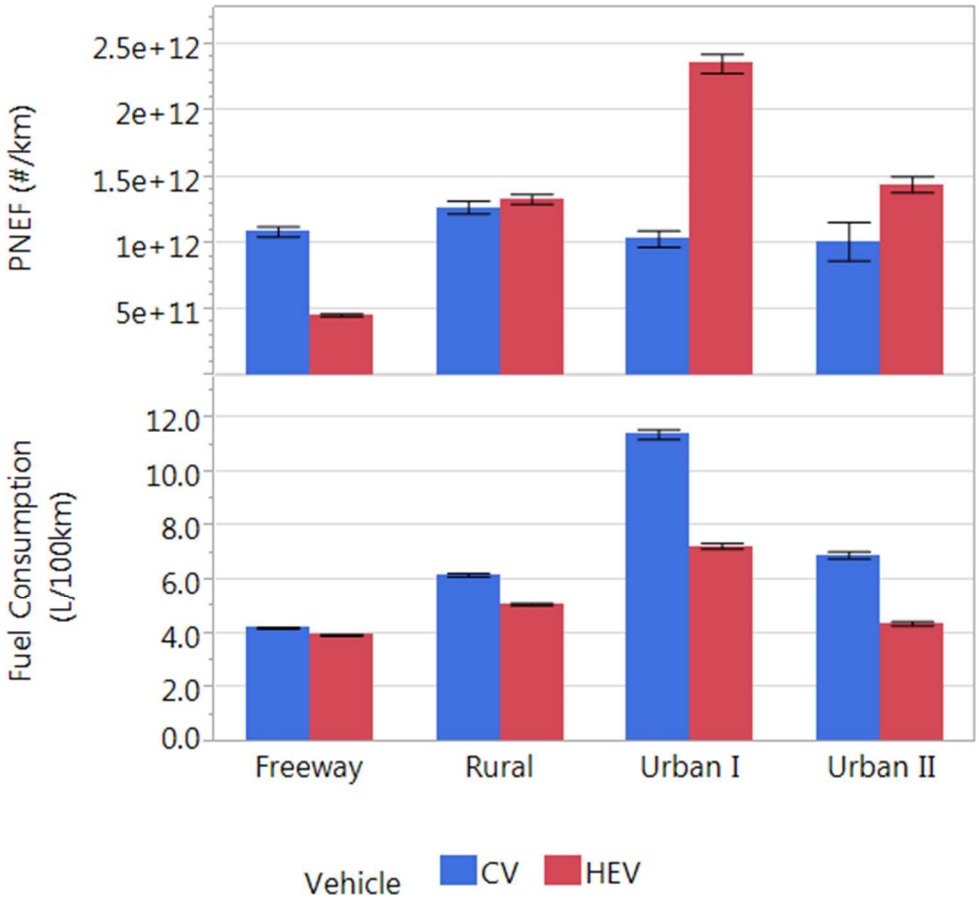

Figure 39. Bar graph of mean PN emission factors and Fuel Consumption by vehicle and road section. Error bars are one standard error.

6.6.5 Fuel Consumption

To provide an additional measure of performance, fuel consumption was compared across road sections and between vehicles (see Table 17). Typical measurement of fuel economy in distance

travelled per unit of fuel (miles per gallon) is common in the U.S., but for the purpose of relative comparison to emission factors, fuel consumption, more commonly used in Europe, is expressed as units of fuel volume consumed per distance travelled, or liters per 100 kilometer (see Eq. 5.15 and Eq. 5.16). As shown in Table 2, the reported, or sticker value 'city' fuel economy of the 2010 Toyota Camry CV is 22 mpg (FC_{CITY} = 10.7 L/100km) and the reported (sticker value) 'highway' fuel economy is 32 mpg (FC_{HWY} = 7.34 L/100 km) (U.S. DOE 2013). The reported 'city' fuel economy of the 2010 Toyota Camry HEV is 33 mpg (FC_{CITY} = 7.11 L/100km) and the reported 'highway' fuel economy is 34 mpg (FC_{HWY} = 6.92 L/100km) (U.S. DOE 2013).

Overall, differences in vehicle computed mean FC were greatest in Urban I and Urban II driving, with FC_{CV} (11.73 and 7.04 L/100km, respectively) on average 1.6 times greater than FC_{HEV} (7.33 and 4.44 L/100 km, respectively). For Rural and Freeway driving, differences between vehicles were diminished, with FC_{CV} only 20% and 7% greater than FC_{HEV}, respectively (see Table 17).

The reported 'city' sticker FC values above (CV = 10.7 L/100 km and HEV = 7.11 L/ 100 km) are similar to Urban I measured FC values in both vehicles (CV = 11.7 L/ 100 km and HEV = 7.33 L/100 km; see Table 17). Reported 'highway' FC above (CV = 7.34 L/100 km and HEV = 6.92 L/ 100 km), however, differ significantly from those measured in Freeway driving (CV = 4.25 and HEV = 3.96 L/100km; see Table 17). The discrepancy in 'highway' sticker FC values and Freeway measured FC values may be due to potential differences in the characteristics of the drive cycle However, the 3% relative difference between vehicles (see Equation 5.17) for sticker value highway FC is similar to the 7% relative difference between vehicles for measured Freeway FC.

The overall differences between vehicle PN emission factors shown in Table 17 and Figure 39 strike a contrast to the fuel conserving benefits of the HEV. Where HEV fuel conserving benefits

are greatest in stop-and-go traffic common to urban driving, these conditions lead to frequent RIEVs with high associated PN emissions. By comparison, during Freeway driving, where operationally the HEV behaved most like the CV, the HEV had similar FC compared to the CV and yet showed a two-fold reduction in mean PNEF compared to the CV.

6.6.6 VSP Modal Comparisons

Graphical examination of the mean PNER by VSP bin (rounded to the nearest whole kW/ton) is helpful in comparing the response of each vehicle under different road loads. As demonstrated in previous sections, mean PNER under RIEV operation was significantly greater than was PNER for Stabilized On operation for either vehicle, and, as shown in Figure 29, RIEV mode share was greatest between VSP bins 4 and 8 kW/ton. To demonstrate the modal differences in RIEVs, Figure 40 shows a plot of the probability of a RIEV occurring within each VSP bin (as a percent of all records in that bin) for each road section. (Note that Urban I and Urban II road sections are combined.) In Figure 40, only the first second of the RIEV (t = 1) is included in the computation of the probability of the RIEV occurring. This plot shows higher likelihood of a RIEV between VSP bin 0 and 10 kW/ton compared with negative VSP bins and VSP bins greater than 10 kW/M) for both Rural and Urban driving. As expected, due to RIEVs being limited to on- and off-ramp, Freeway RIEV probability is lower than Urban and Rural road sections. Peak RIEV probability occurs at VSP bin = 4 kW/ton for both Rural and Urban driving.

In Figure 41, log of mean PNER is plotted by VSP bin across three road sections by vehicle, where Urban I and II have again been combined into one category. In general, mean PNER is seen to range two orders of magnitude between the lowest and highest VSP bins ($\sim 10^9$ to $\sim 10^{11}$ #/s). In VSP bins less than 0 kW/ton, the differences in vehicle PNER appears to range between

less than a half order of magnitude. During Freeway driving, PNER appears least sensitive to VSP, and the HEV is observed to behave most similar to CV of the three road categories. In Rural and Urban driving, the PNER magnitude between VSP bins 0 and 15 kW/ton appeared to increase. In this 0 – 15 VSP bin range, $PNER_{HEV}$ consistently exceeds that of $PNER_{CV}$. This effect of HEV RIEVs is further demonstrated in Figure 42, which shows the mean share of total PN Inventory, as a percent attributed to each VSP bin (-22 kW/ton to 28 kW/ton) for each road section and vehicle, with blue = CV and red = HEV.

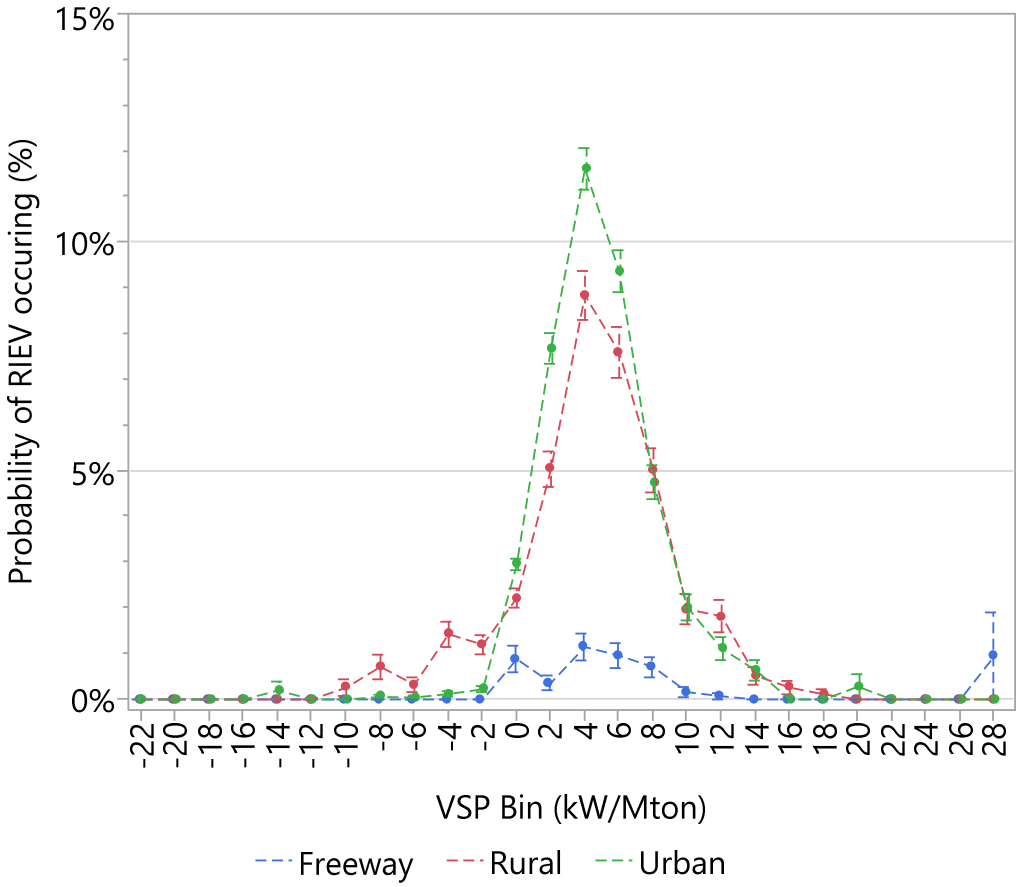

Figure 40. Plot of probability of RIEV occurring as a percent of all records within each VSP bin for Urban, Rural and Freeway driving. Standard error bars shown.

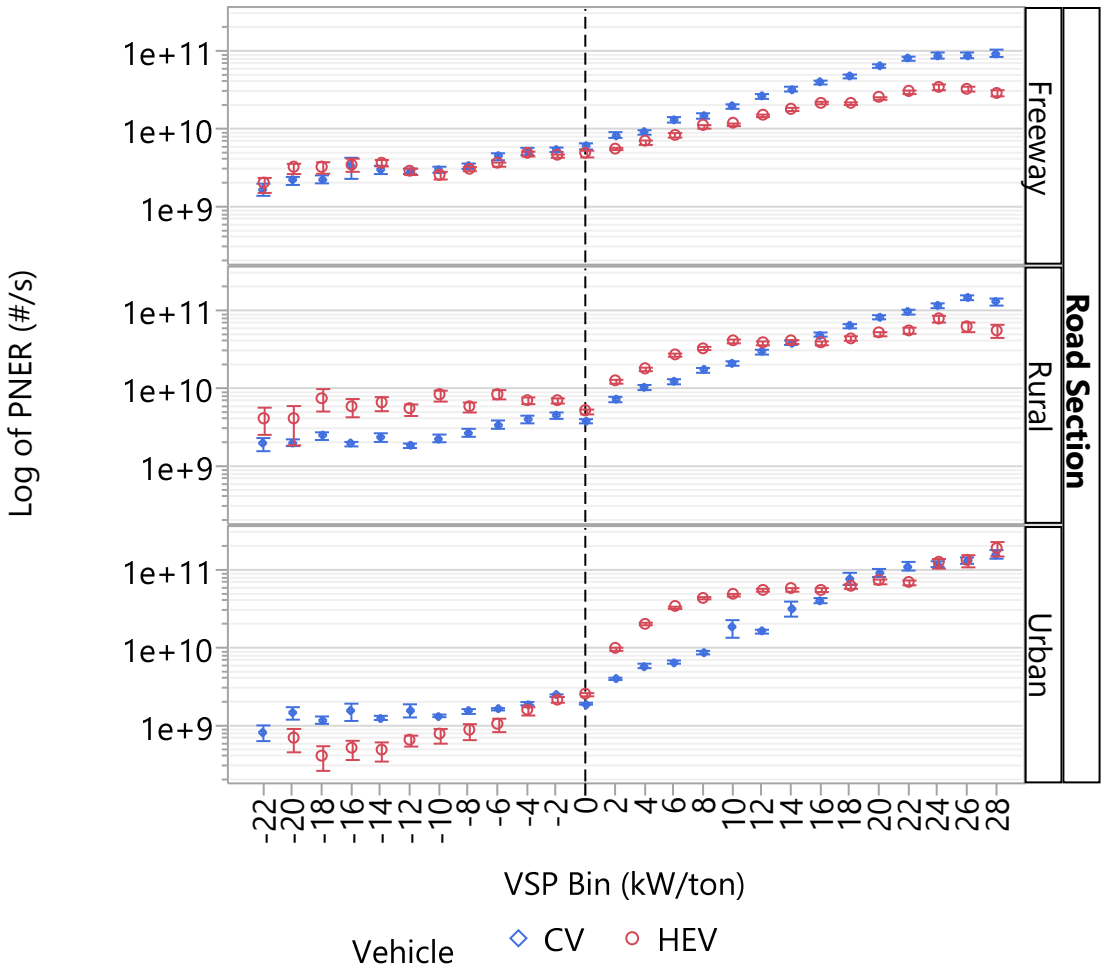

Figure 41. Log of vehicle mean PNER by VSP bin (2 kW/ton) for each road section, with standard error bars. Note Urban I and Urban II road sections are combined.

Figure 42 underscores the range of VSP modes which have the greatest share of PN Inventory for each road section. Under Freeway driving, the vehicles behave most similar operationally, and PN Inventory distribution is also similar between vehicles, with peak VSP bin impact upon PN Inventory between bins 18 and 20 kW/ton. In Urban and to a lesser extent Rural road sections, the VSP bins affected most by RIEV emissions shift in the HEV to lower VSP ranges, between 6 and 10 kW/ton. Urban driving had a narrower distribution and higher peak percent share compared to

Rural and Freeway road sections. For all road categories, the total share of all PN Inventory (%) for VSP bins less than or equal to 0 kW/ton ranged from 5% to 17%. Figure 42 demonstrates the importance of VSP bins greater than 0 kW/ton for both vehicles, which accounts for 83% to 95% of road section PN Inventory. These comparisons again highlight the impact of road section upon PN modal emissions. For future modal modelling efforts of HEV PN emissions, it is likely that building a model of HEV behavior based upon CV activity will be appropriate, with consideration of a hybridization factor and, as a result of the analyses above, a re-ignition factor.

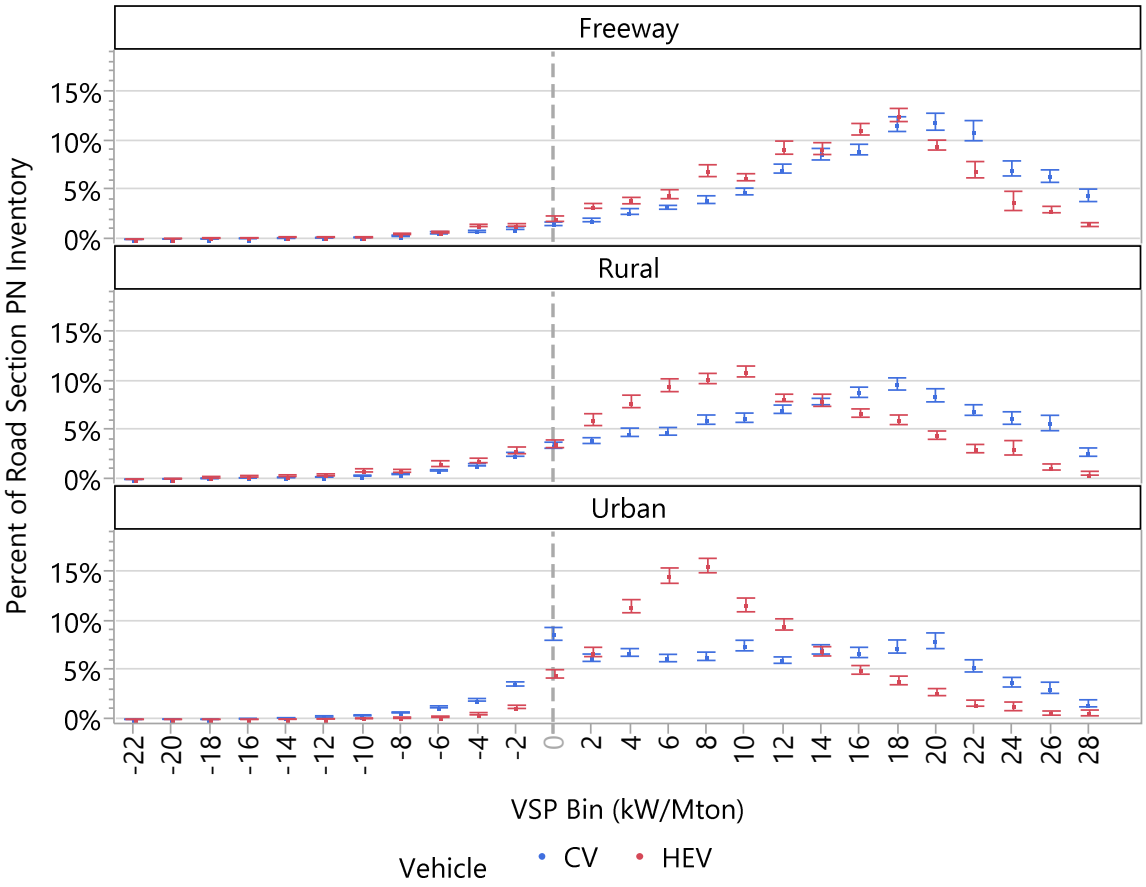

Figure 42. Mean percent share of total PN inventory for each vehicle by VSP bin (rounded to the nerest 2 kW/ton) and by road section. Standard error bars shown.

7 Conclusion

With the increasing popularity of HEVs and their gradual penetration into the U.S. LDV fleet, improved understanding of the unique operation of the HEV drivetrain will be required to effectively model and predict their impact upon emissions inventories under increasingly restrictive fuel efficiency and emission regulations. HEVs have complex coupling between conventional drivetrain components and newer electric propulsion technologies that result in frequent internal combustion engine shutdowns, and subsequent re-ignitions which are associated with high magnitude Particle Number emissions, with potential associated impacts upon health. Traditional means of testing these emissions have relied upon road-side and laboratory studies, but an increasing need exists to study HEV emissions under transient, real-world driving conditions in high temporal resolution and to provide direct comparison with comparable conventional vehicles to better measure relative benefits or liabilities of these new automotive technologies.

In this thesis, a new HEV ICE operational mode framework was developed to define unique on-off modalities, and to characterize the resultant re-ignition events. Average HEV ICE-Off activity by road section varied significantly from only 4% of total Freeway operation to 27% of total rural and 51% of combined total urban operation. Re-ignition events were most frequent in urban driving conditions with approximately 131 - 133 RIEVs hr^{-1} (3.3 - 5.6 km^{-1}) while less frequently associated with rural roadways (103 hr^{-1}, 1.9 km^{-1}) and insignificant during freeway driving (11 hr^{-1}, 0.1 km^{-1}) due to predominantly high speed operation above the ICE-Off threshold of 65 kph. A linear model of percent HEV ICE-Off operation found that overall, 52% of variance was explained by the proportion of total operation spent at idle speeds (<2 kph).

Sixty-five percent of all 3212 RIEVs observed included at least one HEER (record above the 95th percentile of all CV and HEV engine on activity). Characterization of RIEV emissions found that average RIEV PNER was between 2.5 and 4.4 times greater than HEV Stabilized PNER for all road sections. Unexpectedly, no factors measured at the onset of each RIEV were found to have strong explanatory power of the magnitude of the mean PNER during RIEVs. However, a unique non-linear relationship was found between the duration of ICE-Off immediately prior to each RIEV and its mean PNER, with local minima occuring between 1 and 5 seconds of prior ICE-Off and local maxima occuring at 0 seconds (Partial RIEVs) and also between 6 and 12 seconds. Overall, total share particle number inventory emitted during HEV operation associated with re-ignition events on averaged ranged from low of 5% for Freeway driving to a high of 60% for Urban I driving. For future emission benefits, potential retooling of the HEV ECU fuzzy logic control of ICE-Off mode to 1) decrease the likelihood of prior ICE-Off duration at the local PNER maxima, and 2) increase the likelihood of the prior ICE-Off duration at the local PNER minima could result in significant reductions in HEV PN emissions.

Overall comparisons of PN emissions by road section found that Freeway driving resulted in the greatest HEV PN emission benefits, with a mean HEV emission factor on average 2.4 times lower than that of the CV. Conversely, during combined Urban driving, the HEV benefit was lost, with mean HEV PNEF 1.4 to 2.4 times greater than that of the CV. These results contrast the fuel consumption benefits of the HEV during Urban driving (40% lower HEV mean FC than that of the CV) and the reduced HEV benefit during Freeway driving (7% lower mean HEV FC than that of the CV). During Rural driving there was little difference in mean PNEF between vehicles.

Some limitations were observed in this study which may have impacted overall results. An overall decrease in the mean speeds within Freeway and Rural driving resulted in a decrease in

road load from the beginning to the end of the study, likely as a result of the single driver familiarity with the route and adoption of a less aggressive driving style. While this would not necessarily impact modal emissions based upon VSP, it would shift the distribution of VSP modes and potentially could have impacted mean run PN emission factors and rates. Also, assumptions of equal variance among the populations during ANOVA and t-tests may have been violated, and thus the powers of the observations in rejecting or failing to reject null hypotheses may have been diminished. The computed parameter *RIEV spatial density*, with a common denominator based upon the distance travelled along the 100-m chainage bin, may not meet the test of independence of measurements because of the fixed spatial reference of the 100-m chainage bins. Additionally, fuel consumption computations based upon estimated fuel rate regressions from the scantool parameter were not independently validated, and thus analysis may be compromised by unknown factors. However, relative differences in aggregate fuel consumption between vehicles matched that of reported EPA fuel economy "sticker" values, providing some credibility to the comparison of HEV energy benefits by road section. Lastly, while the choice of two Camry vehicles for comparison is logical based upon the popularity of the Toyota hybrid line, and that the Hybrid Synergy Drive platform is shared by over 70% of the HEVs on the road today, it may be challenging to make generalizations about the applicability of the results found in this investigation to all hybrids makes and models.

Despite some of the limitations described above, this body of work presents a thorough introduction to the HEV re-ignition event and a overview of the modal differences between the hybrid and conventional ICE. This thesis also lays the framework for future investigations regarding disaggregate emissions analysis of emerging hybrid-electric automotive technologies. The results found here furthermore suggest that RIEV spatial density is an important factor when comparing overall PN emissions between HEV and CVs, and that this factor becomes more

critical in urban or city driving. The broader implications of RIEVs indicate that HEV PN emissions are more sensitive to different driving conditions than those of conventional vehicles, and HEVs, while demonstrably energy conserving, are not necessarily lower emitting. As it is likely that the U.S. will eventually create regulations governing LDV PN emissions similar to those implemented currently in Europe, the results found here suggest unexpected implications of hybridization upon PN emissions. As LDV HEV model market share increases, it is critical to understand how these differences in emission patterns can potentially impact overall fleet PN emissions as HEVs continue to displace CVs in the global LDV fleet.

8 Future Work

While much groundwork has been presented in this thesis surrounding the nascent understanding of unique HEV ICE operation compared to CV operation, the impact of re-ignitions upon PN emissions and the relative differences in PN emissions between the two vehicle types, further research is necessary to investigate some of the unexplained phenomena as well as to expand upon the understanding of the broader implications of hybridization upon emission. Three general areas of investigation are suggested here.

In this study, a single HEV model and vehicle was used for comparison of PN emissions across a wide range of driving conditions. Expansion of this sample size to include a larger population of HEV models would be necessary to improve the generalization of the ICE HEV operation, and to possibly refine of the OpMode framework to incorporate different hybrid drivetrains other than the Toyota HSD® family of vehicles. In addition, there are likely significant impacts of vehicle condition, specifically the mileage driven, which remain unaccounted for in this study of relatively new vehicles. As vehicles age, it is likely that overall performance deteriorates, and PN emissions are likely to increase with mileage as exhaust systems approach the end of their life cycle and engine components begin to wear out (Wenzel and Ross 1998). Continued development of PEMS, through miniaturization and simplification, that can be more easily transferred between vehicles and dramatically reduce installation time, calibration, data collection and analysis of results will be essential to facilitate expansion of further on-board studies. In addition to expansion of the population of vehicles sampled, a more randomized approach to the route selection would generate independent data measurements when analyzing in spatial frameworks, generating statistical tests with greater significance and broader application.

While not explored fully here, it does appear that HEV ICE OpModes are spatially correlated to specific roadway features such as intersections. HEV ICE OpModes are thus likely predictable and potential models of their likelihood may be generated based upon VSP as well as quantifiable characteristics of the roadway. Furthermore, with the evidence presented here of greater likelihood of RIEVs occurring within specific VSP thresholds, it may be possible to develop dynamic "look ahead" models of RIEVs using measures of road load. With improved vehicle to grid communication, predictive models of vehicle performance such as fuel use are useful in understanding the impact of driver behavior upon emissions and energy use (Ganji and Kouzani 2010; Larsson et al. 2012). Furthermore, a more robust investigation of the hybridization factor to better understand the proportion of BES and ICE power supplied to the wheels would likely improve the modeling of PNER and fuel rates in different modes. While each HEV drivetrain is likely to have a unique hybridization factor and RIEV pattern, future modeling of these phenomena will improve and refine the understanding of factors that potentially impact emissions and energy use.

Lastly, a more thorough examination of the impact of RIEVs upon other pollutants, as well as a more refined approach to studying the factors leading up to each RIEV, is warranted. While CO_2 emission rates likely correlate with fuel rates, criteria pollutants (for example, HC, NOx, and CO), and air toxics with associated carcinogenic effects (for example benzene, formaldehyde, acetaldehyde, 1,3-butadiene) can form as byproducts of incomplete combustion (U.S. EPA 1995). The emission rates of these and other pollutants may be potentially significantly higher during RIEVs, as a result of incomplete combustion processes, than other modes. To develop a better understanding of the potential variation in engine conditions which lead up to each RIEV, it is suggested that a study using higher temporal resolution data be conducted to measure engine parameters, such as fuel injection, which may have the greatest impact upon RIEV emissions of a

variety of pollutants. The results of such a study may, eventually, lead to improved design of the HEV ECU logic systems that control the engine off and on decision-making, and while maintaining fuel conserving benefits, also in balance consider the potential reduction of pollutant emissions resulting from RIEVs.

9 Bibliography

Agus, Emily L., David T. Young, Justin J. N. Lingard, Robert J. Smalley, James E. Tate, Paul S. Goodman, and Alison S. Tomlin. 2007. "Factors Influencing Particle Number Concentrations, Size Distributions and Modal Parameters at a Roof-Level and Roadside Site in Leicester, UK." *Science of The Total Environment* 386 (1–3): 65–82.

Banvait, H., S. Anwar, and Yaobin Chen. 2009. "A Rule-Based Energy Management Strategy for Plug-in Hybrid Electric Vehicle (PHEV)." In *American Control Conference, 2009. ACC '09.*, 3938–43.

Barth, Matthew, John F. Collins, George Scora, Nicole Davis, and Joseph M. Norbeck. 2006. "Measuring and Modeling Emissions from Extremely Low-Emitting Vehicles." *Transportation Research Record: Journal of the Transportation Research Board* 1987: 21–31.

Bayindir, Kamil Çağatay, Mehmet Ali Gözüküçük, and Ahmet Teke. 2011. "A Comprehensive Overview of Hybrid Electric Vehicle: Powertrain Configurations, Powertrain Control Techniques and Electronic Control Units." *Energy Conversion and Management* 52 (2): 1305–13.

Bitsche, Otmar, and Guenter Gutmann. 2004. "Systems for Hybrid Cars." *Journal of Power Sources*, Eighth Ulmer Electrochemische Tage, 127 (1–2): 8–15.

Boriboonsomsin, Kanok, and Matthew Barth. 2009. "Impacts of Road Grade on Fuel Consumption and Carbon Dioxide Emissions Evidenced by Use of Advanced Navigation Systems." *Transportation Research Record: Journal of the Transportation Research Board* 2139: 21–30.

Brandt, E.P., Yanying Wang, and J.W. Grizzle. 2000. "Dynamic Modeling of a Three-Way Catalyst for SI Engine Exhaust Emission Control." *IEEE Transactions on Control Systems Technology* 8 (5): 767–76.

Burtscher, H. 2005. "Physical Characterization of Particulate Emissions from Diesel Engines: A Review." *Journal of Aerosol Science* 36 (7): 896–932.

Car Mart. 2014. "Mazda to Use Hybrid Synergy Drive under License from Toyota." Accessed July 29. http://www.sgcarmart.com/news/article.php?AID=3249.

CCRPC. 2012. "CCRPC - Traffic Data." *Transportation Data - Annual Average Daily Traffic*. http://www.ccrpc.us/data/traffic.php.

Chaturvedi, N.A, R. Klein, J. Christensen, J. Ahmed, and A Kojic. 2010. "Algorithms for Advanced Battery-Management Systems." *IEEE Control Systems* 30 (3): 49–68.

Chau, K. T, and Y. S Wong. 2002. "Overview of Power Management in Hybrid Electric Vehicles." *Energy Conversion and Management* 43 (15): 1953–68.

Christenson, Martha, Aaron Loiselle, Deniz Karman, and Lisa A. Graham. 2007. *The Effect of Driving Conditions and Ambient Temperature on Light Duty Gasoline-Electric Hybrid Vehicles (2): Fuel Consumption and Gaseous Pollutant Emission Rates*. SAE Technical Paper 2007-01-2137. Warrendale, PA: SAE International.

Coelho, Margarida C., H. Christopher Frey, Nagui M. Rouphail, Haibo Zhai, and Luc Pelkmans. 2009. "Assessing Methods for Comparing Emissions from Gasoline and Diesel Light-Duty Vehicles Based on Microscale Measurements." *Transportation Research Part D: Transport and Environment* 14 (2): 91–99.

Collins, John F., P. Shepherd, Thomas D. Durbin, J. Lents, Joseph M. Norbeck, and Matthew Barth. 2007. "Measurements of In-Use Emissions from Modern Vehicles Using an On-Board Measurement System." *Environmental Science & Technology* 41 (18): 6554–61.

Dallmann, Timothy R., and Robert A. Harley. 2010. "Evaluation of Mobile Source Emission Trends in the United States." *Journal of Geophysical Research: Atmospheres* 115 (D14).

Dargay, Joyce. 2007. "Vehicle Ownership and Income Growth, Worldwide: 1960-2030." *The Energy Journal* 28 (4): 143–70.

De Vlieger, I. 1997. "On Board Emission and Fuel Consumption Measurement Campaign on Petrol-Driven Passenger Cars." *Atmospheric Environment* 31 (22): 3753–61.

DOE. 2012. "Alternative Fuels Data Center: AFVs in Use." *Energy Efficiency & Renewable Energy*. October 24. http://www.afdc.energy.gov/data/tab/vehicles/data_set/10300.

Duarte, G. O., R. A. Varella, G. A. Gonçalves, and T. L. Farias. 2014. "Effect of Battery State of Charge on Fuel Use and Pollutant Emissions of a Full Hybrid Electric Light Duty Vehicle." *Journal of Power Sources* 246 (January): 377–86.

Durbin, Thomas D., Kent Johnson, J. Wayne Miller, Hector Maldonado, and Don Chernich. 2008. "Emissions from Heavy-Duty Vehicles under Actual on-Road Driving Conditions." *Atmospheric Environment* 42 (20): 4812–21.

Eccleston, B. H., and R. W. Hurn. 1978. *Ambient Temperature and Trip Length-Influence on Automotive Fuel Economy and Emissions*. SAE Technical Paper 780613. Warrendale, PA: SAE International.

Electric Drive Transportation Association. 2014. "Electric Drive Sales." *Electric Drive Sales*. http://www.electricdrive.org/index.php?ht=d/sp/i/20952/pid/20952.

EPA. 2009. *Development of Emission Rates for Light-Duty Vehicles in the Motor Vehicle Emissions Simulator (MOVES2009)*. EPA-420-P-09-002. Assessment and Standards Division Office of Transportation and Air Quality U.S. Environmental Protection Agency.

———. 2012. *Our Nation's Air - Status and Trends through 2010*. EPA-454/R-12-001. http://www.epa.gov/airtrends/2011/.

Ericsson, Eva. 2001. “Independent Driving Pattern Factors and Their Influence on Fuel-Use and Exhaust Emission Factors.” *Transportation Research Part D: Transport and Environment* 6 (5): 325–45.

Farnlund, J., C. Holman, and P. Kageson. 2001. “Emissions of Ultrafine Particles from Different Types of Light Duty Vehicles,” Swedish National Road Administration Publication 2001:10.

Federal Highway Administration. 2014. “Chapter 3: Functional Classification - Flexibility - Publications - Environment - FHWA.” September 19,2012. *Flexibility in Highway Design: Chapter 3, Functional Classification*. http://www.fhwa.dot.gov/environment/publications/flexibility/ch03.cfm.

Fontaras, Georgios, Panayotis Pistikopoulos, and Zissis Samaras. 2008. “Experimental Evaluation of Hybrid Vehicle Fuel Economy and Pollutant Emissions over Real-World Simulation Driving Cycles.” *Atmospheric Environment* 42 (18): 4023–35.

Frey, H. Christopher, Alper Unal, Nagui M. Rouphail, and James D. Colyar. 2003. “On-Road Measurement of Vehicle Tailpipe Emissions Using a Portable Instrument.” *Journal of the Air & Waste Management Association (1995)* 53 (8): 992–1002.

Friedrich, G., and A Girardin. 2009. “Integrated Starter Generator.” *IEEE Industry Applications Magazine* 15 (4): 26–34.

Ganji, B., and AZ. Kouzani. 2010. “A Study on Look-Ahead Control and Energy Management Strategies in Hybrid Electric Vehicles.” In *2010 8th IEEE International Conference on Control and Automation (ICCA)*, 388–92.

Gauderman, W. James, Edward Avol, Frank Gilliland, Hita Vora, Duncan Thomas, Kiros Berhane, Rob McConnell, et al. 2004. “The Effect of Air Pollution on Lung Development from 10 to 18 Years of Age.” *New England Journal of Medicine* 351 (11): 1057–67.

Gierczak, Christine A., Thomas J. Korniski, Timothy J. Wallington, and James W. Butler. 2006. *Laboratory Evaluation of the SEMTECH-G® Portable Emissions Measurement System (PEMS) For Gasoline Fueled Vehicles*. SAE Technical Paper 2006-01-1081. Warrendale, PA. SAE International.

Gonder, Jeffrey, and Tony Markel. 2007. *Energy Management Strategies for Plug-In Hybrid Electric Vehicles*. SAE Technical Paper 2007-01-0290. Warrendale, PA. SAE International.

Gouriou, F, J. -P Morin, and M. -E Weill. 2004. “On-Road Measurements of Particle Number Concentrations and Size Distributions in Urban and Tunnel Environments.” *Atmospheric Environment* 38 (18): 2831–40.

Gramotnev, G., R. Brown, Z. Ristovski, J. Hitchins, and L. Morawska. 2003. “Determination of Average Emission Factors for Vehicles on a Busy Road.” *Atmospheric Environment* 37 (4): 465–74.

Harada, Jun, Tsutomu Tomita, Hiroyuki Mizuno, Zenichiro Mashiki, and Yasushi Ito. 1997. *Development of Direct Injection Gasoline Engine*. SAE Technical Paper 970540. Warrendale, PA: SAE International.

Harris, Stephen J., and M. Matti Maricq. 2001. "Signature Size Distributions for Diesel and Gasoline Engine Exhaust Particulate Matter." *Journal of Aerosol Science* 32 (6): 749–64.

Health Effects Institute. 2013. *Understanding the Health Effects of Ambient Ultrafine Particles*. Boston, Massachusetts: Health Effects Institute.

Holder, C., and J. Gover. 2006. "Optimizing the Hybridization Factor for a Parallel Hybrid Electric Small Car." In *IEEE Vehicle Power and Propulsion Conference, 2006. VPPC '06*, 1–5.

Holmén, Britt A., Mitchell K. Robinson, Matthew B. Conger, and Karen M. Sentoff. 2014. *Light-Duty Gasoline Hybrid-Electric and Conventional Vehicle Tailpipe Emissions Under Real-World Operating Conditions*. TRC Report 14-007. University of Vermont Transportation Research Center.

Holmén, Britt A., Mitchell Robinson, Karen Sentoff, Paul Montane, and Kevin Hathaway. 2009. "The On-Board Tailpipe Emissions Measurement System (TOTEMS): Proof-of-Concept," TRC Report 10-015. University of Vermont Transportation Research Center.

Huang, Cheng, Diming Lou, Zhiyuan Hu, Qian Feng, Yiran Chen, Changhong Chen, Piqiang Tan, and Di Yao. 2013. "A PEMS Study of the Emissions of Gaseous Pollutants and Ultrafine Particles from Gasoline- and Diesel-Fueled Vehicles." *Atmospheric Environment* 77 (October): 703–10.

Jackson, Eric, and Lisa Aultman-Hall. 2010. "Analysis of Real-World Lead Vehicle Operation for Modal Emissions and Traffic Simulation Models." *Transportation Research Record: Journal of the Transportation Research Board* 2158 (December): 44–53.

Jamriska, Milan, Lidia Morawska, and Kerrie Mergersen. 2008. "The Effect of Temperature and Humidity on Size Segregated Traffic Exhaust Particle Emissions." *Atmospheric Environment* 42 (10): 2369–82.

Jamriska, M., and L Morawska. 2001. "A Model for Determination of Motor Vehicle Emission Factors from on-Road Measurements with a Focus on Submicrometer Particles." *Science of The Total Environment* 264 (3): 241–55.

Jetter, Jeff, Shinji Maeshiro, Seiji Hatcho, and Robert Klebba. 2000. *Development of an On-Board Analyzer for Use on Advanced Low Emission Vehicles*. SAE Technical Paper 2000-01-1140. Warrendale, PA: SAE International.

Jimenez, J.L. 1999. "Understanding and Quantifying Motor Vehicle Emissions with Vehicle Specific Power and TILDAS Remote Sensing." Doctorate Dissertation, Massachusetts Institute of Technology.

Kasper, A., H. Burtscher, J. P. Johnson, D. B. Kittelson, W. F. Watts, U. Baltensperger, and E. Weingartner. 2005. *Particle Emissions from SI-Engines During Steady State and Transient Operating Conditions*. SAE Technical Paper 2005-01-3136. Warrendale, PA: SAE International.

Kawahashi, A. 2004. "A New-Generation Hybrid Electric Vehicle and Its Supporting Power Semiconductor Devices." In *The 16th International Symposium on Power Semiconductor Devices and ICs, 2004. Proceedings. ISPSD '04*, 23–29.

Kayes, David, Simone Hochgreb, M. Matti Maricq, Diane H. Podsiadlik, and Richard E. Chase. 2000. *Particulate Matter Emission During Start-up and Transient Operation of a Spark-Ignition Engine (2): Effect of Speed, Load, and Real-World Driving Cycles*. SAE Technical Paper 2000-01-1083. Warrendale, PA: SAE International.

Kittelson, D. B. 1998. "Engines and Nanoparticles: A Review." *Journal of Aerosol Science* 29 (5–6): 575–88.

Kittelson, D. B., W. F. Watts, and J. P. Johnson. 2004. "Nanoparticle Emissions on Minnesota Highways." *Atmospheric Environment* 38 (1): 9–19.

Kittelson, D. B., W. F. Watts, J. P. Johnson, J. J. Schauer, and D. R. Lawson. 2006. "On-Road and Laboratory Evaluation of Combustion aerosols—Part 2:: Summary of Spark Ignition Engine Results." *Journal of Aerosol Science* 37 (8): 931–49.

Koot, M., J. T B A Kessels, B. de Jager, W. P M H Heemels, P. P J Van den Bosch, and M. Steinbuch. 2005. "Energy Management Strategies for Vehicular Electric Power Systems." *IEEE Transactions on Vehicular Technology* 54 (3): 771–82.

Koupal, John, Larry Landman, Edward Nam, James Warila, Carl Scarbro, Edward Glover, and Robert Giannelli. 2005. *MOVES2004 Energy and Emission Inputs Draft Report*. EPA420-P-05-003. EPA Office of Transportation and Air Quality.

Kousoulidou, Marina, Georgios Fontaras, Leonidas Ntziachristos, Pierre Bonnel, Zissis Samaras, and Panagiota Dilara. 2013. "Use of Portable Emissions Measurement System (PEMS) for the Development and Validation of Passenger Car Emission Factors." *Atmospheric Environment* 64 (January): 329–38.

Kutlar, Osman Akin, Hikmet Arslan, and Alper Tolga Calik. 2005. "Methods to Improve Efficiency of Four Stroke, Spark Ignition Engines at Part Load." *Energy Conversion and Management* 46 (20): 3202–20.

Larsson, V., L. Johannesson, B. Egardt, and A Lassson. 2012. "Benefit of Route Recognition in Energy Management of Plug-in Hybrid Electric Vehicles." In *American Control Conference (ACC), 2012*, 1314–20.

Lee, Hyungmin, Cha-Lee Myung, and Simsoo Park. 2009. “Time-Resolved Particle Emission and Size Distribution Characteristics during Dynamic Engine Operation Conditions with Ethanol-Blended Fuels.” *Fuel* 88 (9): 1680–86.

Lenaers, Guido. 1996. “On-Board Real Life Emission Measurements on a 3 Way Catalyst Gasoline Car in Motor Way-, Rural- and City Traffic and on Two Euro-1 Diesel City Buses.” *Science of The Total Environment*, Highway and Urban Pollution, 189–190 (October): 139–47.

Li, Hu, Gordon E Andrews, Dimitrios Savvidis, Basil Daham, Karl Ropkins, Margaret Bell, and James Tate. 2008. *Comparisons of the Exhaust Emissions for Different Generations of SI Cars under Real World Urban Driving Conditions*. 2008-01-0754. Warrendale, PA: SAE International.

Liu, Jinming, and Huei Peng. 2008. “Modeling and Control of a Power-Split Hybrid Vehicle.” *IEEE Transactions on Control Systems Technology* 16 (6): 1242–51.

Liu, Zhen, and H.X. Li. 2012. “Thermal Modeling for Vehicle Battery System: A Brief Review.” In *2012 International Conference on System Science and Engineering (ICSSE)*, 74–78.

Lutsey, Nicholas, and Daniel Sperling. 2009. “Greenhouse Gas Mitigation Supply Curve for the United States for Transport versus Other Sectors.” *Transportation Research Part D: Transport and Environment* 14 (3): 222–229.

MacNee, W., and K. Donaldson. 2003. “Mechanism of Lung Injury Caused by PM10 and Ultrafine Particles with Special Reference to COPD.” *The European Respiratory Journal. Supplement* 40 (May): 47 – 51.

Manzie, Chris, Harry Watson, and Saman Halgamuge. 2007. “Fuel Economy Improvements for Urban Driving: Hybrid vs. Intelligent Vehicles.” *Transportation Research Part C: Emerging Technologies* 15 (1): 1–16.

MECA. 2013. *Ultrafine Particulate Matter and the Benefits of Reducing Particulate Numbers in the United States: A Report to the Manufacturers of Emission Controls Association*. Manufacturers of Emission Controls Association.

Merkisz, Jerzy, Jacek Pielecha, and Wojciech Gis. 2009. *Gaseous and Particle Emissions Results from Light Duty Vehicle with Diesel Particle Filter*. SAE Technical Paper 2009-01-2630. Warrendale, PA: SAE International.

Mulawa, Patricia A., Steven H. Cadle, Kenneth Knapp, Roy Zweidinger, Richard Snow, Randy Lucas, and Joseph Goldbach. 1997. “Effect of Ambient Temperature and E-10 Fuel on Primary Exhaust Particulate Matter Emissions from Light-Duty Vehicles.” *Environmental Science & Technology* 31 (5): 1302–7.

Muta, Koichiro, Makoto Yamazaki, and Junji Tokieda. 2004. *Development of New-Generation Hybrid System THS II - Drastic Improvement of Power Performance and Fuel Economy*. SAE Technical Paper 2004-01-0064. Warrendale, PA: SAE International.

NREL. 2009. *Fuel Savings from Hybrid Electric Vehicles*. TP-540-42681. National Renewable Energy Laboratory.

Pope, C. Arden, Richard T. Burnett, Michael J. Thun, Eugenia E. Calle, Daniel Krewski, Kazuhiko Ito, and George D. Thurston. 2002. "Lung Cancer, Cardiopulmonary Mortality, and Long-Term Exposure to Fine Particulate Air Pollution." *JAMA: The Journal of the American Medical Association* 287 (9): 1132–41.

Puentes, Robert, and Adie Tomer. 2009. *The RoadLess Traveled: An Analysis of Vehicle Miles Traveled Trends in the U.S.* The Brookings Institution.

Rajagopalan, A., Washington, G., Rizzoni, G., and Guezennec, Y. 2003. *Development of Fuzzy Logic and Neural Network Control and for Parallel Hybrid Vehicles for Advanced Emissions Modeling*. SR-540-32919. Center for Automotive Research: The Ohio State University.

Reyes, F., M. Grutter, A. Jazcilevich, and R. González-Oropeza. 2006. "Tecnical Note: Analysis of Non-Regulated Vehicular Emissions by Extractive FTIR Spectrometry: Tests on a Hybrid Car in Mexico City." *Atmospheric Chemistry and Physics* 6 (12): 5339–46.

Robinson, Mitchell K. 2011. "Second-by-Second on-Board Real-World Particle Number Emissions for Comparable Conventional and Hybrid-Electric Gasoline Vehicles in a City Driving Environment." Masters of Science, Burlington, Vermont: University of Vermont.

Robinson, Mitchell K., and Britt A. Holmén. 2011. "Onboard, Real-World Second-by-Second Particle Number Emissions from 2010 Hybrid and Comparable Conventional Vehicles." *Transportation Research Record: Journal of the Transportation Research Board* 2233: 63–71.

Samaras, Constantine, and Kyle Meisterling. 2008. "Life Cycle Assessment of Greenhouse Gas Emissions from Plug-in Hybrid Vehicles: Implications for Policy." *Environmental Science & Technology* 42 (9): 3170–76.

Sawyer, R. F, R. A Harley, S. H Cadle, J. M Norbeck, R Slott, and H. A Bravo. 2000. "Mobile Sources Critical Review: 1998 NARSTO Assessment." *Atmospheric Environment* 34 (12–14): 2161–81.

Schouten, N.J., M.A Salman, and N.A Kheir. 2002. "Fuzzy Logic Control for Parallel Hybrid Vehicles." *IEEE Transactions on Control Systems Technology* 10 (3): 460–68.

Sentoff, Karen M. 2013. "Characterization of Gas-Phase Emissions from Comparable Conventional and Hybrid Gasoline Vehicles during Real-World Operation." Masters of Science, Civil and Environmental Engineering, Burlington, Vermont: University of Vermont.

Smith, Kandler, and Chao-Yang Wang. 2006. “Power and Thermal Characterization of a Lithium-Ion Battery Pack for Hybrid-Electric Vehicles.” *Journal of Power Sources* 160 (1): 662–73.

Tae, Kim. 2008. “Fuel Economy Benefits of Look-Ahead Capability in a Mild Hybrid Configuration.” Proceedings of the 17th World Congress of IFAC, Seoul, Korea, July.

Tan, Pi-qiang, Shuai-shuai Ruan, Zhi-yuan Hu, Di-ming Lou, and Hu Li. 2014. “Particle Number Emissions from a Light-Duty Diesel Engine with Biodiesel Fuels under Transient-State Operating Conditions.” *Applied Energy* 113 (January): 22–31.

Toyota. 2010a. “Toyota Technical Training: Engine Control System II Course 874 Technician Handbook.” Toyota Motor Sales, USA, Inc.

———. 2010b. “Toyota Technical Training: Engine Control Systems I Course 852.” Toyota Motor Sales, USA, Inc.

Tribioli, Laura, Michele Barbieri, Roberto Capata, Enrico Sciubba, Elio Jannelli, and Gino Bella. 2014. “A Real Time Energy Management Strategy for Plug-in Hybrid Electric Vehicles Based on Optimal Control Theory.” *Energy Procedia*, ATI 2013 - 68th Conference of the Italian Thermal Machines Engineering Association, 45: 949–58.

Truex, Timothy J., John F. Collins, Jeff J. Jetter, Benjamin Knight, Tadayoshi Hayashi, Noriyuki Kishi, and Norio Suzuki. 2000. *Measurement of Ambient Roadway and Vehicle Exhaust Emissions-An Assessment of Instrument Capability and Initial On-Road Test Results with an Advanced Low Emission Vehicle*. SAE Technical Paper 2000-01-1142. Warrendale, PA: SAE International.

TSI, Inc. 2010. “Engine Exhaust Particle Sizer Spectrometer 3090.” http://www.tsi.com/engine-exhaust-particle-sizer-spectrometer-3090/.

UNEP. 2009. *Hybrid Electric Vehicles: An Overview of Current Technology and Its Application in Developing and Transitional Countries*. Nairobi Kenya: United Nations Environment Program. https://cleanenergysolutions.org/.

U.S. DOE. 2013. “FuelEconomy.gov.” http://fueleconomy.gov/.

———. 2014. “SEED - DOE - EERE: Alternative Fuels and Advanced Vehicles Data Center (AFDC).” *Sustainability Education and Economic Development*. http://www.theseedcenter.org/Resources/Resource-Center/DOE---EERE--Alternative-Fuels-and-Advanced-Vehicle.

U.S. EIA. 2014. *Annual Energy Outlook 2014*. AEO2014. US Energy Information Administration. http://www.eia.gov/forecasts/aeo/.

U.S. EPA. 1993. *Federal Test Procedure Review Project: Preliminary Technical Report.* EPA 420-R-93-007. http://www.epa.gov/otaq/sftp.htm.

———. 1995. *Air Toxics from Motor Vehicles*. EPA 400-F-92-004. http://www.epa.gov/oms/consumer/02-toxic.pdf.

———. 2014a. *Light-Duty Vehicle and Light-Duty Truck - Clean Fuel Fleet Exhaust Emission Standards - Emission Standards Reference Guide*. http://www.epa.gov/otaq/standards/light-duty/ld-cff.htm.

———. 2014b. *National Ambient Air Quality Standards (NAAQS)*. http://www.epa.gov/air/criteria.html.

———. 2014c. *Characterization of the Chemical Composition of Atmospheric Ultrafine Particles*. Reports & Assessments. http://cfpub.epa.gov/ncer_abstracts/index.cfm/fuseaction/display.abstractdetail/abstract/5579.

Villatico, Federico. 2008. "Efficiency Comparison between FC and ICE in Real Urban Driving Cycles." *International Journal of Hydrogen Energy* 33 (12): 3235-3242.

Wenzel, Tom, and Marc Ross. 1998. *Characterization of Recent-Model High-Emitting Automobiles*. SAE Technical Paper 981414. Warrendale, PA: SAE International.

Yu, S., G. Dong, and L. Li. 2008. "Transient Characteristics of Emissions during Engine Start/stop Operation Employing a Conventional Gasoline Engine for HEV Application." *International Journal of Automotive Technology* 9 (5): 543–49.

Zhai, Haibo, H. Christopher Frey, and Nagui M. Rouphail. 2011. "Development of a Modal Emissions Model for a Hybrid Electric Vehicle." *Transportation Research Part D: Transport and Environment* 16 (6): 444–50.

Zhai, Haibo, H. Christopher Frey, and Nagui M. Rouphail. 2008. "A Vehicle-Specific Power Approach to Speed- and Facility-Specific Emissions Estimates for Diesel Transit Buses." *Environmental Science & Technology* 42 (21): 7985–91.

Zhang, K. Max, Anthony S. Wexler, Debbie A. Niemeier, Yi Fang Zhu, William C. Hinds, and Constantinos Sioutas. 2005. "Evolution of Particle Number Distribution near Roadways. Part III: Traffic Analysis and on-Road Size Resolved Particulate Emission Factors." *Atmospheric Environment* 39 (22): 4155–66.

Zhao, Jinxing, and Min Xu. 2013. "Fuel Economy Optimization of an Atkinson Cycle Engine Using Genetic Algorithm." *Applied Energy* 105 (May): 335–48.

Zheng, Zhongqing, Thomas D. Durbin, Jian Xue, Kent C. Johnson, Yang Li, Shaohua Hu, Tao Huai, Alberto Ayala, David B. Kittelson, and Heejung S. Jung. 2014. "Comparison of Particle Mass and Solid Particle Number (SPN) Emissions from a Heavy-Duty Diesel Vehicle under On-Road Driving Conditions and a Standard Testing Cycle." *Environmental Science & Technology* 48 (3): 1779–86.

Zhu, Yuan, Yaobin Chen, Guangyu Tian, Hao Wu, and Quanshi Chen. 2004. “A Four-Step Method to Design an Energy Management Strategy for Hybrid Vehicles.” In *American Control Conference, 2004. Proceedings of the 2004*, 1:156–61 vol.1.

Appendix A **EPA MOVES OpModes**

Table A1. Adapted Operating Mode Description (EPA 2009)

Operating Mode (OpMode)	Operating Mode Description	Vehicle Specific Power (VSP) [kW/ton]	Speed (v) [mph]	Acceleration (a) [mph/s]
0	Deceleration/Braking			[$a_t \leq -2$] OR [$a_t < -1$ & $a_{t-1} < -1$ & $a_{t-2} < -1$]
1	Idle		$-1 \leq v < 1$	Note: t = time (seconds)
11	Coast	VSP < 0	$0 \leq v < 25$	
12	Cruise/Acceleration	$0 \leq$ VSP < 3	$0 \leq v < 25$	
13	Cruise/Acceleration	$3 \leq$ VSP < 6	$0 \leq v < 25$	
14	Cruise/Acceleration	$6 \leq$ VSP < 9	$0 \leq v < 25$	
15	Cruise/Acceleration	$9 \leq$ VSP < 12	$0 \leq v < 25$	
16	Cruise/Acceleration	$12 \leq$ VSP	$0 \leq v < 25$	
21	Coast	VSP < 0	$25 \leq v < 50$	
22	Cruise/Acceleration	$0 \leq$ VSP < 3	$25 \leq v < 50$	
23	Cruise/Acceleration	$3 \leq$ VSP < 6	$25 \leq v < 50$	
24	Cruise/Acceleration	$6 \leq$ VSP < 9	$25 \leq v < 50$	
25	Cruise/Acceleration	$9 \leq$ VSP < 12	$25 \leq v < 50$	
27	Cruise/Acceleration	$12 \leq$ VSP < 18	$25 \leq v < 50$	
28	Cruise/Acceleration	$18 \leq$ VSP < 24	$25 \leq v < 50$	
29	Cruise/Acceleration	$24 \leq$ VSP < 30	$25 \leq v < 50$	
30	Cruise/Acceleration	$30 \leq$ VSP	$25 \leq v < 50$	
33	Cruise/Acceleration	VSP < 6	$50 \leq v$	
35	Cruise/Acceleration	$6 \leq$ VSP < 12	$50 \leq v$	
37	Cruise/Acceleration	$12 \leq$ VSP < 18	$50 \leq v$	
38	Cruise/Acceleration	$18 \leq$ VSP < 24	$50 \leq v$	
39	Cruise/Acceleration	$24 \leq$ VSP < 30	$50 \leq v$	
40	Cruise/Acceleration	$30 \leq$ VSP	$50 \leq v$	

Appendix B **TOTEMS Instrumentation**

Table B1. Total On-board Emissions Measurement System (TOTEMS) Instrumentation Description

Instrument	Acronym	Model	Purpose	Label No.
Emissions Analysis				
Fourier Transform Infrared Spectrometer	FTIR	MKS MultiGas2030HS	Gas-Phase Emissions Analysis at 1-hertz	1
Personal Sampling Pump	SKC	SKC Leland Legacy	Draw Exhaust Sample through FTIR	2
Engine Exhaust Particle Sizer	EEPS	TSI 3090	Particle Size Distribution (D_p = 5.6 - 560 nm)	3
Ultrafine Condensation Particle Counter	UCPC	TSI 3025A	Total Particle Number (D_p = 3 - 3000 nm)	4
Rotating Disk Diluter	MD19-2E	Matter Engineering 379020	1st Stage Particle Sample Dilution	5
Air Supply Evaporation Tube	ASET	TSI 379030	2nd Stage Particle Sample Dilution	6
Exhaust Parameters & Sample Transport				
Tailpipe Adapter	TA	Custom Built	Extends Tailpipe to Provide Sampling Ports and House Pitot Tube	7
Thermocouple Type T	T1	Omega GTMQSS-125E-2	Exhaust Sample Temperature at end of Heated Line	8
Thermocouple Type J	T2	Omega GTMQSS-125E-3	Exhaust Temperature in Tailpipe Adapter	9
Thermocouple Type T	T3	Omega GTMQSS-125E-2	Exhaust Sample Temperature at Inlet of FTIR	10
Thermocouple Type T	T4	Omega GTMQSS-125E-2	Exhaust Sample Temperature at Inlet EEPS/UCPC	11
Differential Pressure Transducers (4)	DiffP#	Omega PX-277	Exhaust Flow Rate	12
Static Pressure Sensor		Omega PX181-030G5V	Exhaust Flow Rate	-
Heated Line	HL	Atmoseal IGH-120-S-6/X-G13	Transport of Exhaust Sample from Tailpipe to FTIR, CPC, and EEPS	13
Vehicle Operation, Spatial Location & Environment				
Scan Tool	SCN	Toyota Techstream	Records Vehicle Operation Parameters from Vehicle's ECU(s)	14
Garmin GPS Receiver	GAR	Garmin GPS16-HVS	Spatial Position of Vehicle	15
Geologger	GEO	Geostats DL-04 V2.4	Spatial Position of Vehicle	-
Accelerometer	ACC	Crossbow CXLO2LF3	Acceleration in X, Y, and Z Directions	-
Temperature and Relative Humidity Loggers (2)	RHT	Onset HOBO U23-001	Ambient and Interior Conditions	16
Video Camera	VID	Canon Optura 30	Driver Perspective of Roadway	17
Power Supply				
Automatic Transfer Switch	ATS	GoPower Electric GP-ATS-30	Uninterrupted Transfer from Grid to On-board Power Supply	18
Absorbent Glass Mat Lead-Acid Batteries (2)		Lifeline GPL-8DA	On-board power supply	-
Deep Cycle Battery Charger		Xantrex TrueCharge 40	Three Stage Battery Charger to Large AGM Marine Batteries	19
Optima Yellow Top Battery		Optima D31A	Pressure transducer DC power supply	20
Power Inverter		Vector VEC56D	Conversion from DC to AC power	-
Data Acquisition				
On-Board Emissions PC		Dell Optiplex GX620	Records data from instruments	21
FTIR Laptop		Dell Latitude D630	Records data from FTIR	22
Labview Device 1	L1	Labview DAQCard-6024E	National Instruments SCB-68 Connector Block and DAQCard for Data Acquisition from Crossbow, Static Pressure, and Thermocouples	23
Labview Device 2	L2	Labview DAQCard-6024E	Connector Block and DAQCard for Data Acquisition from Differential Pressure Transducers and Dilution System	24

Table B2. EEPS Channel Particle Diameters. Source: Robinson, 2011

Channel	Lower Limit (nm)	Upper Limit (nm)	Midpoint (nm)
1	5.6234	6.4938	6.04
2	6.4938	7.4989	6.98
3	7.4989	8.6596	8.06
4	8.6596	10.0000	9.31
5	10.0000	11.5478	10.75
6	11.5478	13.3352	12.41
7	13.3352	15.3993	14.33
8	15.3993	17.7828	16.55
9	17.7828	20.5353	19.11
10	20.5353	23.7137	22.07
11	23.7137	27.3842	25.48
12	27.3842	31.6228	29.43
13	31.6228	36.5174	33.98
14	36.5174	42.1697	39.24
15	42.1697	48.6968	45.32
16	48.6968	56.2341	52.33
17	56.2341	64.9382	60.43
18	64.9382	74.9894	69.78
19	74.9894	86.5964	80.58
20	86.5964	100.0000	93.06
21	100.0000	115.4782	107.46
22	115.4782	133.3521	124.09
23	133.3521	153.9927	143.30
24	153.9927	177.8279	165.48
25	177.8279	205.3525	191.10
26	205.3525	237.1374	220.67
27	237.1374	273.8420	254.83
28	273.8420	316.2278	294.27
29	316.2278	365.1741	339.82
30	365.1741	421.6965	392.42
31	421.6965	486.9675	453.16
32	486.9675	562.3413	523.30

Table B3. EEPS Instrument Detection Limits (IDLs) by Run.

RUN	VEHICLE	IDL (#/cc)
5	CV	984
6	CV	1190
7	CV	1203
8	CV	696
9	CV	835
10	CV	980
11	CV	955
12	CV	915
13	HEV	910
14	HEV	1090
15	HEV	911
16	HEV	816
17	HEV	809
18	HEV	590
19	HEV	597
20	HEV	1110
21	HEV	1935
22	HEV	5351
23	HEV	3165
24	HEV	2829
25	HEV	1572
26	HEV	3274
27	HEV	1946
28	HEV	3512
29	HEV	2953
30	HEV	1782
31	CV	375
32	CV	1160
33	CV	723
34	CV	521
35	CV	629
36	CV	846
37	CV	594
38	CV	999
39	CV	882
40	CV	796

RUN	VEHICLE	IDL (#/cc)
41	HEV	753
42	HEV	646
43	HEV	1171
44	HEV	1640
45	HEV	1715
46	HEV	1477
47	HEV	1683
48	HEV	1220
49	HEV	647
50	HEV	735
51	HEV	342
52	HEV	1410
53	HEV	2101
54	CV	592
55	CV	920
56	CV	2213
57	CV	905
58	CV	2281
59	CV	1771
60	CV	1283
61	CV	2246
62	CV	778
63	CV	2401
64	CV	1332
65	CV	1613
66	CV	738
67	CV	886
68	HEV	2306
69	HEV	1227
70	HEV	32088
71	HEV	1596
72	HEV	2398
73	HEV	1460
74	HEV	1498
75	HEV	1006
76	HEV	792
77	HEV	1193
78	HEV	1063
79	HEV	972

Appendix C **Driving Route Details**

Table B1. Driving Route Turn-by-Turn Directions Logsheet

Time	Direction	Facility Name	Notes
	–	ENGINE ON	*Start Phase 3
	L	Colchester Avenue	
	R	North Prospect Street	
	R	Riverside Avenue	
	R	Cumberland Farms Gulf Station	
	R	Riverside Avenue	
	R	Colchester Avenue	
	–	START OF RUN AT VOTEY HALL	*Start Phase 4
	R	Mansfield Avenue	
	L	Mansfield Avenue	
	C	North Street	
	R	North Willard Street	
	L	Archibald Street	
	L	Intervale Avenue	
	L	North Street	
	R	North Winooski Avenue	
	R	Pearl Street	
	R	Elmwood Avenue	
	L	Allen Street	
	R	Murray Street	
	L	North Street	
	L	Park Street	
	C	Battery Street	
	L	King Street	
	R	South Champlain Street	
	L	Maple Street	
	L	South Prospect Street	
	R	Main Street / US-2 E	
	R	I-89 South	
	R	Exit 11 for US-2	
	C	Richmond Park and Ride (entranc	*Start Phase 5
	L	West Main Street / US-2 E	*End Phase 5
	R	Bridge Street	
	R	Huntington Road	
	R	Hinesburg Road	
	C	East Hill Road	
	R	South Road	
	R	Oak Hill Road	
	L	US-2 / Williston Road	
	R	Patchen Road	
	C	Grove Street	
	L	Chase Street	
	C	Barrett Street	
	L	Colchester Avenue	
	–	END OF RUN AT VOTEY HALL	*End Phase 6
	–	ENGINE OFF	*End Phase 7

Appendix D **Tailpipe Exhaust Flow Rate and Fuel Rate Estimations**

Equation D1. Flowrate computation from Differntial Pressure Sensor Voltage and Selection. Source: Sentoff, 2013.

$$QExhaust = \begin{cases} \sqrt{83609.257 * (DiffP4 - 5)} & if\ 0.4 \le (DiffP4 - 5) < 4.6 \quad (R^2 = 0.87) \\ \sqrt{394516.8 * DiffP3} & if\ 0.4 \le DiffP3 < 9.6 \quad (R^2 = 0.98) \\ \sqrt{2129720.5 * DiffP2} & if\ 0.4 \le DiffP2 < 9.6 \quad (R^2 = 0.94) \\ \sqrt{14499240 * DiffP1} & if\ 0.4 \le DiffP1 < 9.6 \quad (R^2 = 0.70) \end{cases}$$

where: DiffP1 = Omega Differential Pressure Sensor 1 Raw Voltage Signal
DiffP2 = Omega Differential Pressure Sensor 2 Raw Voltage Signal
DiffP3 = Omega Differential Pressure Sensor 3 Raw Voltage Signal
DiffP4 = Omega Differential Pressure Sensor 4 Raw Voltage Signal

Appendix E **Estimated Flowrate Development**

Table E1. Table of Correlations for CV between Computed Flow Rate and Scantool Parameters. Correlations computed and generated using JMP 11.0, pairwise method.

	Computed Flowrate	CALCLOAD	SPEED	RPM	INJVOL	MAF
Computed Flowrate	1.0000	0.9003	0.3403	0.7657	0.9206	0.9684
CALCLOAD	0.9003	1.0000	0.2891	0.7100	0.9634	0.9261
SPEED	0.3403	0.2891	1.0000	0.6312	0.3153	0.3850
RPM	0.7657	0.7100	0.6312	1.0000	0.7470	0.8373
INJVOL	0.9206	0.9634	0.3153	0.7470	1.0000	0.9320
MAF	0.9684	0.9261	0.3850	0.8373	0.9320	1.0000

Note: highlighted value is largest correlation with Computed Flowrate.

Figure E1. Scatterplot Matrix for CV, Computed Flowrate and Scantool Parameters.

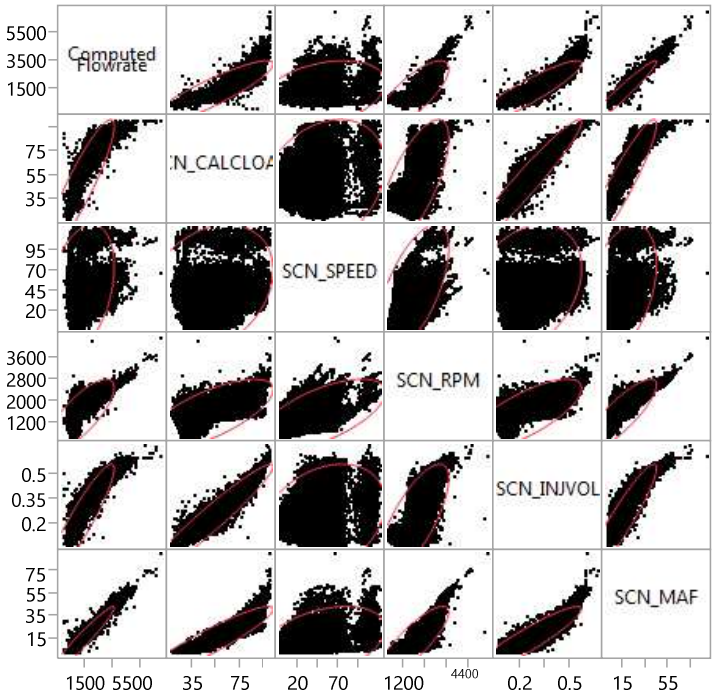

Table E2. Table of Correlations for HEV between Computed Flow Rate and Scantool Parameters. Correlations computed and generated using JMP 11.0, pairwise method.

	Computed Flowrate	CALCLOAD	SPEED	RPM	INJVOL	MAF
Computed Flowrate	1.0000	0.8025	0.5214	0.9429	0.0000	0.0000
CALCLOAD	0.8025	1.0000	0.5267	0.8960	0.0000	0.0000
SPEED	0.5214	0.5267	1.0000	0.5909	0.0000	0.0000
RPM	0.9429	0.8960	0.5909	1.0000	0.0000	0.0000
INJVOL	0.0000	0.0000	0.0000	0.0000	1.0000	0.0000
MAF	0.0000	0.0000	0.0000	0.0000	0.0000	1.0000

Note: highlighted value is largest correlation with Computed Flowrate.

Figure E2. Scatterplot Matrix for HEV, Computed Flowrate and Scantool Parameters.

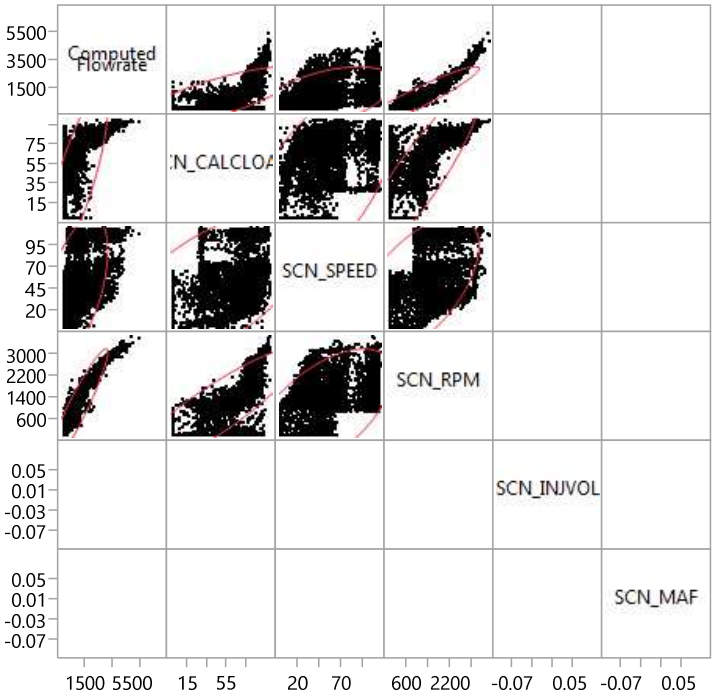

Figure E3. Bivariate Fit of Computed Flowrate By CV MAF

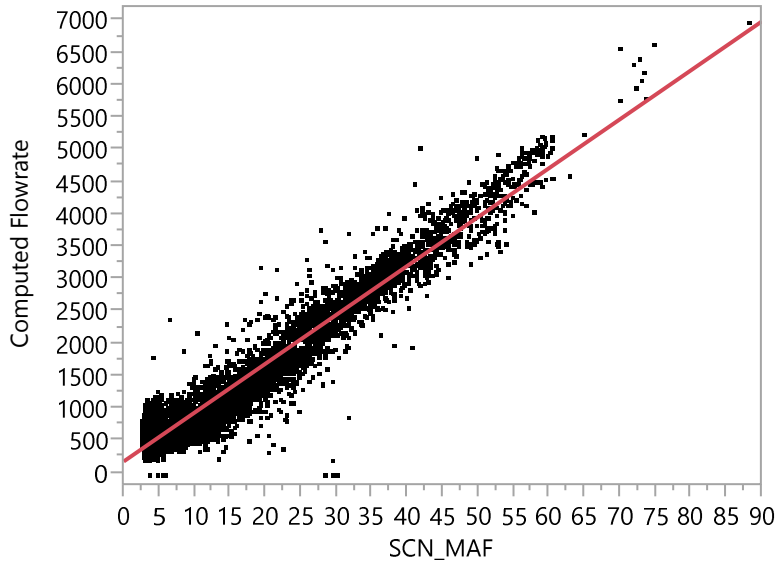

Linear Fit

Computed Flowrate = 170.16366 + 75.679416*SCN_MAF

Summary of Fit

RSquare	0.937891
RSquare Adj	0.937885
Root Mean Square Error	244.4266
Mean of Response	1158.817
Observations (or Sum Wgts)	11266

Analysis of Variance

Source	DF	Sum of Squares	Mean Square	F Ratio
Model	1	1.0162e+10	1.016e+10	170094.2
Error	11264	672960517	59744.364	**Prob > F**
C. Total	11265	1.0835e+10		<.0001*

Parameter Estimates

Term	Estimate	Std Error	t Ratio	Prob>|t|
Intercept	170.16366	3.324078	51.19	<.0001*
SCN_MAF	75.679416	0.183499	412.42	<.0001*

Figure E4. Bivariate Fit of Computed Flowrate By CV Engine Speed (RPM)

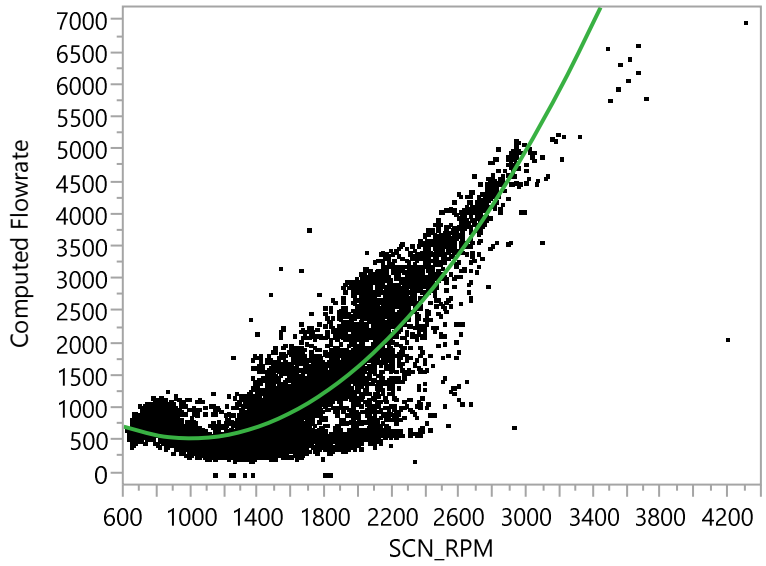

Polynomial Fit Degree=2

Polynomial Fit Degree=2

Computed Flowrate = -953.4604 + 1.1773292*SCN_RPM + 0.0011192*(SCN_RPM-1525.94)^2

Summary of Fit

RSquare	0.763124
RSquare Adj	0.763082
Root Mean Square Error	477.365
Mean of Response	1158.817
Observations (or Sum Wgts)	11266

Analysis of Variance

Source	DF	Sum of Squares	Mean Square	F Ratio
Model	2	8268550790	4.1343e+9	18142.55
Error	11263	2566582026	227877.3	**Prob > F**
C. Total	11265	1.0835e+10		<.0001*

Parameter Estimates

Term	Estimate	Std Error	t Ratio	Prob>|t|
Intercept	-953.4604	13.68989	-69.65	<.0001*
SCN_RPM	1.1773292	0.008852	133.01	<.0001*
(SCN_RPM-1525.94)^2	0.0011192	1.221e-5	91.68	<.0001*

Figure E5. Bivariate Fit of Computed Flowrate By HEV Engine Speed (RPM)

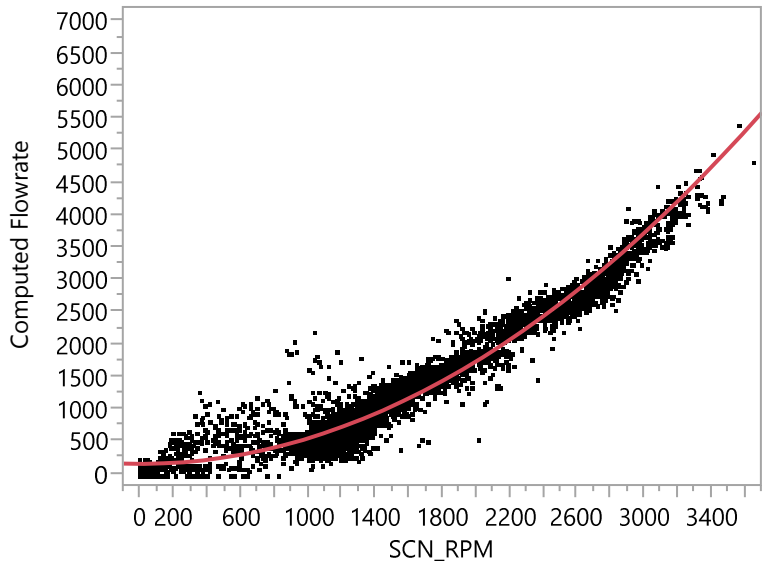

Transformed Fit to Square

Computed Flowrate = 145.35715 + 0.0003972*Square(SCN_RPM)

Summary of Fit

RSquare	0.965019
RSquare Adj	0.965015
Root Mean Square Error	181.2668
Mean of Response	839.9271
Observations (or Sum Wgts)	9364

Analysis of Variance

Source	DF	Sum of Squares	Mean Square	F Ratio
Model	1	8486124166	8.4861e+9	258269.4
Error	9362	307613262	32857.644	**Prob > F**
C. Total	9363	8793737427		<.0001*

Parameter Estimates

Term	Estimate	Std Error	t Ratio	Prob>|t|
Intercept	145.35715	2.318805	62.69	<.0001*
Square(SCN_RPM)	0.0003972	7.816e-7	508.20	<.0001*

Figure E6. Bivariate Fit of HEV Injection Volume by HEV Calculated Load

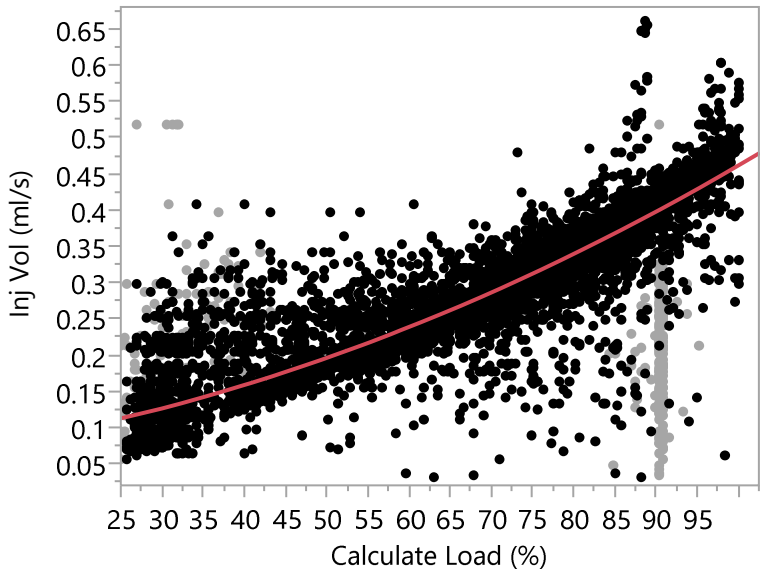

Inj Vol Lag (cyl 1) = -0.056341 + 0.0049178*Calculate Load + 2.6251e-5*(Calculate Load-67.3778)^2

Summary of Fit

RSquare	0.821095
RSquare Adj	0.821049
Root Mean Square Error	0.044007
Mean of Response	0.286074
Observations (or Sum Wgts)	7792

Analysis of Variance

Source	DF	Sum of Squares	Mean Square	F Ratio
Model	2	69.230081	34.6150	17874.06
Error	7789	15.084239	0.0019	**Prob > F**
C. Total	7791	84.314320		<.0001*

Parameter Estimates

Term	Estimate	Std Error	t Ratio	Prob>|t|
Intercept	-0.056341	0.002448	-23.01	<.0001*
Calculate Load	0.0049178	0.00003	163.56	<.0001*
(Calculate Load-67.3778)^2	2.6251e-5	1.322e-6	19.86	<.0001*

Appendix F **Correlation Matrices for RIEV PNER and Measured Parameters**

Figure F1. Correlation matrix of measured factors at t=0 before re-ignition and peak RIEV PNER.

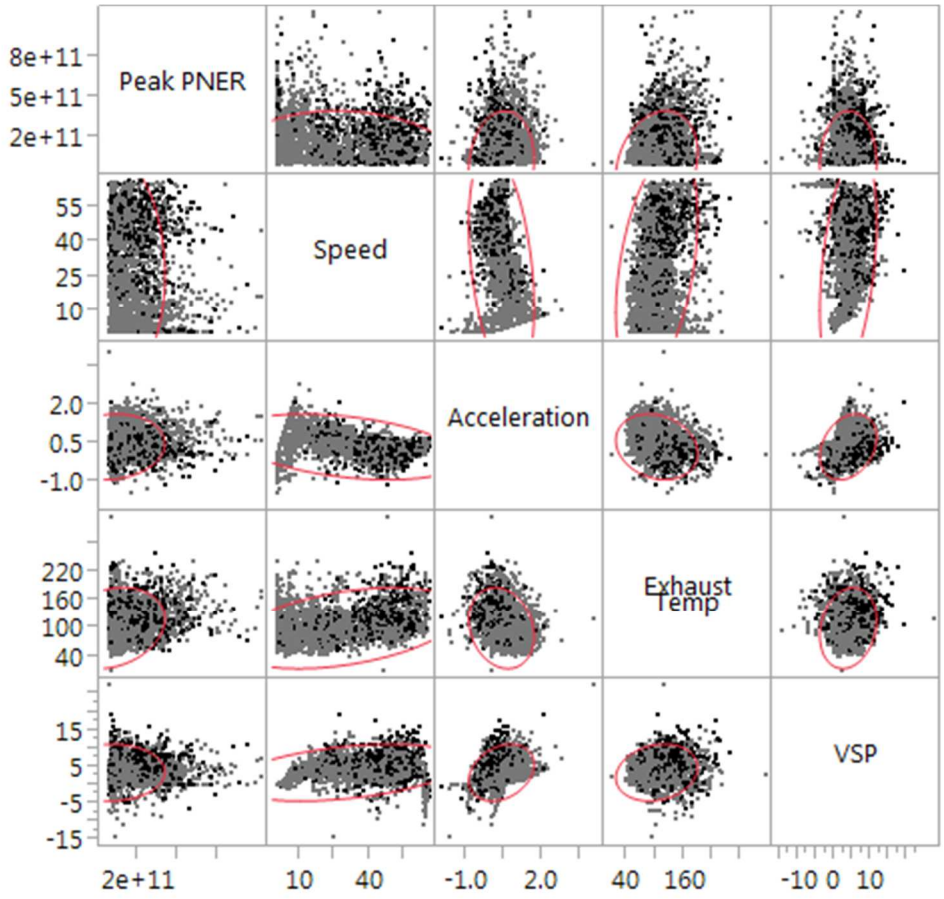

	Peak PNER	Speed	Acceleration	Exhaust Temp	VSP
Peak PNER	1.0000	-0.0795	0.0982	0.2254	0.0199
Speed	-0.0795	1.0000	-0.3675	0.4085	0.3910
Acceleration	0.0982	-0.3675	1.0000	-0.1991	0.2870
Exhaust Temp	0.2254	0.4085	-0.1991	1.0000	0.1879
VSP	0.0199	0.3910	0.2870	0.1879	1.0000

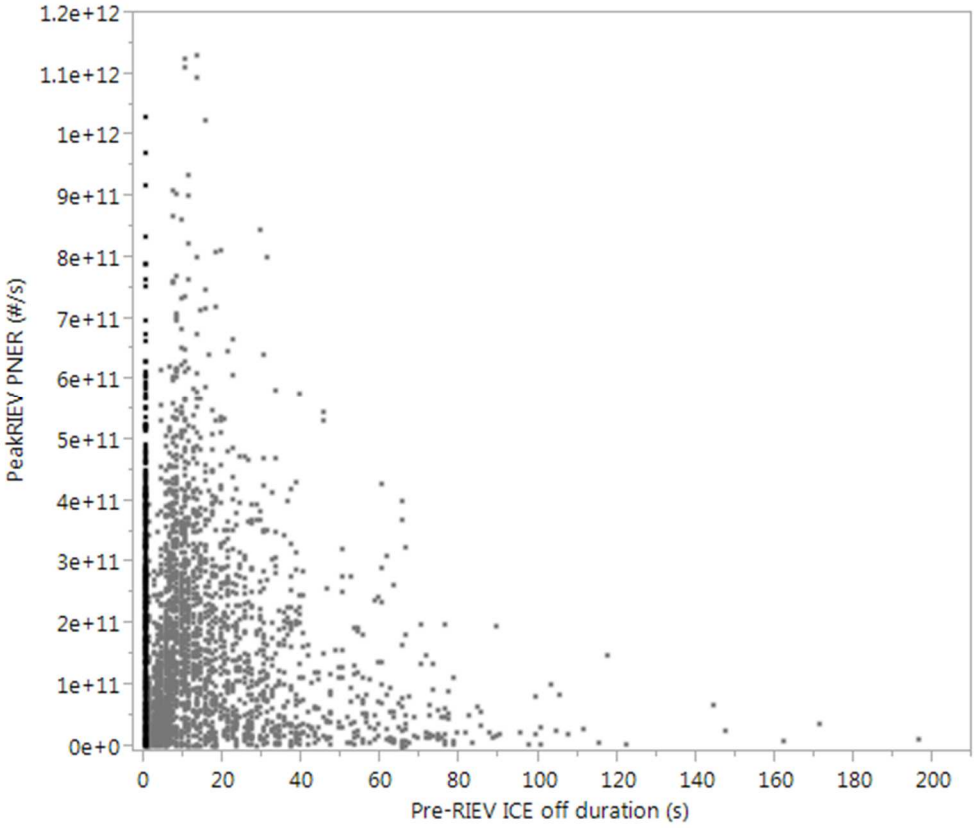

Figure F2. Scatterplot of peak PNER (#/s) during re-ignition events vs. previous period of ICE-Off (s) for all 3224 RIEVs. Bold points represent all partial RIEVs.

Appendix G **Analysis of Vehicle Specific Power Parameters**

Figure G1. Distribution of VSP (kW/ton) for all data.

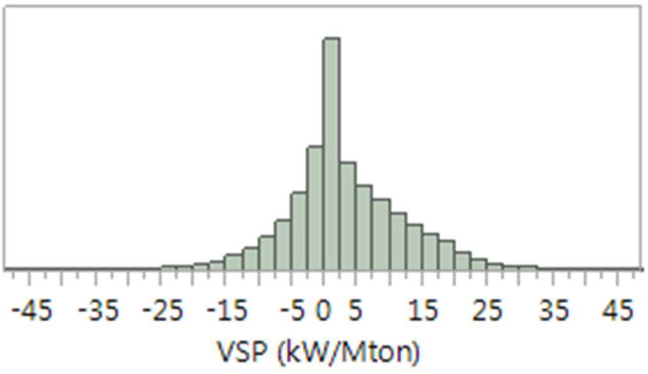

Quantiles

100.0%	maximum	168.067
99.5%		29.5753
97.5%		21.9463
90.0%		14.8886
75.0%	quartile	7.94645
50.0%	median	1.42432
25.0%	quartile	-1.4104
10.0%		-6.5657
2.5%		-13.518
0.5%		-21.088
0.0%	minimum	-104.81

Std Dev	3.0790778
Std Err Mean	8.8310605
Upper 95% Mean	0.0194603
Lower 95% Mean	3.1172194
Mean	3.0409361
N	205934

Appendix H **Run Summaries**

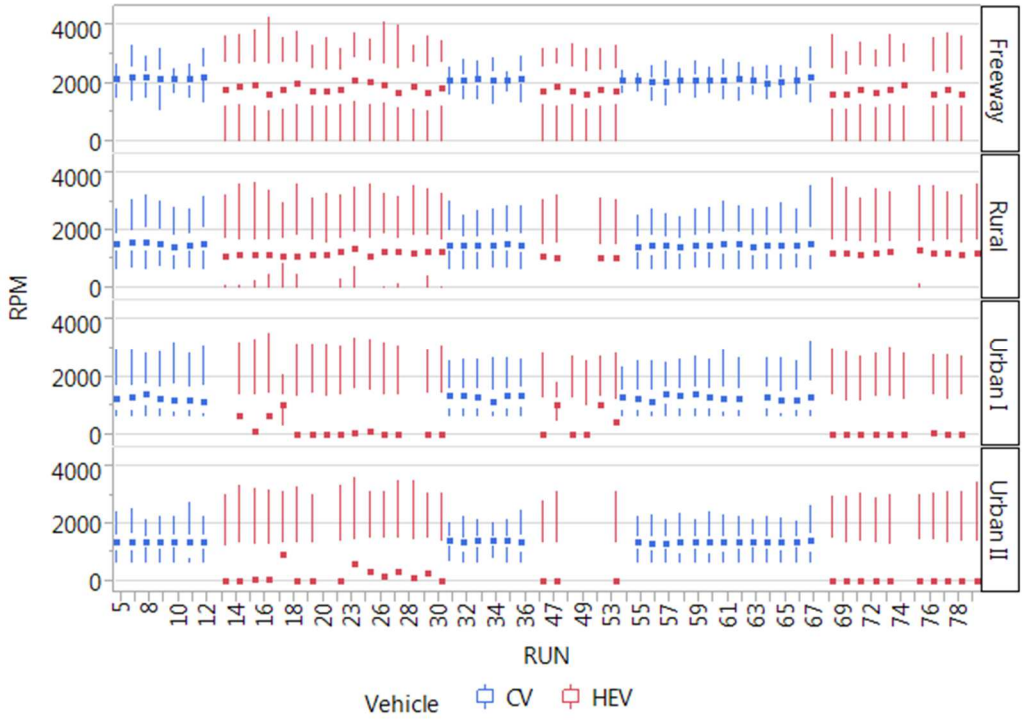

Figure H1. Box plots of RPM by run and road section, CV (blue) and HEV (red).

Table H1. Summary of RIEVs for each Run and Road Section.

	Freeway RIEV type		Rural RIEV type		Urban I RIEV type		Urban II RIEV type	
RUN	Full	Partial	Full	Partial	Full	Partial	Full	Partial
13	4	0	25	3	0	0	28	6
14	1	0	24	3	38	4	25	4
15	2	0	21	0	36	2	26	8
16	2	1	28	5	36	7	29	6
17	1	0	25	7	5	1	20	5
18	2	1	22	5	47	2	21	4
19	1	0	27	4	44	3	25	4
20	0	0	29	7	55	3	0	0
21	1	0	25	10	43	5	22	5
23	0	0	22	8	48	6	31	11
25	2	0	25	8	42	8	28	11
26	1	0	22	10	47	14	32	7
27	2	0	28	10	52	6	23	10
28	0	0	25	1	0	0	24	6
29	5	1	25	10	56	9	27	9
30	2	2	24	6	38	1	31	9
46	1	0	29	3	36	9	25	6
47	0	0	29	3	1	1	29	7
48	1	1	0	0	44	4	0	0
49	2	0	0	0	40	13	0	0
51	1	0	27	12	27	2	0	0
53	2	0	31	9	32	7	21	10
68	1	1	28	8	41	9	20	2
69	2	1	24	5	47	4	25	5
71	1	0	23	7	49	8	19	8
72	1	0	23	11	49	5	24	2
73	1	0	22	5	41	5	23	10
74	3	0	0	0	46	5	0	0
75	0	0	20	4	0	0	19	11
76	2	0	24	4	39	8	16	3
77	1	1	25	4	42	8	32	10
78	1	0	26	3	42	2	19	3
79	0	0	19	16	0	0	27	22
TOTALS	**46**	**9**	**747**	**191**	**1163**	**161**	**691**	**204**

Note: Red Filled Sections were excluded from analysis.

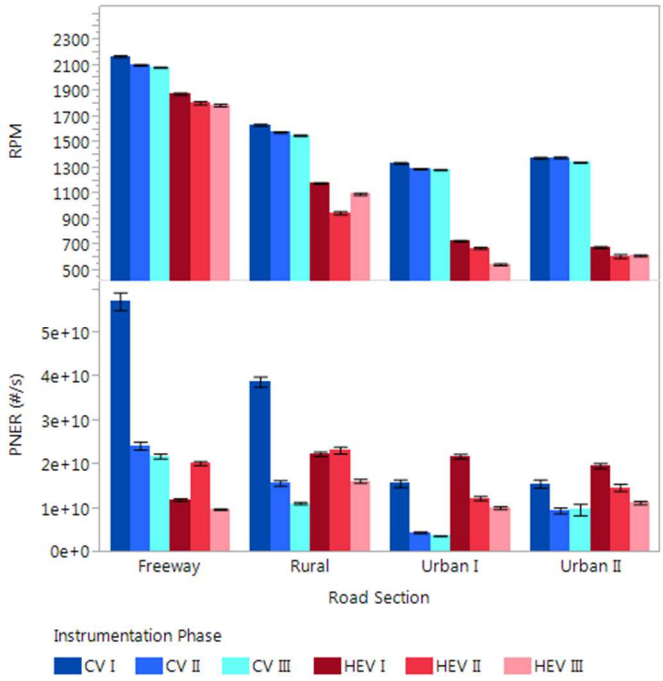

Figure H2. Bar Graph of mean PNER and RPM by road section and six run groups.

Table H2. Conventional vehicle run summaries of total duration (Time), total particle number count (PN) and total fuel consumed (FC) for each road section. Red sections are excluded from analysis.

	Freeway			Rural			Urban I			Urban II		
RUN	Time (s)	PN (10^{12})	FC (ml)	Time (s)	PN (10^{12})	FC (ml)	Time (s)	PN (10^{12})	FC (ml)	Time (s)	PN (10^{12})	FC (ml)
5	584	33.50	744.3	1009	49.80	1026.3	1072	17.20	855.3	864	16.40	639.3
7	565	36.90	736.9	984	42.60	986.3	1089	9.60	870.4	828	21.40	655.7
8	568	36.40	748.1	1073	42.20	1031.3	982	30.90	840.7	790	18.20	621.2
9	597	31.10	696.1	986	41.10	986.6	1163	15.60	927.6	848	9.78	614.1
10	606	37.70	730.5	1176	30.30	1022.9	1216	21.10	999.4	827	9.73	644.6
11	614	27.20	738.4	1063	33.60	1024.4	1280	15.70	1007.8	967	9.98	737.5
12	579	33.90	733.6	994	43.70	1001.5	1278	17.10	1037.3	888	8.63	707.8
31	596	14.20	716.3	1052	17.00	988.6	1206	4.07	851.9	821	6.22	615
32	599	7.99	715.2	1105	9.84	1019.6	1314	3.93	974.8	914	7.11	690.7
33	598	10.80	713.3	1111	19.30	1021.5	1170	5.61	872.4	855	7.85	648.2
34	603	4.50	724.1	1121	10.10	1034.2	1547	2.79	1080.5	793	7.01	600.3
35	596	29.10	739.4	1090	26.20	1062.1	1181	11.50	903.5	789	13.70	614
36	593	20.80	722.1	1091	21.60	1032.3	1215	6.81	908.8	908	6.54	709
54	593	11.50	713.9				1329	3.47	951.6			
55	593	18.30	745.1	1218	10.20	1059.1	1336	4.78	1005.8	895	6.79	692.4
56	609	14.50	719.6	1213	10.40	1091.9	1432	4.58	1103.8	1006	5.32	777.7
57	601	13.00	723.9	1090	7.09	1047.2	1027	4.46	835.9	939	2.53	712.8
58	593	9.57	721.9	1218	7.98	1119	1229	4.62	983.4	989	40.50	744.3
59	616	12.80	768.6	1093	9.52	1028.4	1212	4.07	935	890	7.35	656.5
60	595	8.53	728.7	1070	9.32	1027.5	1264	4.14	974.6	898	5.03	682.9
61	587	16.00	720.9	1095	17.40	1093	1293	7.42	1062.6	865	7.32	703.7
62	588	9.63	717.5	1130	11.20	1016	1296	3.81	964.6	886	5.38	681.7
63	587	21.60	720.2	1165	20.20	1058.7				829	7.91	664.5
64	594	9.49	732.2	1104	11.70	1012.9	1251	3.89	990.1	864	7.73	670.5
65	592	5.57	714.6	1124	11.30	1041.2	1511	3.97	1124.3	982	5.46	708.7
66	574	13.80	700.5	1080	12.10	1004.4	1317	5.12	1000.3	846	5.39	645.5
67	577	18.20	721.6	1079	26.50	1064	1051	8.38	942	875	8.01	723.4

Table H3. Hybrid vehicle run summaries of total duration (Time), total particle number count (PN) and total fuel consumed (FC) for each road section. Red sections are excluded.

	Freeway			Rural			Urban I			Urban II		
RUN	Time (s)	PN (10^{12})	FC (ml)	Time (s)	PN (10^{12})	FC (ml)	Time (s)	PN (10^{12})	FC (ml)	Time (s)	PN (10^{12})	FC (ml)
13	585	6.47	667.4	1004	28.70	809				966	18.60	392.4
14	573	5.11	684	1020	25.40	822.8	963	23.60	552.3	784	16.10	386.9
15	565	5.97	656.7	988	13.00	810.5	1035	22.30	534.5	838	13.90	434.2
16	596	10.00	665.8	998	25.40	822.9	992	34.90	582.2	825	21.70	418.6
17	578	3.48	655.4	986	16.90	832	957	9.86	798.8	700	9.76	422.4
18	565	3.91	677.8	988	18.30	833.6	1162	18.90	535.8	822	11.90	422.8
19	601	5.08	688.7	1079	23.80	860.2	1175	32.60	618.3	940	15.30	412.1
20	575	3.83	656.2	1129	20.10	855.8	1332	24.90	644.3			
21	595	4.67	667.7	1073	24.90	879.6	1166	23.20	554.4	933	18.70	467.5
23	562	10.20	685.2	1014	23.40	888.6	1098	32.60	603.3	895	13.60	492.2
25	576	12.20	690.9	1123	27.80	830.9	1137	25.30	638.4	807	18.70	447.9
26	585	10.30	673.3	1093	31.80	910	1313	33.60	644.1	830	20.90	446.7
27	596	5.21	674.9	1138	21.00	949.4	1248	20.50	622.4	821	11.90	453.8
28	605	9.27	667.4	1090	25.50	875.8				826	21.10	445.2
29	653	9.49	684	1013	29.50	863.1	1276	28.70	652.5	820	20.80	449.3
30	599	8.37	687.9	1059	21.80	863	1065	18.30	509.8	950	19.20	415.6
46	591	13.80	686.8	1161	30.30	806.7	1348	19.80	615	829	12.40	393.4
47	611	14.00	686.9	1089	29.10	804	1219	11.60	1006.2	810	11.40	391.4
48	603	12.80	678.4				1252	11.80	513.3			
49	641	7.90	685.6				1507	14.40	492.7			
51	608	10.00	667.4	1178	22.60	767	1087	15.40	598.5			
53	612	16.10	685.2	1169	25.10	763.6	1183	20.80	568.9	825	12.70	397.3
68	641	12.30	668.3	1100	24.80	858.5	1292	16.50	584.9	817	12.30	424
69	652	3.38	690.6	1123	13.00	857.5	1552	14.40	580.6	936	8.47	407.5
71	590	7.27	676.1	1113	34.40	807.4	1603	16.60	583.7	971	18.50	447
72	601	7.12	673.7	1114	22.30	816.3	1361	19.80	571.1	956	7.98	399.2
73	601	5.66	674.4	1111	13.20	887.4	1226	12.00	544.3	1010	9.27	396.1
74	599	4.13	697.4				1545	11.80	596.4			
75				1077	17.60	905.40				826	9.27	405.6
76	625	4.51	698.7	1096	12.70	832.3	1170	14.60	575.4	802	7.54	421.1
77	598	3.20	672.2	1140	8.68	882.6	1473	10.90	556.9	991	8.54	445.6
78	610	6.81	688.8	1171	16.10	840.5	1117	9.24	558.8	879	8.31	375.7
79				1274	21.30	938.3				1128	11.80	526.3

Appendix I **Particle Number Emission Factors**

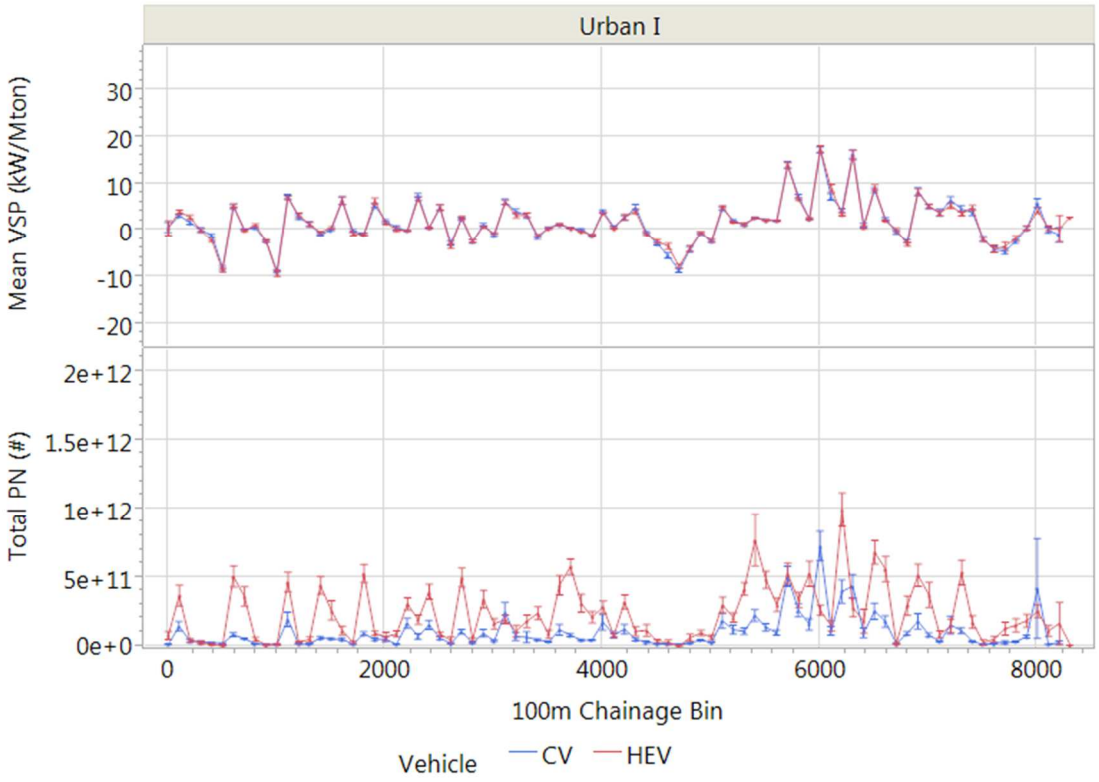

Figure I1. Distance series plot of Mean VSP (top, kW/ton) and Total PN emitted (bottom, #) by 100-m chainage bin for Urban I driving. CV = blue and HEV = red. Standard error bars are shown.

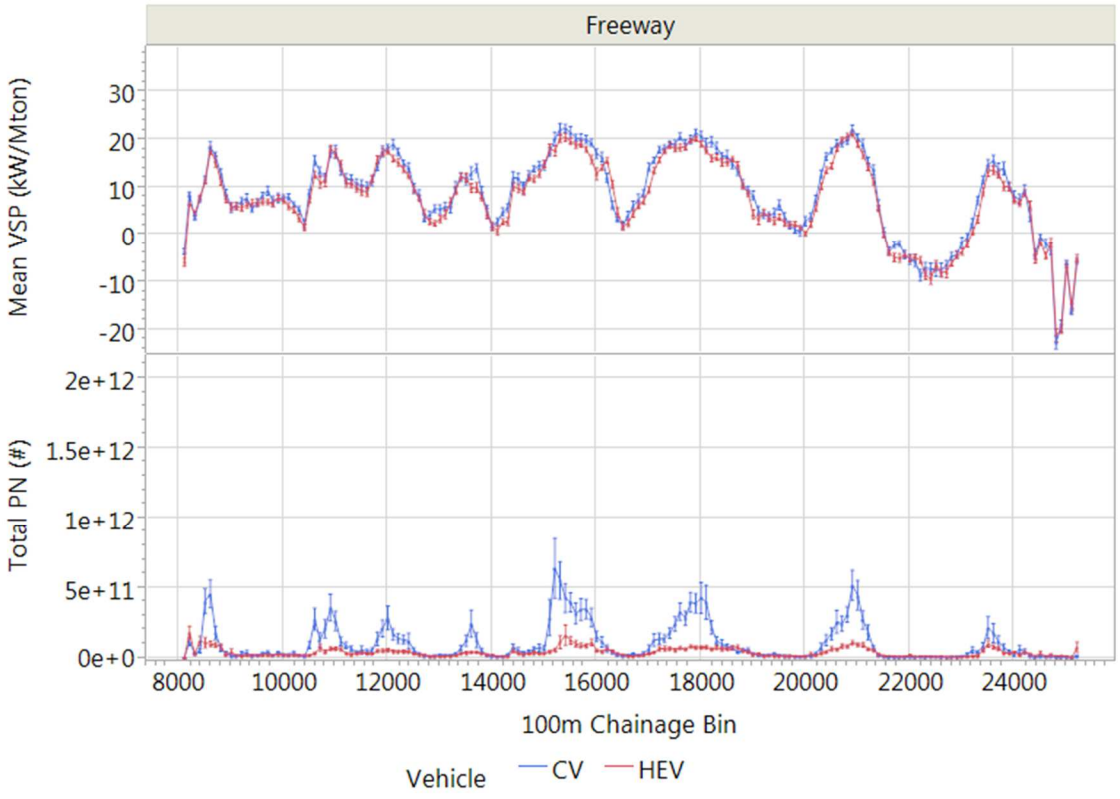

Figure I2. Distance series plot of Mean VSP (top, kW/ton) and Total PN emitted (bottom, #) by 100-m chainage bin for Freeway driving. CV = blue and HEV = red. Standard error bars are shown.

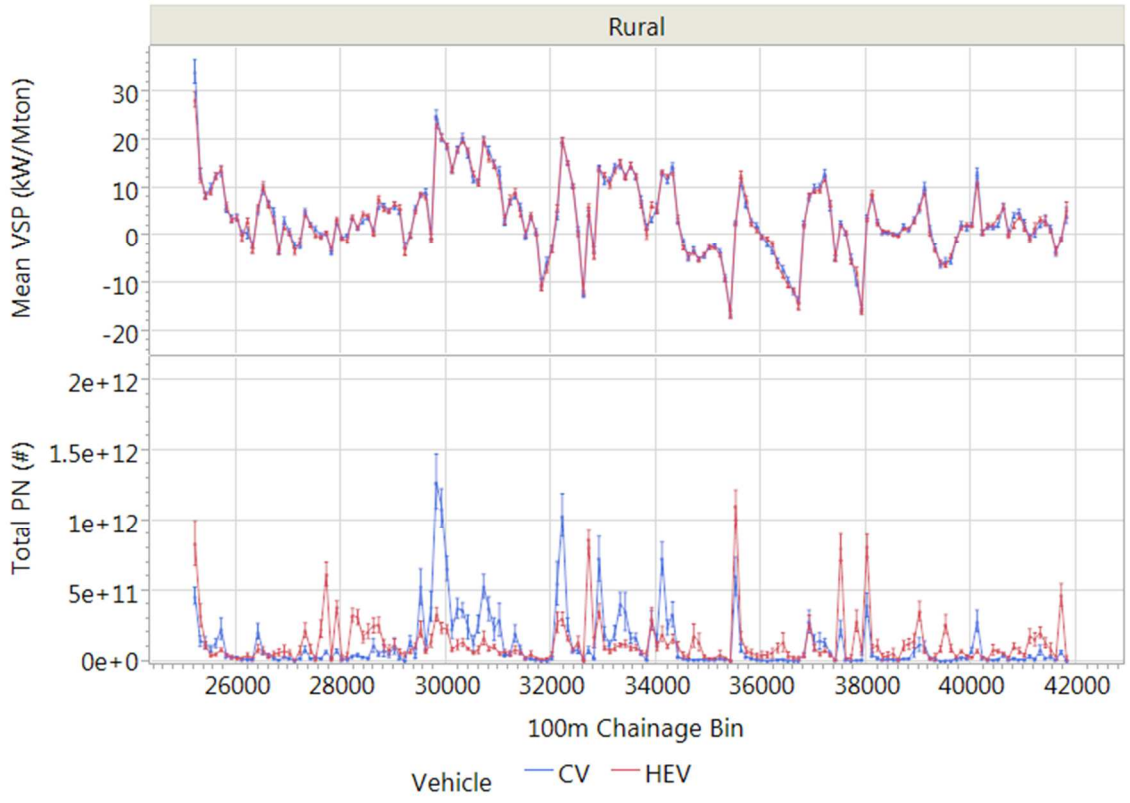

Figure I3. Distance series plot of Mean VSP (top, kW/ton) and Total PN emitted (bottom, #) by 100-m chainage bin for Rural driving. CV = blue and HEV = red. Standard error bars are shown.

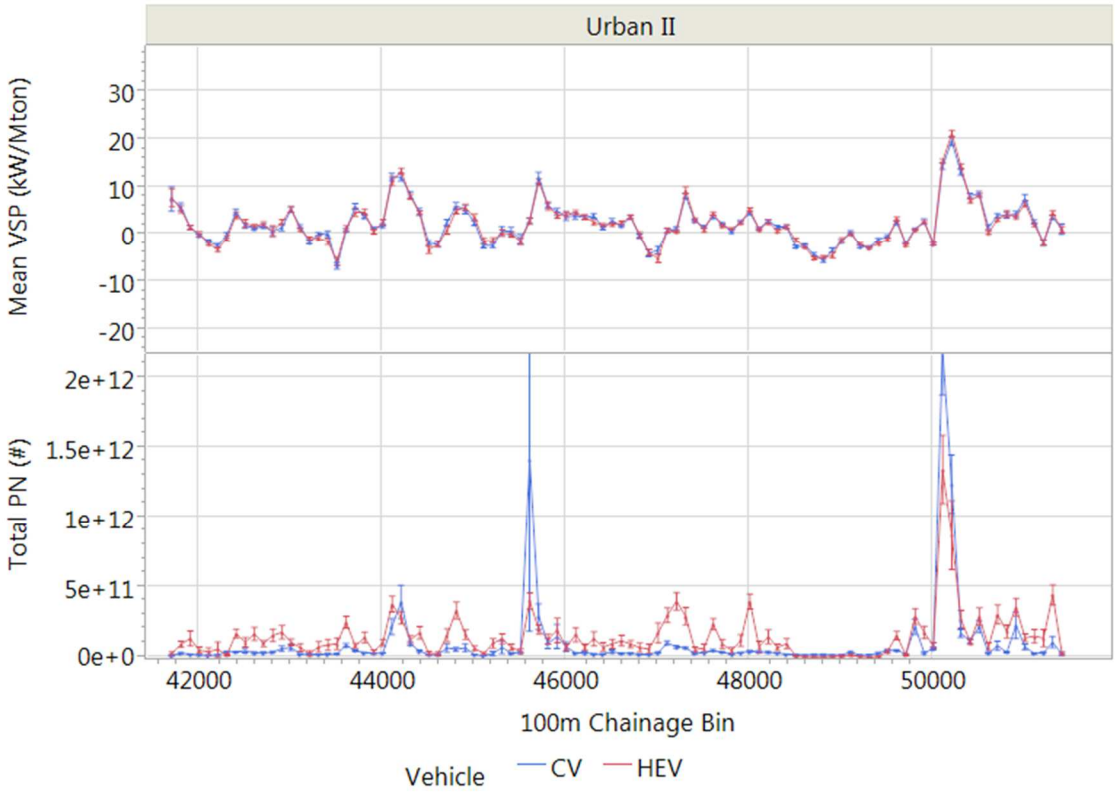

Figure I4. Distance series plot of Mean VSP (top, kW/ton) and Total PN emitted (bottom, #) by 100-m chainage bin for Urban II driving. CV = blue and HEV = red. Standard error bars are shown.